THESIS FOR THE DEGREE OF DOCTOR OF PHILOSOPHY IN MACHINE AND VEHICLE SYSTEMS

Traffic Situation Management for Driving Automation of Articulated Heavy Road Transports

From driver behaviour towards highway autopilot

PETER NILSSON

Department of Mechanics and Maritime Sciences
CHALMERS UNIVERSITY OF TECHNOLOGY

Göteborg, Sweden 2017

Traffic Situation Management for Driving Automation of Articulated Heavy Road Transports
From driver behaviour towards highway autopilot
PETER NILSSON
ISBN 978-91-7597-630-3

Doktorsavhandlingar vid Chalmers tekniska högskola
Ny serie nr. 4311
ISSN 0346-718X
Department of Mechanics and Maritime Sciences
Chalmers University of Technology
SE-412 96 Göteborg
Sweden
Telephone: +46 (0)31-772 1000

Chalmers Reproservice
Göteborg, Sweden 2017

To Elin and Linnea.

Traffic Situation Management for Driving Automation of Articulated Heavy Road Transports
From driver behaviour towards highway autopilot
Thesis for the degree of Doctor of Philosophy in Machine and Vehicle Systems
PETER NILSSON
Department of Mechanics and Maritime Sciences
Chalmers University of Technology

Abstract

In this thesis traffic situation management for driving automation of long combination vehicles is discussed. The automation targets high-speed driving in multiple-lane, one-way roads. Traffic situation predictions, traffic situation manoeuvres and driving principles are studied specifically. Traffic situation predictions relates to the functions used to predict how an observed traffic situation will evolve in the future. Traffic situation manoeuvres relates to decision-making regarding driving principles and control on a tactical level of driving. The developed methods and principles assume the existence of vehicle environment sensing functionalities. Furthermore, the methods have been verified using motion platform driving simulator experiments and desktop simulations.

In the proposed methods for traffic situation predictions, models of the subject vehicle, driver, road and surrounding traffic have been formulated. These models capture both subject vehicle dynamics and predicted motion of surrounding traffic. Also, a unique driver steering model for articulated vehicles has been derived. Moreover, traffic situation predictions for multiple-lane one-way road driving has been derived by using driver steering and acceleration models in a closed loop with the subject vehicle model. Also, a second approach to calculate actuation trajectories has been developed and evaluated using a model predictive control framework including on-line optimisation. The derived traffic situation manoeuvres include maintain-lane, lane changes and non-evasive abort manoeuvres.

It is envisaged that studying the important characteristics of manual driving will give insight into how to design driving automation especially in regard to mixed traffic with both manually driven and automated vehicles. Driving principles for driving automation are derived by using back-to-back comparisons of manual and automated driving in simulator experiments. Driving principles for initiation and execution of lane-change manoeuvres with surrounding traffic as well as managing mandatory road exits and lane changes in dense traffic have been studied and some driving principles for automation have been derived.

Keywords: articulated heavy-vehicles, long combination vehicles, vehicle dynamics, vehicle model, driver model, driving automation, driving simulator, driving principles

Acknowledgements

The research presented in this thesis has been financially supported by Volvo Group Trucks Technology and VINNOVA, Sweden's innovation agency. This support is gratefully acknowledged.

First I would like to express my deep gratitude to my supervisors Adjunct Prof. Leo Laine and Prof. Bengt Jacobson for your great enthusiasm and guidance. At Volvo GTT, I especially want to thank my managers Stefan Edlund, Malin Larking and Inge Johansson for providing me with the possibility to conduct this research. Thanks also to my steering group members Lena Larsson, Lennart Cider, Fredrik Sandblom, Martin Sanfridson and Johan Lindberg. To my friend and roommate Kristoffer Tagesson - genius by simplicity. To Sachin Janardhanan, Niklas Fröjd and Pontus Larsson for superior support in the driving simulator studies. Thanks also to my oldest colleagues Anders, Andreas, Carl-Johan, Fredrik, Larses, Nicolas, Peter and Sofi for supporting me during good and difficult periods. I am grateful for all the support I received at VTI in setting up simulator studies. A special thanks goes to to Bruno Augusto, Jesper Sandin, Frida Reichenberg and Eleni Kalpaxidou. At Chalmers University of Technology, I would like to thank Adi, Anton, Britta, Fredrik, Manjurul, Mathias, Ola, Pär, Sixten, Sonja, Toheed, Tushar and Weitao for inspiring discussions and a pleasant working environment. I am also thankful to Associate Prof. Tamás Keviczky at TU Delft, for ideas and advise during the project. To Niels van Duijkeren for invaluable programming skills.

Finally, the support I have received from my family is invaluable - thank you Mum, Dad, Stefan and Cristina.

Peter Nilsson
Göteborg, September 2017

Acronyms

ADS	automated driving system
ADS-DV	automated driving system dedicated vehicle
AGV	automated guided vehicle
BASt	Federal Highway Research Institute in Germany
CoG	centre of gravity
DAE	differential algebraic equation
DDT	dynamic driving task
EMS	European modular system
FA	functionality area
FD	functionality domain
FA-TSM	functionality area traffic situation manoeuvre
FA-TSO	functionality area traffic situation observation
FA-TSP	functionality area traffic situation prediction
FD-HMI	functionality domain human machine interface
FD-MSDM	functionality domain motion support device management
FD-RM	functionality domain route management
FD-RSiM	functionality domain route situation management
FD-TMM	functionality domain transport mission management
FD-TSM	functionality domain traffic situation management
FD-VEM	functionality domain vehicle environment management
FD-VMM	functionality domain vehicle motion management
FSM	finite-state machine
GPS	global positioning system
GPU	graphics processing unit
HMI	human-machine interface
HSSO	high speed steady-state off-tracking
HSTO	high speed transient off-tracking
IDM	intelligent driver model
ISO	International Organization for Standards
LCD	lane change duration
LCT	lateral clearance time
LCV	long combination vehicles
MPC	model predictive control

NHTSA	National Highway Traffic Safety Administration in the U.S.
NMPC	non-linear model predictive control
OCP	optimal control problem
ODD	operational design domain
OpenCL	open computing language
PSO	particle swarm optimization
RA	rearward amplification
RRT	rapidly-expanding random tree
SAE	Society of Automotive Engineers
SLO	straight line off-tracking
SPW	swept path width
SRT	steady-state roll-over threashold
TSM	complete set of functionalities included in FA-TSM
TSP	complete set of functionalities included in FA-TSP
TTC	time to collision
VeMFRA	vehicle motion functionality reference architecture
YDC	yaw damping coefficient

Nomenclature

Maximum acceleration in IDM model	$a^{(\alpha)}$
Acceleration along the road for surrounding vehicle m in lane n	$a^{(o)}_{m,n}$
Vehicle front cross-sectional area	A_{v}
Translational acceleration vector for the CoG of vehicle unit j	$\mathbf{a}_j$
Longitudinal acceleration limits	$\underline{a}_x$, $\overline{a}_x$
Translational accelerations of vehicle unit j in a body fixed frame	$a_{\mathrm{Xv}j}$, $a_{\mathrm{Yv}j}$
Requested time derivative of the longitudinal velocity of the first vehicle unit in a body fixed frame used in prediction	$a^{\mathrm{req,pred}}_{\mathrm{Xv1}}$
Extremum of lateral acceleration for the CoG of vehicle unit j in a body fixed frame	$a_{\mathrm{Yv}j,\mathrm{ext}}$
Desired deceleration in IDM model	$b^{(\alpha)}$
Air drag coefficient	C_{D}
Horizontal road curvature of segment i	$c^{(i)}_h$
Initial horizontal road curvature of segment i	$c^{(i)}_{\mathrm{h},0}$
Horizontal road curvature rate of segment i	$c^{(i)}_{\mathrm{h},1}$
Cost associated with a lane-change manoeuvre	c_{lc}
Rolling resistance coefficient	c_{r}
Vertical road curvature of segment j	$c^{(j)}_{\mathrm{v}}$
Initial vertical road curvature of segment j	$c^{(j)}_{\mathrm{v},0}$

Vertical road curvature rate of segment j	$c_{\mathrm{v},1}^{(j)}$
Cornering stiffness of vehicle unit j axle k. In case of equivalent wheelbase model.	$C_{\mathrm{Y}jk}$
Cornering stiffness of vehicle unit j axle m. In case of multiple non-steered axles.	$C_{\mathrm{Y}jm}$
Lateral distance offset perpendicular to the road tangent for vehicle unit j axle k	$d_{\mathrm{R}jk}$
Extremum of lateral distance offset for vehicle unit j axle k	$d_{\mathrm{R}jk,\mathrm{ext}}$
Limits of the lateral distance perpendicular to road	$\underline{d}$, $\overline{d}$
Reference for lateral distance perpendicular to road of vehicle unit j axle k	$d_{\mathrm{R}jk,\mathrm{ref}}$
Unit vectors of an inertial frame	$\mathbf{e}_{\mathrm{X_E}}$, $\mathbf{e}_{\mathrm{Y_E}}$
Unit vectors of vehicle unit j in a body fixed frame	$\mathbf{e}_{\mathrm{X}\mathrm{v}j}$, $\mathbf{e}_{\mathrm{Y}\mathrm{v}j}$, $\mathbf{e}_{\mathrm{Z}\mathrm{v}j}$
Unit vectors of vehicle unit j axle k in a wheel fixed frame	$\mathbf{e}_{\mathrm{X}\mathrm{w}jk}$, $\mathbf{e}_{\mathrm{Y}\mathrm{w}jk}$
Unit vectors of vehicle unit j axle k in a road fixed frame	$\mathbf{e}_{s_{\mathrm{R}jk}}$, $\mathbf{e}_{n_{\mathrm{R}jk}}$
Unit vectors for far-point in a road fixed frame	$\mathbf{e}_{s_{\mathrm{Rf}}}$, $\mathbf{e}_{n_{\mathrm{Rf}}}$
Unit vectors of vehicle unit j axle k in a body fixed frame aligned with far-point direction	$\mathbf{e}_{s_{\mathrm{R}jk}\prime}$, $\mathbf{e}_{n_{\mathrm{R}jk}\prime}$
Discretised system	f^{dt}
Body force vector of vehicle unit j	$\mathbf{F}_j$
Body forces of vehicle unit j in a body fixed frame	$F_{\mathrm{X}\mathrm{v}j}$, $F_{\mathrm{Y}\mathrm{v}j}$
Tyre force vector of vehicle unit j axle k	$\mathbf{F}_{jk}$
Tyre forces of vehicle unit j axle k in a wheel fixed frame	$F_{\mathrm{X}\mathrm{w}jk}$, $F_{\mathrm{Y}\mathrm{w}jk}$
Requested longitudinal force	F_X^{req}
Propulsion force vehicle unit 1 axle 2 in a wheel fixed frame	$F_{\mathrm{prop},12}$
Brake force vehicle unit j axle k in a wheel fixed frame	$F_{\mathrm{brake},jk}$
Maximum design brake force of unit j axle k in a wheel fixed frame	$F_{\mathrm{brake},jk}^{\mathrm{max}}$

Vertical force of vehicle unit j axle k in a body fixed frame	$F_{\mathrm{Zv}jk}$
Aerodynamic drag in a body fixed frame	$F_{\mathrm{air},1}$
Gravitational force of vehicle unit j	$F_{\mathrm{grav},j}$
Maximum propulsion force in a wheel fixed frame	$F_{\mathrm{prop}}^{\mathrm{max}}$
Gravitational acceleration	g
Translational jerk of vehicle unit j in a body fixed frame	$j_{\mathrm{Xv}j}$,$j_{\mathrm{Yv}j}$
Yaw inertia of vehicle unit j	J_{Zj}
Gain factors in driver acceleration model	$k_{\dot{\theta}_{\mathrm{p}}}$, $k_{\theta_{\mathrm{p}}}$, $k_{\Delta v}$
Gain factors in driver steering model	k_{f}, k_{n}, k_{nI}
Gain factors in proposed driver steering model	k_{r}, k_{rI}
Desired gain factors in driver steering model	$k_{\mathrm{f,des}}$, $k_{\mathrm{n,des}}$, $k_{\mathrm{nI,des}}$
Weighting factors in MPC cost function	$K_{d_{\mathrm{R}11}}$, $K_{d_{\mathrm{R}j1}}$, $K_{v_{\mathrm{Xv}1}}$, $K_{\Delta s}$, $K_{j_{\mathrm{Xv}1}}$, $K_{j_{\mathrm{Yv}1}}$, $K_{a_{\mathrm{Xv}1}}$, $K_{\dot{\delta}}$
Equivalent wheelbase	l_{eq}
Distance from CoG of unit j to axle k	l_{jk}
Distance from CoG of unit j to connection point front	$l_{j\mathrm{f}}$
Distance from connection point rear of unit j to rear axle	$l_{j\mathrm{r}}$
Actual wheelbase	L_{wb}
Number of rear axles	M
Mass of vehicle unit j	m_j
Relative lane to the targeted global waypoint	N_{rel}
Generalized coordinate i	q_i
Engine power	P_{prop}
Generalized force i	Q_i

Weighting matrix for states in MPC formulation	$\mathbf{Q}_{\mathrm{MPC}}$
Position vector for CoG of vehicle unit j	$\mathbf{r}_j$
Position vector of vehicle unit j axle k	$\mathbf{r}_{jk}$
Rotation matrix for vehicle unit j	$\mathbf{R}_{\mathrm{v}j}$
Rotation matrix for vehicle unit j axle k	$\mathbf{R}_{\mathrm{w}jk}$
Position of far-point in a body fixed frame	$r_{\mathrm{f/o}\prime}$
Velocity of far-point in a body fixed frame	$\dot{r}_{\mathrm{f/o}\prime}$
Rearward amplification using lateral acceleration	$\mathrm{RA}_{a_{\mathrm{y}}}$
Weighting matrix for actuation in MPC formulation	$\mathbf{R}_{\mathrm{MPC}}$
Road arc position	s
Road arc position of the horizontal projection	s_{h}
Distance travelled along the road for vehicle unit j axle k	$s_{\mathrm{R}jk}$
Distance travelled along the road for surrounding vehicle m in lane n	$s_{m,n}^{(o)}$
Far-point velocity along the road	$\dot{s}_{\mathrm{Rf}}$
Lateral tyre slip of vehicle unit j axle k	$S_{\mathrm{Y}jk}$
Desired minimum gap in IDM model	s^*
Current gap in IDM model	s_α
Jam distances in IDM model	$s_0^{(\alpha)}$, $s_1^{(\alpha)}$
Kinetic energy	T
Tandem factor	T_{f}
Safe time headway in IDM model	T^α

Prediction horizon	T_{p}
Lane change duration parameter	T_{lc}
Vehicle actuation vector	$\mathbf{u}$
Optimization vector in MPC formulation	$\mathbf{U}_0$
Reference actuation vector in MPC formulation	$\mathbf{u}^{\mathrm{ref}}$
Utility for lane n	U_n
Tuning parameters in utility function	u_0, u_1
Potential energy	V
Translational velocity vector for CoG of vehicle unit j	$\mathbf{v}_j$
Translational velocities of vehicle unit j in a body fixed frame	$v_{\mathrm{Xv}j}$, $v_{\mathrm{Yv}j}$
Translational velocity vector of vehicle unit j axle k	$\mathbf{v}_{jk}$
Translational velocities of vehicle unit j axle k in a wheel fixed frame	$v_{\mathrm{Xw}jk}$, $v_{\mathrm{Yw}jk}$
Velocity along the road for surrounding vehicle m in lane n	$v_{m,n}^{(o)}$
Acceleration of vehicle α in IDM model	$\dot{v}_\alpha$
Velocity of vehicle α in IDM model	v_α
Desired velocity in IDM model	$v_0^{(\alpha)}$
Speed limits	$\underline{v}_x$, $\overline{v}_x$
Reference speed profile for first vehicle unit	$v_{\mathrm{Xv1,ref}}$
Average speed ahead in lane n	$v_{\mathrm{aver},n}^{(o)}$
Reference speed in lane n	$v_{\mathrm{ref},n}$

Speed in lane n (used in utility calculation)	$\tilde{v}_n$
Legal speed limit in lane n	$\overline{v}_{\mathrm{x},n}$
Position for CoG of vehicle unit j in an inertial coordinate frame	$\bar{X}_j$, $\bar{Y}_j$
Position of road segment i in a local coordinate frame	$x^{(i)}$, $y^{(i)}$
Initial position of road segment i in a local coordinate frame	$x_0^{(i)}$,$y_0^{(i)}$
Acceleration exponent in IDM model	δ
Front wheel steering angle limit	$\overline{\delta}$
Steering angle of vehicle unit j axle k	δ_{jk}
Requested steering wheel angle used in prediction	$\delta^{\mathrm{req,pred}}$
Longitudinal distance from the rear end of L_{wb} to the rear axle m	Δ_m
In case of a lead vehicle: distance between the rear of surrounding vehicle m in lane n and front of the subject vehicle. In case of a lag vehicle: distance between the front of the surrounding vehicle and rear of the subject vehicle.	$\Delta s_{m,n}^{(o)}$
Lower distance limit between the rear of lead vehicle and front of the subject vehicle	$\underline{\Delta s}_{1,n}^{(o)}$
Distance difference along the road between far-point and subject vehicle front axle	Δs_{Rf}
Distance difference along the road between near-point and subject vehicle front axle	Δs_{Rn}
Distance to the targeted global way-point	Δs_{wp}
Safety distance	Δs_{safe}
Speed difference between the desired set speed and the subject vehicle speed	Δv_{set}
Difference between road angle on the inner edge of the lane at last vehicle axle and yaw angle of last vehicle unit	$\Delta\theta_{\mathrm{r}}$
Difference between road angular rate on the inner edge of the lane at last vehicle axle and yaw rate of last vehicle unit	$\Delta\dot{\theta}_{\mathrm{r}}$

Articulation angle and angular rate of the trailing vehicle unit j	$\Delta\psi_j$, $\Delta\dot{\psi}_j$
Yaw angle of vehicle unit j relative to the road	$\Delta\psi_{\mathrm{R}j}$
Ratio between the steering wheel angle and the front wheel steering angle	η_s
Angle between the road tangent vector and the s_{h} axle	$\theta_{\mathrm{R}}^{(j)}$
Far-point angle rate	$\dot{\theta}_{\mathrm{f}}$
Near-point angle and angular rate	θ_{n}, $\dot{\theta}_{\mathrm{n}}$
Object projection angle and angular rate	θ_{p}, $\dot{\theta}_{\mathrm{p}}$
Vehicle state vector	ξ
Reference state vector in MPC formulation	ξ^{ref}
Air density	ρ
Quotient between the angular projection of an object and the angular expansion rate	τ
Angle between the road tangent vector and the X-axis	$\psi_{\mathrm{R}}^{(i)}$
Yaw angle and yaw rate of vehicle unit j	ψ_j, $\dot{\psi}_j$
Road angle at vehicle unit j axle k	$\psi_{\mathrm{R}jk}$
Road angle at far-point position	ψ_{Rf}
Road angle on the inner edge of the lane at last vehicle axle	$\psi_{\mathrm{R}n1\prime}$
Road angular rate on the inner edge of the lane at last vehicle axle	$\dot{\psi}_{\mathrm{R}n1\prime}$
Rotational velocity vector of vehicle unit j	$\boldsymbol{\Omega}_j$
Scalar product	$\bullet$
Cross product	$\times$

Characters in boldface are used for matrices and geometric vectors. Units according to SI and radians. Velocities and accelerations are absolute (w.r.t. an inertial system) if not else is stated.

Thesis

This thesis consists of an extended summary and the following appended papers:

Paper A P. Nilsson, L. Laine, O. Benderius, and B. Jacobson. "A driver model using optic information for longitudinal and lateral control of a long vehicle combination". *Intelligent Transportation Systems (ITSC), 2014 IEEE 17th International Conference on.* IEEE. 2014, pp. 1456–1461

Paper B P. Nilsson, L. Laine, B. Jacobson, and N. Van Duijkeren. "Driver model based automated driving of long vehicle combinations in emulated highway traffic". *Intelligent Transportation Systems (ITSC), 2015 IEEE 18th International Conference on.* IEEE. 2015, pp. 361–368

Paper C P. Nilsson, L. Laine, N. Van Duijkeren, and B. Jacobson. "Automated highway lane changes of long vehicle combinations: A specific comparison between driver model based control and nonlinear model predictive control". *Innovations in Intelligent SysTems and Applications (INISTA), 2015 International Symposium on.* IEEE. 2015, pp. 1–8

Paper D P. Nilsson, L. Laine, and B. Jacobson. A Simulator Study Comparing Characteristics of Manual and Automated Driving During Lane Changes of Long Combination Vehicles. *IEEE Transactions on Intelligent Transportation Systems* PP.99 (2017), pp. 1–11

Paper E P. Nilsson, L. Laine, J. Sandin, and B. Jacobson. On Actions of Long Combination Vehicle Drivers Prior To Lane Changes in Dense Highway Trajectory - A Driving Simulator Study (2017). Submitted to Transportation Research: Part F

The author of this thesis had the main responsibility for the implementation of models, carrying out numerical simulations, analysis and writing of Papers B, D and E. For Paper A, the author collaborated with Benderius in the parametrization of the driver model and writing. For Paper C, the author collaborated with Duijkeren in the the implementation of models.

Related work by the author, not included in the thesis:

P. Nilsson, L. Laine and B. Jacobson. "Performance characteristics for automated driving of long heavy vehicle combinations evaluated in motion simulator". *Intelligent Vehicles Symposium Proceedings, 2014 IEEE.* IEEE. 2014, pp 362-369

P. Nilsson, J. Sandin. "Drivers' assessment of driving a 32 meter A-double with and without full automation in a moving simulator base simulator". *13th International Heavy Vehicle Transport Technology Symposium, San Luis, Argentina.* 2014

N. Duijkeren, T. Keviczky, P. Nilsson and L. Laine. "Real-Time NMPC for Semi-Automated Highway Driving of Long Heavy Vehicle Combinations." *5th IFAC Conference on Nonlinear Model Predictive Control, NMPC'15, Seville, September 17-21, 2015.* 2015

J. Sandin, B. Augusto, P. Nilsson and L. Laine. "A Lane-Change Gap Acceptance Scenario Developed for Heavy Vehicle Active Safety Assessment: A Driving Simulator Study." *Future Active Safety Technology Towards zero traffic accidents, FAST Zero 2015, Göteborg, September 2015.* 2015

J. Sandin, B. Augusto, L. Laine, N. Fröjd and P. Nilsson. "Large Moving Base Simulators and Automation Design for Heavy Vehicles - Case Study for HCT." *International Symposium on Heavy Vehicle Transport Technology (HVTT14).* 2016

Contents

1 Introduction

Safe and effective road freight transports are an important part of today's society, enabling economic development. In 2014, freight transports by road accounted for close to three-quarters of the total inland tonne-kilometres conducted in the European Union [30]. To meet future environmental and productivity goals, an interesting starting point is the use of long combination vehicles (LCVs), as illustrated in Fig. 1.2. These are road transport vehicles whose length and weight fall outside the dimensions permitted under conventional European road regulations. Typically, LCVs include at least two articulated joints and their length generally varies between 27 m and 34 m. The weight and/or volume of goods transported by LCVs increases by a factor 1.5-2.0, compared with a conventional tractor semi-trailer combination. The energy consumption is typically reduced by 15-20% per tonne-kilometre [68].

Road freight transports are mainly carried out on the same public road infrastructure used by passenger cars. When comparing heavy trucks used for freight transports and passenger cars, relevant differences include: a factor of up to 5 in length (affects lateral tracking), a factor of up to 30 in mass (affects both acceleration and braking capacities due to lower specific propulsion and braking effect) and a factor of up to 3 in the height of the centre of gravity (affects roll-over), see Fig. 1.1. The static roll-over limit for heavy trucks can be as low as $0.35g$, whereas the roll-over limit for passenger cars is typically $1.1g$.

In addition to the distinct differences in size and weight, there are further differences related to vehicle behaviour in dynamic manoeuvring, such as lane changes. As a first example of articulated vehicle characteristics, consider the behaviour in cornering, as illustrated in Fig. 1.2.

Figure 1.1: *Difference in height and width between a passenger car and heavy truck combination. This affects the risk of roll-over and available lane space. The static roll-over limit for heavy trucks can be as low as 0.35g, whereas the roll-over limit for passenger cars is typically 1.1g.*

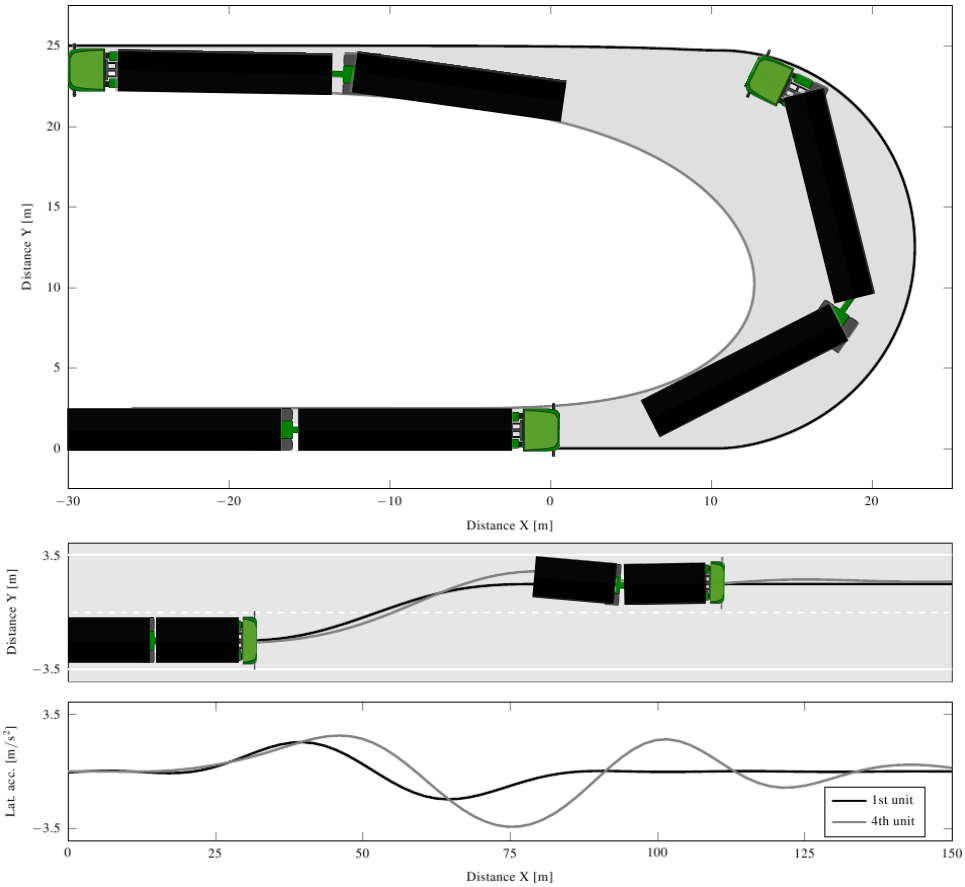

Figure 1.2: *Low speed cornering (top). The shaded area represents the swept path width between the outer corner of the first vehicle unit and the inner corner of the last vehicle unit. Lane-change manoeuvre (bottom). The vehicle speed is* 70 km/h *and a critical steering wheel frequency input. The rearmost unit swings out approximately* 0.5 m *and the lateral acceleration is amplified by a factor of 1.5.*

This shows the vehicle navigating a sharp bend with an outer radius of 12.5 m at low speed. Here, it should be observed that the last vehicle unit is travelling inwards of the first vehicle unit. The effect of the different paths between the first and last axle in the vehicle combination is known as off-tracking. The off-tracking in this example results in a swept path width of 12.5 m.

As a second example, consider the vehicle behaviour in a lane-change manoeuvre. In Fig. 1.2, the vehicle is travelling at 70 km/h and carries out a lane-change manoeuvre with a critical steering wheel frequency of around 0.4 Hz. Due to vehicle dynamics, the last vehicle unit swings out by approximately 0.5 m compared to the first unit. Moreover,

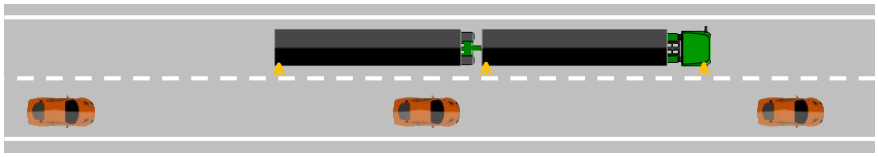

(a) *Long articulated heavy vehicle*

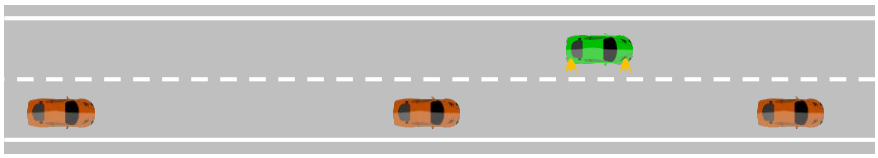

(b) *Passenger car*

Figure 1.3: *Example of a lane change to the right situation in dense highway traffic. Traffic speed typically* 70 km/h *and time gap* 1 s*. There is a sufficient gap for the passenger car but not for the articulated heavy vehicle.*

the maximum magnitude of lateral acceleration of the last vehicle unit is amplified by a factor of 1.5 compared to the first unit, from $2.3\,\mathrm{m/s^2}$ to $3.4\,\mathrm{m/s^2}$, which can pose a significant risk of vehicle roll-over. As mentioned above, the roll-over limit for heavy trucks is often clearly lower than for passenger cars due to the position of the centre of gravity. The amplification effect, known as rearward amplification increases the risk of roll-over.

The manoeuvring characteristics of articulated vehicles result not only in different continuous driving behaviour (i.e. execution of steering and propulsion/braking) but also a different discrete driving behaviour (i.e. initiation of braking and/or a specific manoeuvre). Drivers of articulated vehicles typically refer to extended planning, including an increased planning horizon. Consider a highway driving scenario in dense traffic, see Fig. 1.3. Due to the length of their vehicles, drivers of long articulated vehicles are often exposed to many surrounding vehicles ahead as well as behind. Executing a lane change in such dense traffic (which might be fully possible for a passenger car due to the natural gap size), may be impossible for an articulated vehicle, simply because there are no gaps big enough. To accomplish their lane change manoeuvre, the driver needs to initiate and rely on cooperation from surrounding traffic.

In recent decades, industry and academia has placed an increasing emphasis on driving automation for road vehicles. These efforts have accelerated recently thanks to technological developments which have made high data processing capacity possible. The focus of driving automation has primarily been passenger vehicles and many of the commercial actors have announced the introduction of high-level driving automation features in the near future [33, 95, 97]. However, although it has attracted less attention, the development of driving automation for heavy vehicles is also underway. Nevertheless, the primary motivation for introducing driving automation features is not necessarily shared by passenger vehicles and heavy trucks. For passenger cars, the main motivations

are traffic safety and more free time for the driver. For heavy trucks, however, the main motivations are business operation and traffic safety concerns.

Returning to the above discussion on differences in manoeuvring characteristics between passenger cars and articulated heavy vehicles, it is probably necessary to take these characteristics into account to ensure safe and reliable driving automation features for articulated vehicles. Consideration of manoeuvring characteristics is foreseen in the creation of traffic situation predictions (tactical motion planning) and traffic situation manoeuvres (tactical decision-making). Moreover, it is anticipated that learning from the driver behaviour of professional truck drivers (who often have considerable driving experience) can be an efficient way to aid development of driving automation principles.

1.1 Objective

The objective of this work is to study traffic situation predictions and traffic situation manoeuvres that can be used for high-speed driving automation features of articulated heavy vehicles. High-speed driving refers to vehicle speeds in the range of 0-80 km/h. The primary application is long combination vehicles; often the most demanding in terms of lateral stability. Due to manoeuvring characteristics of these vehicles, traffic situation predictions are likely to incorporate motion constraints. When considering the use of vehicle models to express motion constraints, the models need to be quantified in respect of their level of complexity. This will guarantee reliable and computationally efficient algorithms. Furthermore, traffic situation manoeuvres are strongly linked with driving behaviour and are important in terms of the overall acceptance of the envisaged driving automation. The implementation of driving principles entails the specific design of continuous and discrete motion control for driving automation in a given operational design domain.

1.2 Prerequisites

The work presented in this thesis assumes that the envisaged reference architecture for vehicle motion functionality has been used (developed at Volvo Global Trucks Technology (VGTT)). Methods and strategies developed for traffic situation predictions and traffic situation manoeuvres are given under the following assumptions:

A1 the methods and strategies should include vehicle combinations of up to three articulation joints. The vehicle configuration is known to the vehicle control, in terms of geometry and payload parameters.

A2 the methods and strategies assume the existence of vehicle environment sensing functionalities. This means a vehicle sensor system that measures the subject vehicle's position on the road as well as such things as the relative positions and velocities of surrounding traffic and objects.

A3 the methods and strategies assume the existence of vehicle motion management functionalities. This means a low-level control system that handles coordination of propulsion, braking, and steering.

1.3 Limitations

This work is presented, subject to following limitations:

L1 the primary application of this work is in long combination vehicles based on the modular concept. However, only the A-double combination has been used as an example.

L2 the methods and strategies developed for traffic situation predictions and traffic situation manoeuvres only consider one-way, multiple-lane roads such as highways.

L3 the methods and strategies developed for traffic situation predictions and traffic situation manoeuvres have not been verified using physical testing. Verification has been carried out using motion platform driving simulator experiments and desktop simulations.

L4 the methods and strategies developed for traffic situation predictions and traffic situation manoeuvres have not been adapted to the computing capacity of existing production vehicles.

L5 the main standard for functional safety of electrical automotive systems, ISO-26262, has not been considered.

1.4 Contributions

The scientific contributions of this work are:

C1 Formulation of traffic situation predictions by using models for subject vehicle, driver, road and surrounding traffic.

- C1a Formulation of a unique driver steering model for articulated vehicles.

C2 Traffic situation predictions used in multiple-lane, one-way road driving simulator experiments, including actuation requests for subject vehicle longitudinal and lateral control. The actuation requests are based on driver modelling and model predictive control.

C3 Traffic situation manoeuvres including formulation of decision making for driving automation including maintain-lane, lane changes and non-evasive abort manoeuvres in multiple-lane, one-way roads.

C4 Deriving driving principles for automation by using back-to-back comparison of manual and automated driving in simulator experiments. These derived driving principles are based on human driving behaviour by professional drivers to attain high levels of acceptance.

- C4a Initiation and execution of lane changes with surrounding traffic.
- C4b Managing mandatory road exits and lane changes in dense traffic.

1.5 Outline

Chapter 2 presents long combination vehicles, including typical road usage and manoeuvring characteristics. Chapter 3 illustrates goods transports and their connection to driving automation, as well as existing heavy truck-driving automation demonstrators. Chapter 4 illustrates general vehicle motion function components and presents the Volvo GTT vehicle motion functionality reference architecture. Chapter 5 presents the models of road, subject vehicle, driver and surrounding traffic, used to calculate traffic situation predictions. Chapter 6 presents traffic situation predictions, based on driver modelling and model predictive control. Chapter 7 gives traffic situation manoeuvres, including manoeuvre planning and manoeuvring decisions. Chapters 8 presents some concluding remarks, including scientific contributions, appended papers, industrialisation and future research directions.

2 Long combination vehicles

Long combination vehicles (LCVs) refer to modular road vehicles that are longer and possibly heavier than the currently permitted dimensions in Sweden. Section 2.1 presents a short background on combination vehicles. Section 2.2 gives the typical road usage for LCVs and Section 2.3 presents important manoeuvring characteristics.

2.1 Background

For heavy goods vehicles within the European Union, the maximum authorised weight and length dimensions are regulated by the Council directive 96/53/EC. This directive states that the maximum lengths of tractor semi-trailer combinations and rigid truck-trailer combinations are 16.5 m and 18.75 m, respectively, see Fig. 2.1. The maximum weight is restricted to 40 t, with the exception of domestic transports (including 40-foot ISO containers) in a combined transport operation. For these, the maximum weight is 44 t. As exceptions from the regulation, the maximum lengths in Sweden and Finland are 24 m and 22 m, respectively.

Aditionally, the directive gives member states the option of using longer and heavier vehicle combinations within their territories, provided that the combinations are based on the European modular system (EMS) [5], or do not significantly affect international competition in the transport sector. In Sweden, longer and heavier vehicle combinations based on the EMS concept were introduced in 1997. There are three permitted types of combinations, each carrying one short module and one long module, giving a total vehicle length of 25.25 m and a maximum permitted weight of 60 t, see Fig. 2.2a.

The term long combination vehicles refers to modular road vehicles that are longer and possibly heavier than those permitted in Sweden, i.e. longer than 25.25 m and possibly heavier than 60 t. The primary motives for LCV utilisation are increased transport productivity and reduced environmental impact. It is predicted that LCVs may be

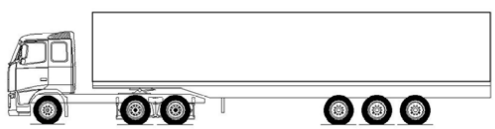

(a) *Tractor semi-trailer combination. Reproduced from [5].*

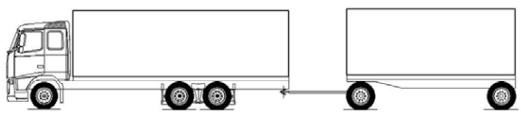

(b) *Rigid truck-trailer combination. Reproduced from [5].*

Figure 2.1: *Examples of existing vehicle combinations in Europe.*

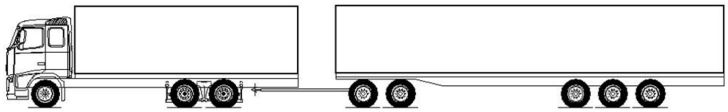

(a) *Existing EMS combination in Sweden. Reproduced from [5].*

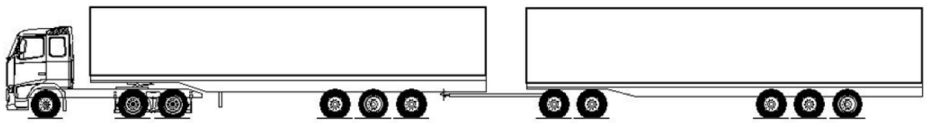

(b) *A-double combination. Reproduced from [5].*

Figure 2.2: *Examples of modular vehicle combinations.*

one way to meet future environmental targets and emission legislation on transported goods. The predicted LCVs typically range between 27-34 m in length and have at least two articulated joints. In a pilot project [68] conducted in Sweden, the productivity and energy consumption of a 90 t vehicle combination of 30 m in length was improved by approximately 20 percent. This was when compared to a conventional Nordic 60 t combination of 25.25 m in length.

The main concerns regarding a general introduction of LCVs relate to road infrastructure and traffic safety. An introduction of LCVs in Sweden would most likely require additions to the existing classification of road types. Such an initiative has been ongoing in Sweden since 2016 [115]. There are also several studies concerning the traffic safety impact of longer and heavier vehicles such as LCVs [3, 7, 60]. However, it is not clear whether and how traffic safety would be affected by an introduction of LCVs.

2.2 Typical road usage

In Sweden, the public road network is currently divided into three buoyancy classes: BK1, BK2 and BK3. As mentioned in Section 2.1, an initiative for introducing a fourth buoyancy class is ongoing [115]. These classes restrict maximum gross combinations of weight and static load per axle and axle groups and minimise the distance between axle groups. BK1 roads, on which the highest weights are permitted, cover about 95 % of the public road network. Today's heavy goods vehicles are allowed on all BK1 roads. However, LCVs are not expected to be driven on all existing BK1 roads and a further specification of the road weight classes in some form is envisaged and proposed [117] as part of a general introduction of LCVs. The intention is to allow modular LCVs mainly on roads with the highest weight class. Before driving on other roads, they can be decoupled into shorter conventional combinations. For example, the A-double combination, which

consists of a tractor unit, semi-trailer, dolly-converter and a second semi-trailer, can be converted to a standard tractor semi-trailer when approaching city areas.

When determining the road usage in a general LCV introduction, other road infrastructure limitations besides weight restrictions (such as oncoming traffic and types of intersection) may need to be taken into consideration. One traffic situation that has been specifically studied is overtaking situations in oncoming traffic [3]. Even though no significant increased accident risk associated with overtaking was found, this thesis considers one-way, multiple lane roads to be the primary application for LCVs.

2.3 Manoeuvring characteristics of articulated heavy vehicles

Performance-based standards are a basis for regulating articulated heavy vehicles incorporating specific performance criteria with quantified required level of performance [59]. One example of performance-based characteristics for the longitudinal and lateral directions have been defined in [103]. The characteristics for longitudinal direction are: startability, gradeability, acceleration capability, stopping distance, and down-grade holding capability. The characteristics for lateral direction are: rearward amplification (RA), swept path width (SPW), high-speed transient off-tracking (HSTO), high-speed steady-state off-tracking (HSSO), yaw damping coefficient (YDC), straight line off-tracking (SLO), lateral clearance time (LCT), steady-state rollover threshold (SRT), and deceleration capability in a turn. The most important lateral characteristics for high-speed manoeuvring are RA, HSTO, HSSO and YDC, which are described as follows:

- RA is the relationship between the maximum motion of the first and last vehicle units during a specified steering manoeuvre [51] and vehicle speed. RA is usually given in the metrics lateral acceleration gain or yaw velocity gain. It expresses the increased risk of a last unit roll-over or swing-out.

- The off-tracking characteristics, HSTO and HSSO, both describe the lateral deviation between the path of the front axle and the path of the most severely off-tracking axle of the last unit. Examples of HSTO and HSSO are given in Figures 2.3 and 2.4. These measures express the additional space needed for the last unit in a specific steering manoeuvre and vehicle speed.

- The YDC is the damping ratio of the least damped articulation joint's angle during free-yaw oscillations of the vehicle combination, after a specific steering manoeuvre and vehicle speed. A longer decay time might result in higher driver workload and increased risk of the safety of other road users.

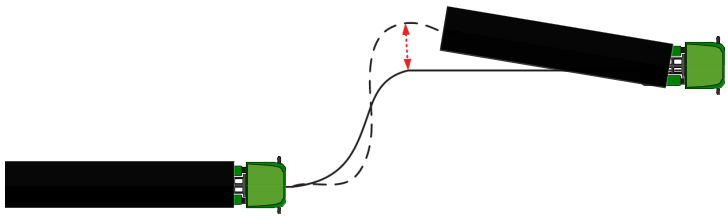

Figure 2.3: *Lane-change manoeuvre illustrating HSTO, RA and YDC. Reproduced from [103].*

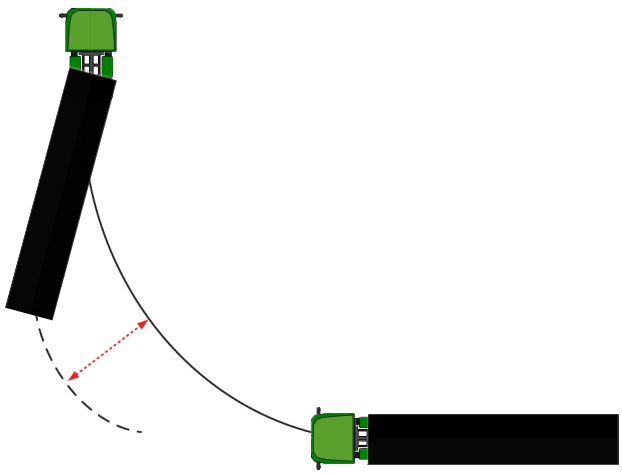

Figure 2.4: *Steady-state manoeuvre illustrating HSSO. Reproduced from [103].*

3 Goods transports and driving automation

Somewhat simplified, goods transport is the movement of goods from location A to location B. This is a task that seldom or never adds value to the goods. The existence of goods transport is due to the location of raw materials or production operation rarely corresponding to the location of demand for goods. In general terms, goods transports include elements such as infrastructure, vehicle and business operation. Moreover, goods transports are divided into different transport modes such as road, rail, air, water, pipelines, and so on. Section 3.1 illustrates goods transports and their connection to driving automation. Section 3.2 presents existing standards for driving automation for motor vehicles on public roads. Section 3.3 presents existing heavy truck-driving automation demonstrators.

3.1 Goods transports

The nature of goods transport has given rise to a strong business operation focus, which has historically contributed to continuously improved transport solutions. Typically, such solutions are related to logistics planning, vehicle, infrastructure, and automation. In the case of in-house logistics, automated transport applications (vehicle without a driver) were carried out in the 1950s [32]. The first so-called automated guided vehicles (AGVs) were used in production plants and warehouses. In early systems, the navigation was implemented using electrical conductors embedded in the floors. Today's systems, entails free navigation using laser scanners and cameras. Regarding out-door private property logistics, there are several examples of AGVs being used to improve productivity. At a container terminal in Germany, battery-operated AGVs move containers between ship and yard [46]. Automated trucks are also used at one of the world's largest iron-ore mines in Australia [61].

By using the existing **public road infrastructure**, heavy truck goods transports assist other modes of transport to improve overall transport accessibility. Considering both domestic and international goods transports in Sweden 2014, goods transported by heavy trucks constituted approximately 65% of the total goods transported [107], see Fig. 3.1. Also notable is that only 8% of the domestic transports involving heavy trucks were distances greater than 300 km. Typically, other transport modes are more cost-effective for longer distances.

Road transports, including heavy trucks, carry several types of commodities. Common goods in Sweden are products from the mining industries, from the agricultural and forestry industries and piece-goods transports [107]. As a first example to illustrate typical heavy truck transports, consider the timber transport [34], as shown in Fig. 3.2. In this example, the transport takes place between the logging location and a pulp production plant. The vehicle combination has a total length of 24 m and a maximum weight of 60 t. The vehicle combination consists of a 3-axle rigid vehicle and a 4-axle trailer. The total transport consists of approximately 61 km of driving. Out of these 3 km are on forest road, 17 km are on poorly maintained roads and 41 km are on well-maintained roads. The time distribution for a typical transport mission is: 40% driving with load, 36% driving

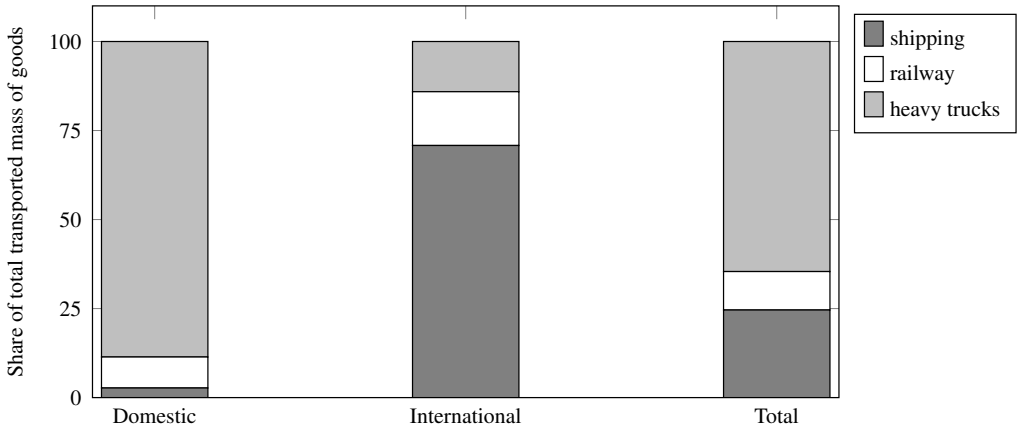

Figure 3.1: *Proportion of transported mass of goods in Sweden 2014. Based on [107].*

without load, 15% loading and 9% unloading.

As a second example of typical heavy truck road transports, consider a container transport included in a so-called intermodal transport, see Fig. 3.2. Here, the transportation of goods is made using two different modes (road and sea) and the sealed container is lifted and replaced when changing modes. The benefits of intermodal transports are standardised load carriers as well as lower environmental impact and improved traffic safety, as compared with corresponding direct road transports [78]. The disadvantages include the limited number of goods transfer terminals, high terminal investment costs and low usage of volume and/or weight for the load carriers [78]. In the example shown [125], the transport takes place out between the harbour and an industrial area. Typically, one driver carries out two trips per day. One trip involves driving back and forth from the harbour. One trip consists of approximately 128 km driving on well-maintained roads. The vehicle combination has a length of 16.5 m and a maximum weight of 40 t. The

Figure 3.2: *Illustration of two different road transport applications of heavy trucks. Theses applications include different vehicle combinations driven on different types of roads.*

combination consists of a 3-axle tractor vehicle and a 3-axle semi-trailer. The time distribution for one transport is: 24% driving with load, 24% driving without load, 33% waiting time at harbour, 5% loading, 5% unloading and 9% resting time.

Returning to the discussion on business operation focus in goods transports, a few things can be noted based on the heavy truck road transport examples given above. Firstly, logistics planning of such things as number of vehicle units, number of drivers, number of trips per day, potential goods on the return trip, resting times and so on is essential. Secondly, the vehicle specification needs to be as optimised as possible for the given transport mission. Consideration must be given to road condition, topography, curve density and the like, cf [26]. Finally, the transport mission often includes activities other than driving such as paper work (for Customs), loading and securing the goods, and unloading. Some of these are carried out by the driver. The management of these factors together contributes to the success of the business operation.

Considering the recent focus in industry and academia on driving automation for road vehicles, it is essential to clarify similarities and differences between passenger and goods transports to understand the potential benefits for each category. Driving automation for passenger cars is mainly motivated by concerns of mobility, traffic safety, and freeing up time for the driver. In most cases, this requires a high level of automation; to such degree that the driver is not expected to be the fall-back solution in a sudden critical event. For heavy truck goods transports, however, driving automation is mainly fuelled by a business operation focus and traffic safety concerns. Although traffic safety is a shared motivation for passenger vehicles and heavy goods transports, consideration must be given to the types of accidents and associated factors. These are necessarily not the same for heavy trucks and passenger cars [96]. For example, a the driver of a heavy truck might need assistance in reducing speed while negotiating a turn to avoid roll-over accidents, while passenger car accidents are often associated with some form of distraction [96].

Table 3.1: Levels of driving automation as proposed by SAE J3016 [104], BASt [39], NHTSA [82].

Automation level	0	1	2	3	4	5
SAE	No driving automation	Driver assistance	Partial driving automation	Conditional driving automation	High driving automation	Full driving automation
BASt	Driver only	Assisted	Partial automation	High automation	Full automation	-
NHTSA	No automation	Function specific automation	Combined function automation	Limited self-driving automation	Full self-driving automation	-

3.2 Driving automation on public roads

Standards for describing levels of driving automation for motor vehicles on public roads have been proposed by the organisations SAE [104], BASt [39] and NHTSA [82], see summary in Table 3.1. Perhaps the most common is the standard from SAE which consists of six levels. Essential to this standard are respective roles of the human driver and the driving automation system in relation to each other. Moreover, to accurately describing a driving automation system feature such as automated parking, it is necessary to identify both the level of driving automation and its operational design domain (ODD). ODD covers the specific conditions in which a given driving automation system is designed to function; for example, a geographically-defined area or vehicle speed range. Furthermore, the dynamic driving task (DDT) includes all real-time operational and tactical functions needed to operate a vehicle in traffic. Strategic driving tasks, such as trip scheduling and selection of destinations and waypoints are excluded. In the SAE terminology, *driving automation system* is a generic term referring to any level 1-5 system, whereas an automated driving system (ADS) is used to describe a level 3-5 system. Moreover, an ADS-dedicated vehicle (ADS-DV) is a vehicle designed to operate exclusively by a level 4 or 5 ADS for all trips.

In a level 1 system (driver assistance), the driving automation system carries out part of the DDT by executing either longitudinal or lateral motion control. The driver carries out the remainder of the DDT, engages and disengages the system and supervises and intervenes as necessary, to ensure safe operation. In a level 2 system (partial driving automation), the role distribution between the human driver and the system is the same as in a level 1 system, with the exception that the driving automation system carries out both longitudinal and lateral motion control. In a level 3 system (conditional driving automation), the driving automation system (while engaged), performs the entire DDT, determines whether ODD limits are about to be exceeded, determines whether there is a relevant system failure, disengages an appropriate time after failure (or immediately in the case of driver request). While ADS is engaged, the driver serves as DDT fall-back in case of system failure and determines how to achieve a minimal risk condition. In a level 4 system (high driving automation), the ADS (when engaged) carries out the entire DDT, serves as DDT fall-back and transitions to a minimal risk condition in case of:

Figure 3.3: *Vehicle platoon from the European Truck Platooning Challenge 2016. Reproduced from [29].*

system failure, a user not responding to a requested to intervene, or a user request for the system to implement a minimal risk condition. Moreover, the ADS only disengages after it achieves a minimal risk condition or a driver is carrying out the DDT. The driver (while ADS is engaged) may serve as DDT fall-back following a request to intervene, may request that ADS be disengaged and may become the driver after a requested disengagement. In a level 5 system (full driving automation), the role distribution between the human driver and the system are the same as in a level 4 system, with the exception that the ADS can operate the vehicle under all driver manageable road conditions (unlimited ODD).

The SAE standard for driving automation 2016 [104] has been updated since 2014 [105], and further updates of the standard are expected.

3.3 Driving automation demonstrators for heavy trucks

Demonstrators involving vehicle platooning are perhaps the most common example of heavy truck applications including driving automation features equal to, or higher than, SAE level 2. In the concept of vehicle platooning, a collection of vehicles travels together in a coordinated formation. By operating the vehicles at short inter-vehicular distances, the overall aerodynamic drag (and thus the fuel consumption) can be reduced.

In the U.S., the California PATH programme has shown the technical feasibility of driving two trucks at an inter-vehicular distance of $3-10\,\mathrm{m}$ at vehicle speeds $80-90\,\mathrm{km/h}$. The experiments have shown fuel consumption savings in the range of 5% for the lead truck and 10% to 15% for the following truck [19, 110].

In Europe, the CHAUFFEUR project (lead by DaimlerChrysler) carried out platooning using two heavy-duty tractor semi-trailer combinations [36]. In the subsequent project CHAUFFEUR 2, longitudinal and lateral control was implemented using the sensors available in series production vehicles [37]. The German KONVOI project (2005-2009), studied the impact (on driver acceptance, traffic flow and environment) and the legal and economic implications of platoons [49]. In the European project SARTRE, the lead vehicle of the platoon was a manually driven heavy vehicle, with the following vehicles

under automated longitudinal and lateral control. A platoon comprising five vehicles was demonstrated on public roads near Barcelona, Spain in 2012 [13, 14].

In Japan, the national project Energy ITS [121], started in 2008, included platooning in which three fully automated trucks were tested under highway conditions. Measurements showed fuel consumption savings of about 14%.

More recently, the COMPANION project [21] led by Scania, aimed to contribute to future standardisation and policy development for European transportation. In the European Truck Platooning Challenge 2016 [29] launched by the Netherlands, six truck brands drove semi-automated truck platoons on public roads from several European cities to the Netherlands. The initiative targeted a joint effort between authorities and industry.

Aside from vehicle platooning there is a small number of other examples of single heavy truck driving automation demonstrators. In 2015, the Freightliner Inspiration Truck [35] became the first commercial vehicle equipped with level 3 driving automation (NHTSA) [82] to operate on an open public highway in the U.S. In Europe, Daimler [22] has demonstrated driving level 2 and 3 automation (BASt) [39].

4 Vehicle motion functionality architecture

A motion functionality architecture describe how functions connected to the vehicle motion are divided and how they relate to each other. Section 4.1 gives a brief background and illustrates general vehicle motion function components for driving automation. Section 4.2 presents the Volvo GTT vehicle motion functionality reference architecture.

4.1 Background

A simplified interpretation of the concept *system architecture*[1] is that it represents the construction plan of the system. Typical mechanical architectures for vehicles includes frame/body dimensions, wheel sizes and so on. Typical electrical architectures include hardware architecture, software architecture and network architecture. An architecture enables dismantling and decoupling into smaller building components. It facilitates reuse, introduction of new components and parallelisation of the development process. In accordance with the concept of system architecture, a motion functionality architecture is a way to describe how functions connected to the vehicle motion are divided and how they relate to each other. A motion functionality architecture does not include the actual technical implementation in terms of hardware and software.

One example of functionality for high-level driving automation, based on [9], is given in Fig. 4.1. The main components are perception, decision and control and vehicle platform manipulation. Firstly, perception refers to the functions concerned with interpretation of data collected by vehicle sensors. The subcomponents sensing and sensor fusion include functions that sense physical variables of the surrounding environment and the subject vehicle, as well as combining the information from multiple sensors. Localisation functions determine the position of the subject vehicle (typically using GPS and inertial sensors) with respect to a global map. Semantic understanding functions and the world model are

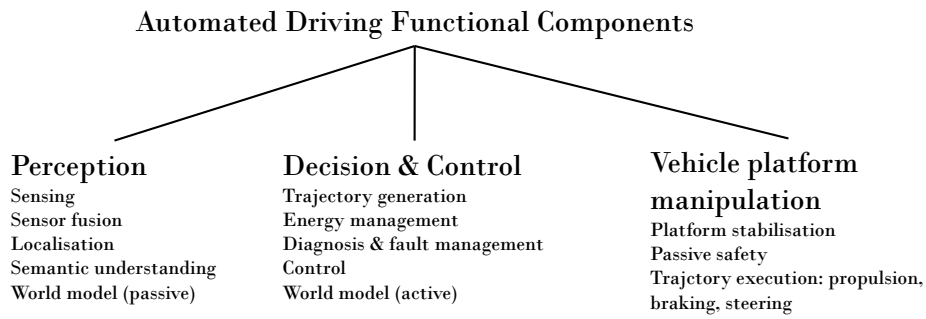

Figure 4.1: *Typical function components for high-level driving automation. Based on [9]*

[1] According to [52], architecture is "fundamental concepts or properties of a system in its environment embodied in its elements, relationships, and in the principles of its design and evolution"

responsible for interpretation of what has been detected, such as representing drivable areas and storing physical variables of the surrounding environment.

Secondly, decision and control refers to functions concerning the vehicle behaviour in context of the vehicle's environment. The subcomponents are trajectory generation, energy management, diagnosis and fault management, control and world model. A function related to trajectory generation calculates feasible trajectories (typically position, orientation and velocity of the subject vehicle), representing the motion given a specific actuation. The control functions are used for instant response to unforeseen events from the environment, such as automated emergency braking. These functions complement, or are redundant to the former trajectory generation functions. World model refers to functions that can predict the environment's evolution when given a sequence of inputs.

Finally, vehicle platform manipulation means functions directly related to the motion of the subject vehicle. Its subcomponents are vehicle stability functions, passive safety and trajectory execution. The stability functions are related to anti-lock braking, electronic stability programs and so on. Functions related to trajectory execution are responsible for coordinating the use of the available actuators, given the trajectory generated by decision and control. A function architecture for the motion of an automated vehicle can be achieved by distributing the components described above, cf [9].

4.2 Volvo GTT vehicle motion functionality reference architecture

In the presented work, the Volvo GTT vehicle motion functionality reference architecture (VeMFRA) [73] has been used as a reference for dismantling and structuring functionality. One of the cornerstones of VeMFRA is the layers used to organise sets of functionalities. The layer order and functions included in each layer are organised based on their temporal and spatial extension. Upper layers (longer extension) are dependent on the existence of lower layers. Lower layers provide aggregated capabilities to the next upper layer. Moreover, VeMFRA defines generic elements for hierarchical structuring. The main elements are ordered from top to bottom: functionality domain (FD) and functionality area (FA). The main functionality domains are: FD-Transport mission management (FD-TMM), FD-Route management (FD-RM), FD-Route situation management (FD-RSiM), FD-Traffic situation management (FD-TSM), FD-Vehicle motion management (FD-VMM), FD-Motion support device management (FD-MSDM), FD-Vehicle environment management (FD-VEM) and FD-Human machine interface (FD-HMI), see Fig. 4.2.

The **FD-Transport mission management** includes functions related to fleet management and route assignment. As an example, functions in this layer can provide weekly or daily plans for each vehicle managed by a fleet owner. The functions aim to optimise vehicle usage and provide information for fleet optimisation with respect to energy consumption and cost, see Fig 4.3. Functions related to **FD-Route management** handles the vehicle performance for an actual designated route i.e. a delivery from point A to point B. Typically the range for this FD is within the spatial horizon of 100 km. One example is route planning as provided by, say, Google. The **FD-Route situation management** includes functionalities related to road segments, typically $1-5$ km, of a planned route.

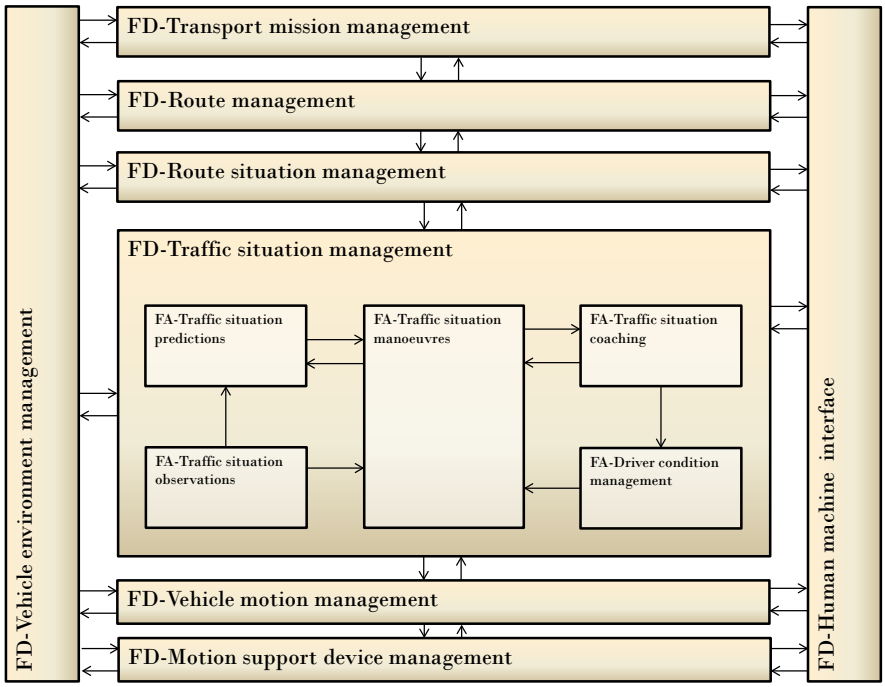

Figure 4.2: *Overview of envisaged vehicle motion reference architecture for Volvo GTT. Arrows represent data flow.*

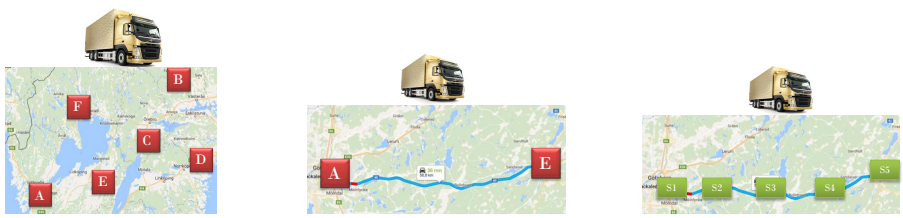

(a) *FD-TMM* (b) *FD-RM* (c) *FD-RSiM*

Figure 4.3: *Illustration of the spatial resolution for the function domains Traffic mission management (FD-TMM), Route management (FD-RM) and Route situation management (FD-RSiM).*

One example of an existing function within this domain is the Volvo I-See function [1] used for fuel-saving. Another example is functionalities related to planning road junctions and exists during highway driving. If comparing VeMFRA with the driving assignment carried out by a human driver, the layers FD-RM and FD-RSiM can be associated with the *strategic* level of the driving as defined by Michon [79].

FD-Traffic situation management, cf control and decision in Section 4.1, is related

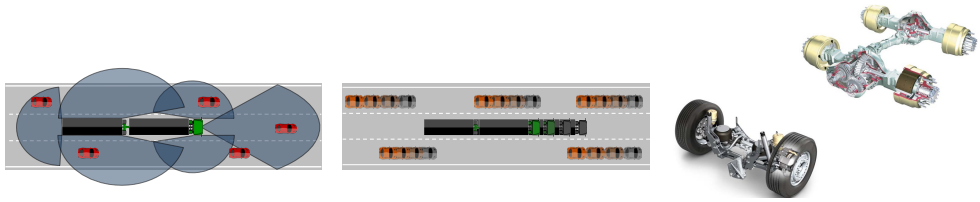

(a) *FD-VEM* (b) *FD-TSM* (c) *FD-VMM*

Figure 4.4: *Illustration of the functional domains Vehicle environment management (FD-VEM), Traffic situation management (FD-TSM) and Vehicle Motion management (FD-VMM).*

to functions with a temporal horizon of up to 10 s. The main attributes include: continuous control and decision-making with respect to the subject vehicle behaviour in an observed traffic situation, see Fig. 4.4. If comparing with the driving task for a human driver, FD-TSM can be associated with *tactical* [79] manoeuvring including such things as gap acceptance and overtaking. When driving on public roads, the functions in FD-TSM often include consideration of obstacles and surrounding traffic. This, in combination with the subject vehicle stability limits, results in safety-critical functionalities. One example of an existing function in FD-TSM is the adaptive cruise control [28]. The **FA-Traffic situation observations** (FA-TSO) include functions concerning the creation of instant observation of the traffic situation around the subject vehicle. Typically, observed information includes number of lanes, lane widths, subject vehicle position in lane and motion states of subject and surrounding vehicles. This is similar to the passive world model in perception, described in Section 4.1 above. **FA-Traffic situation predictions** (FA-TSP) relates to the functions used to predict how the observed traffic situation will evolve in the future. Throughout this work, the term *traffic situation predictions* (TSPs) refers to the complete set of functions included in FA-TSP. The objective of FA-TSP is to generate feasible manoeuvres for the subject vehicle, such that the vehicle motion fulfils requirements on such things as safety, efficiency and driving comfort. Given the objective above, typical FA-TSP functionalities include predictions of the subject vehicle and surrounding traffic. This is similar to the active world model in decision and control, described above in Section 4.1. The **FA-Traffic situation manoeuvres** (FA-TSM) can be described as decision-making regarding driving principles and control on a tactical level. Candidate actuation requests for a set of traffic manoeuvres can be generated by FA-TSP. However, FA-TSP does not necessarily determine why nor when a specific manoeuvre is executed. The manoeuvre planning and manoeuvre decision are made instead by the functionalities associated with FA-TSM to achieve tactical as well as strategical goals. Throughout this work, the term *traffic situation manoeuvres* (TSMs) refers to the complete set of functions included in FA-TSM.

FD-Vehicle motion management (compare with vehicle platform manipulation in Section 4.1) encapsulates knowledge of available actuations and coordinates the use of the actuators within the vehicle. Typically, these functions are related to a temporal horizon of up to 1 s. If comparing with the driving task for a human driver [79], FD-VMM

can be associated with *control* including automatic action patterns. Functions related to **FD-Motion support device management** handle the organisation of monitoring, measurement and control of devices, typically actuators and sensors. **FD-Vehicle environment management**, see perception in Section 4.1, is related to functions that represent the external environment of the vehicle operation. Examples of functions in FD-VEM are lane and road sign detection. Finally, functions in **FD-Human machine interface** (FD-HMI) include detection and response to drivers' intentions. One example of a function in this layer is activation and deactivation of a driving support system.

5 Modelling for traffic situation predictions

In the traffic situation predictions, models of the **road**, **subject vehicle**, **driver** and **surrounding traffic** (see Fig. 5.1) are used to calculate candidate actuation requests for steering and acceleration. Moreover, these models are used to evaluate the actuation feasibility for a given prediction horizon. The individual models are described in Sections 5.1-5.4.

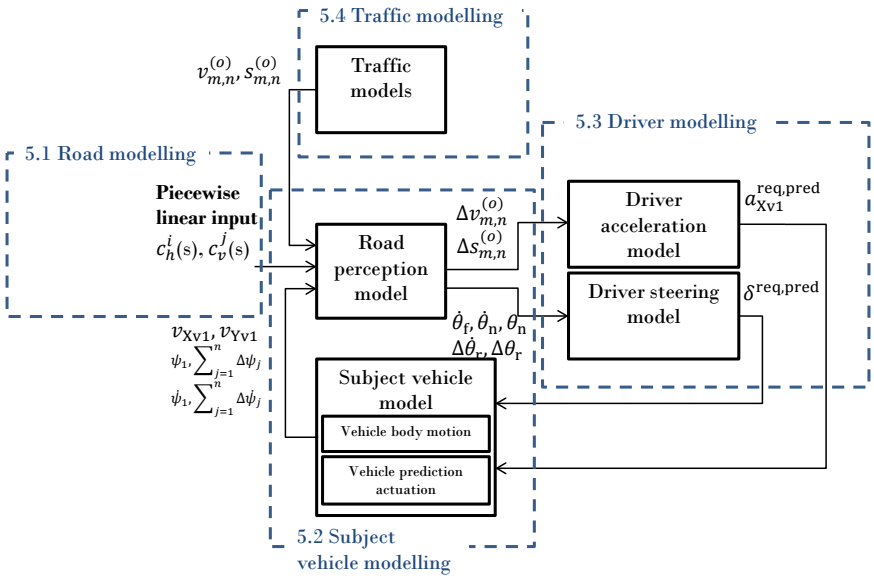

Figure 5.1: *Illustration of combined road, subject vehicle, driver and surrounding traffic model. Arrows represent data flow.*

5.1 Road modelling

5.1.1 Background

The design of public roads is regulated by national authorities; in Sweden this is the Swedish Transport Administration. The design elements in Sweden [116] for the horizontal road geometry are: straight lines, circular arcs and clothoids. A clothoid is a spiral whose curvature $c(s)$ is a linear function of its length [77].

The recommended minimum radius in the horizontal plane for roads with a reference speed of 110 km/h is 900 m in the case of new construction and 800 m in case of reconstruction [116]. The corresponding minimum radii for a road with a reference speed of 60 km/h are 140 m and 100 m [116]. The horizontal curvature of the roads used in the simulator experiments described in [90, 94] and Papers D and E are illustrated in the top row of Fig. 5.2.

The design elements in Sweden [116] for the vertical road geometry are: straight lines, circular arcs and parabolae. The recommended minimum concave radii for roads with a reference speed of 110 km/h are in the interval of 2000 m to 9000 m. The corresponding minimum radii for roads with a reference speed of 60 km/h are 600 m to 1750 m. The vertical curvature of the roads used in the simulator experiments described in [90, 94] and Papers D and E are illustrated in the bottom row of Fig. 5.2.

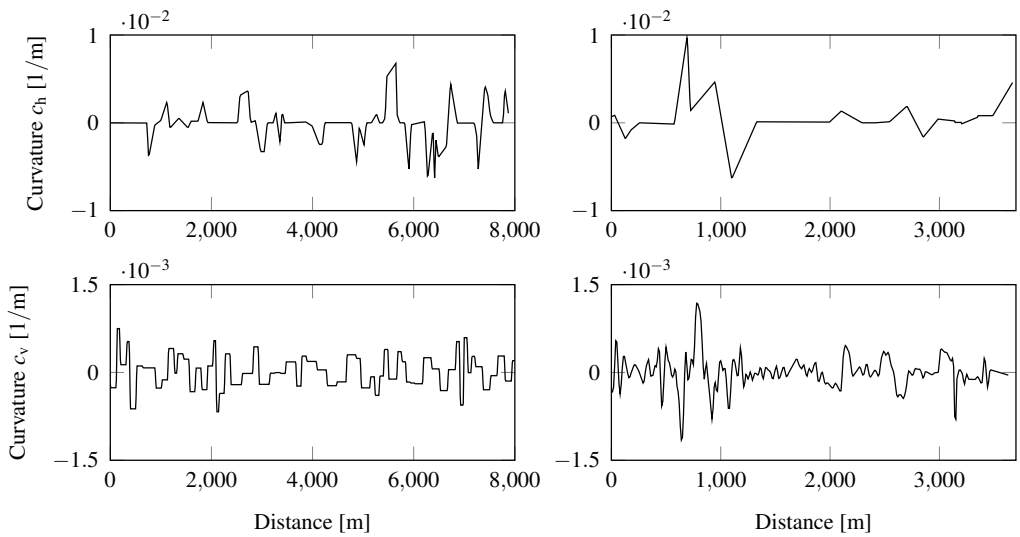

Figure 5.2: *The horizontal (top row) and vertical (bottom row) curvature of the roads used in the simulator experiments described in [90, 94] (left-hand panel), and Papers D and E (right-hand panel).*

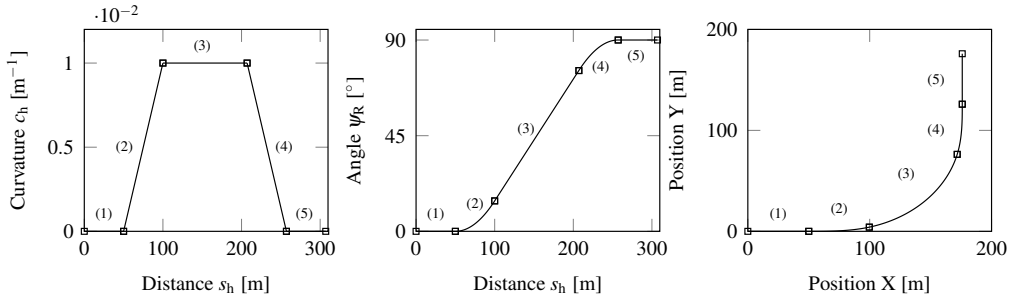

Figure 5.3: *Illustration of a road model in the horizontal plane, consisting of five clothoid spline segments. The start and end of each segment is marked with a black square. The left and middle panels show the curvature c_h and the road angle ψ_R for each segment as a function of the distance, s_h. The right panel shows the position given a fixed reference frame OXY.*

5.1.2 Design

In the proposed road model, the projection of the road in the horizontal plane is represented by a curve denoting a **clothoid spline** as circles whilst straight lines may be considered as limiting forms of clothoids. The curve representing the vertical road geometry is a clothoid spline, expressed using the total distance, s. The proposed road model consists of n clothoid segments for the horizontal description and m clothoid segments for the vertical description. The reason for using a different number of segments for the horizontal and vertical descriptions is due to the different minimum radii, see Section 5.1.1. Fig. 5.3 illustrates a road section consisting of five clothoid segments. The horizontal and vertical curvatures $c_h(s_\mathrm{h})$ and $c_\mathrm{v}(s)$ of segment i and j are described as

$$c_\mathrm{h}^{(i)}(s_\mathrm{h}) = c_{\mathrm{h},0}^{(i)} + c_{\mathrm{h},1}^{(i)} \cdot s_\mathrm{h} \tag{5.1}$$

$$c_\mathrm{v}^{(j)}(s) = c_{\mathrm{v},0}^{(j)} + c_{\mathrm{v},1}^{(j)} \cdot s \tag{5.2}$$

where s_h is the arc position of the horizontal projection, s is the total arc position, $c_{\mathrm{h},0}^{(i)}$ and $c_{\mathrm{v},0}^{(j)}$ are the initial curvatures and $c_{\mathrm{h},1}^{(i)}$ and $c_{\mathrm{v},1}^{(j)}$ are the curvature rates. It is assumed that the segments are connected to each other such that G^2 continuity is ensured, i.e. the position, heading and curvature of two segments are equal at their joints.

Furthermore, the curvatures $c_\mathrm{h}^{(i)}$ and $c_\mathrm{v}^{(j)}$ of each segments i and j are defined as

$$c_\mathrm{h}^{(i)} = \frac{\mathrm{d}\psi_\mathrm{R}^{(i)}}{\mathrm{d}s_\mathrm{h}} \tag{5.3}$$

$$c_\mathrm{v}^{(j)} = \frac{\mathrm{d}\theta_\mathrm{R}^{(j)}}{\mathrm{d}s} \tag{5.4}$$

where $\psi_R^{(i)}$ is the angle between the road tangent vector and the X-axis, and $\theta_\mathrm{R}^{(j)}$ is the angle between the tangent vector and the s_h axle. Using the chain rule and (5.3)-(5.4),

the angular velocities $\dot{\psi}_{\mathrm{R}}^{(i)}$ and $\dot{\theta}_{\mathrm{R}}^{(i)}$ can be written as

$$\dot{\psi}_{\mathrm{R}}^{(i)} = c_h^{(i)} \cdot \dot{s}_{\mathrm{h}} \tag{5.5}$$

$$\dot{\theta}_{\mathrm{R}}^{(j)} = c_v^{(j)} \cdot \dot{s} \tag{5.6}$$

For the horizontal plane, the position of each segment of the road in a local coordinate frame is described as

$$x_l^{(i)}(s_{\mathrm{h}}) = x_0^{(i)} + \int \cos(\psi_{\mathrm{R}}^{(i)}(s_{\mathrm{h}}))\mathrm{d}s_{\mathrm{h}} \tag{5.7}$$

$$y_l^{(i)}(s_{\mathrm{h}}) = y_0^{(i)} + \int \sin(\psi_{\mathrm{R}}^{(i)}(s_{\mathrm{h}}))\mathrm{d}s_{\mathrm{h}} \tag{5.8}$$

where $x_0^{(i)}$ and $y_0^{(i)}$ are initial values and

$$\psi_{\mathrm{R}}^{(i)}(s_{\mathrm{h}}) = c_{\mathrm{h},0}^{(i)} \cdot s_{\mathrm{h}} + \frac{c_{\mathrm{h},1}^{(i)}}{2} \cdot s_{\mathrm{h}}^2 \tag{5.9}$$

The integrals (5.7)-(5.8), include the Fresnels integrals [77] and do not have a closed form solution. However, an approximate solution can be found using Taylor expansion.

5.2 Subject vehicle modelling

5.2.1 Background

Vehicle planar dynamics refer to the vehicle motion in a plane horizontal to the vehicle, with longitudinal, lateral and yaw degrees of freedom. A **vehicle model** is defined as the system of equations needed to describe the dynamics of a vehicle during acceleration, braking and/or cornering manoeuvres. The model is often expressed as a system of non-linear differential-algebraic equations (DAEs). These DAEs are based on kinematic and inertial properties of the vehicle, as well as constitutive relations between motion and force quantities. One example of a commonly used constitutive relation is a tyre model where the tyre force is related to the tyre velocity.

A vehicle model is used in the traffic situation predictions to calculate future predicted motion of the subject vehicle. Important motion characteristics, such as vehicle accelerations, velocities and positions, are used to verify the feasibility of the calculated candidate actuation requests. As mentioned in Section 2.3, highly important lateral motion characteristics for articulated heavy vehicles are connected to off-tracking and rearward amplification, see example in Fig. 5.4. Important criteria for a subject vehicle model used in the traffic situation predictions are:

i) the model can capture important motion characteristics in the operating speed range of the vehicle. In highway driving, the operating speed range is typically 0-80 km/h;

ii) the model can handle relevant driving scenarios. The driving scenarios considered in this work are typically related to maintain-lane manoeuvring, lane changes and prospective non-severe avoidance manoeuvres;

iii) the model is tunable in terms of physically interpretable parameters;

iv) the model is computationally efficient to allow real-time execution.

One way to approach the above criteria is to use a two-track-model, see illustration in Fig. 5.5. In a two-track model, each wheel is modelled separately and can accordingly exhibit varying cornering stiffness. Moreover, yaw moment produced by non-symmetrical

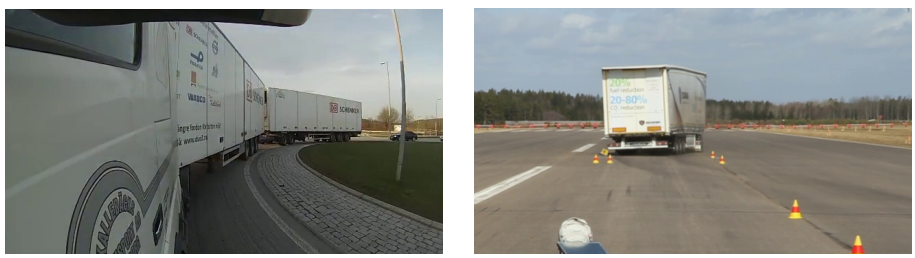

(a) *Off-tracking in low speed roundabout driving using an A-double combination.* (b) *Rearward amplification in a severe lane change manoeuvre.*

Figure 5.4: *Example of important motion characteristics for articulated heavy vehicles.*

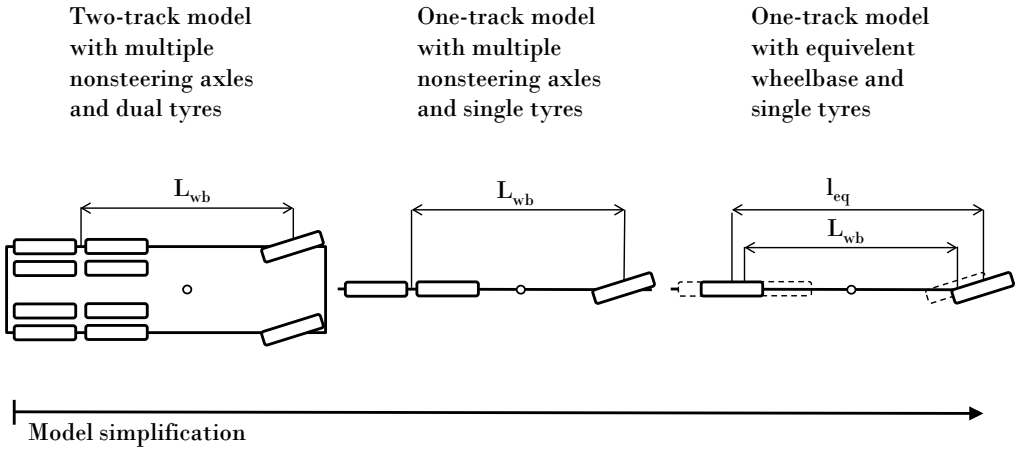

Figure 5.5: *Illustration of single-unit two-track model with multiple nonsteering axles and dual tyres (left), single-unit one-track model with multiple nonsteering axles and single tyres (middle) and single-unit one-track two axles model with equivalent wheelbase and single tyres (right).*

wheel torque interventions are inherently represented. However, the two-track model requires the actuator configuration to be on wheel level which generates a computationally demanding model with many states and multiple inputs. Instead, a **one-track model** [53] (also known as a single-track model or bicycle model) with simplified actuation requests of steering and longitudinal forces is considered. Here, the effects of all tyres on an axle are combined into one virtual tyre, see illustration in Fig. 5.5. Moreover, the concept of an equivalent wheel-base [129] can also be used, which means that groups of axles (such as a tandem or tridem) are collapsed into one axle, see illustration in Fig. 5.5. The motion degrees of freedom included in the model are the longitudinal, lateral, and yaw motion of each vehicle unit.

Furthermore, the general form of the one-track model can be simplified by introducing assumptions related to the vehicle driving conditions. A common simplification is linearisation, in which the physical assumptions are: constant longitudinal velocity, small steering and articulation angles, small side slip angles, and linear tyre constitution. A linear tyre constitution in this context means that the tyre force varies linearly with the lateral slip. In general, vehicle manoeuvring often involves a combination of steering and propulsion or braking. During such conditions, the lateral and longitudinal tyre forces deviate from the values derived under independent conditions. Introduction of longitudinal slip generally tends to reduce the lateral force at a given slip angle and, conversely, the application of a slip angle reduces the longitudinal force under a given propulsion or braking condition. This effect is often referred as combined slip. In addition to linearisation, manoeuvre-dependent assumptions are possible and commonly utilised. One example is steady-state conditions, which are mathematically represented by neglecting state derivatives.

5.2.2 Design

5.2.2.1 Vehicle body motion

The equivalent wheel-base of a multi-axle vehicle is the wheel-base of a two-axle vehicle, with steady-state turning behaviour equivalent to that of the multi-axle vehicle. The equivalent wheel-base is always greater than the actual wheelbase. Assuming linear lateral tyre forces, the equivalent wheelbase is calculated as

$$l_{\mathrm{eq}} = L_{\mathrm{wb}} \cdot \left(1 + \frac{T_{\mathrm{f}}}{L_{\mathrm{wb}}^2} \cdot \left(1 + \frac{\sum_m^M C_{\mathrm{Y}1m}}{C_{\mathrm{Y}11}}\right)\right) \tag{5.10}$$

where L_{wb} is the actual wheelbase, M is the number of rear axles and $C_{\mathrm{Y}11}$ is the cornering stiffness of the front axle. $C_{\mathrm{Y}1m}$ is the cornering stiffness of the m^{th} rear axle. The tandem factor T_{f} is calculated as

$$T_{\mathrm{f}} = \frac{\sum_{m=1}^M \Delta_m^2}{M} \tag{5.11}$$

where Δ_m is the longitudinal distance from the rear end of L_{wb} to the m^{th} rear axle.

In this work, **Lagrangian formalism** [17] is used to derive one-track models with equivalent wheelbase. The first step is to define a set of coordinates which describe the position and orientation of all parts of the system uniquely with respect to an inertial frame. Any set of coordinates having this property is called a set of *generalised coordinates*. The defined generalised coordinates are assumed to be free, i.e. the number of coordinates is equal to the number of degrees of freedom. Secondly, the kinetic and potential energies are written in terms of these coordinates and the force components of the forces acting on the system are computed along these coordinates. These forces are referred to as *generalised forces*. Finally, the substitution of these quantities in Lagrange's equations results in the final formulation. The main advantage of using the Lagrange formalism is that the coupling forces between the vehicle units are inherently represented and the numbers of equations are correspondingly fewer. This approach also has the advantage of requiring only the kinetic and potential energies of the system to be formulated and hence tends to be less prone to error than summing together the coupling forces. On the other hand, Newtonian formalism is more adapted for multi-domain modelling and modularisation. Modularisation can be efficient when modelling articulated vehicles, especially when combined with tools for symbolic equation manipulation [114].

The Lagrangian equations are defined as

$$\frac{d}{dt}\frac{\partial T}{\partial \dot{q}_i} - \frac{\partial T}{\partial q_i} + \frac{\partial V}{\partial q_i} = Q_i \tag{5.12}$$

where $i = 1, ..., N$ with N as the number of generalised coordinates. The generalised coordinates q_i are the dependent variables, T is the kinetic energy, V is the potential energy and Q_i are the generalised forces. Due to the fact that only planar motion is being considered, the potential energy is zero.

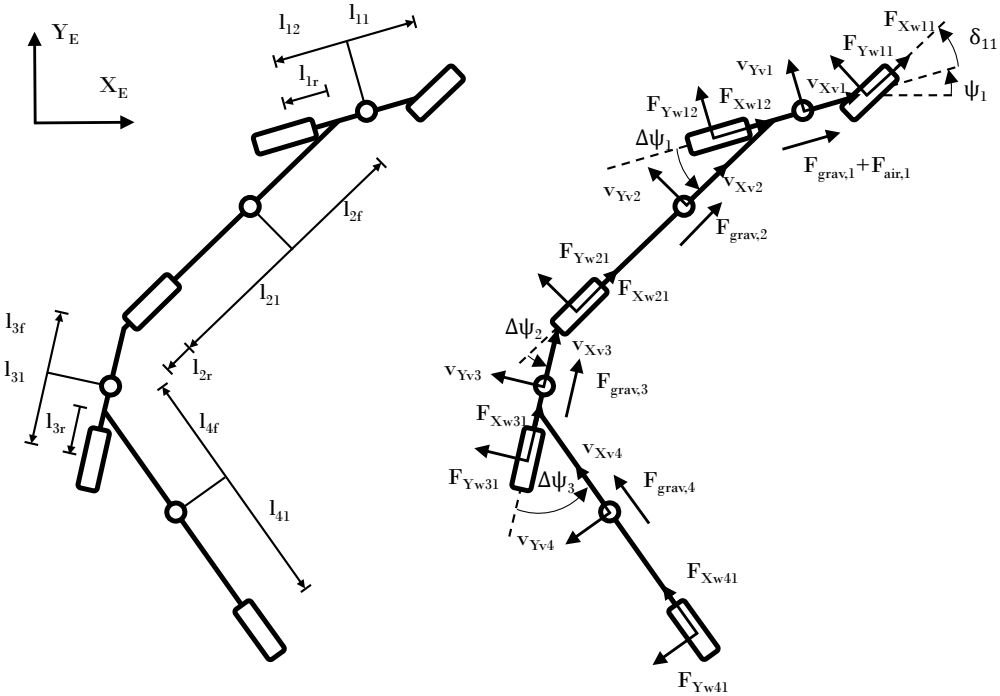

Figure 5.6: *One-track model of an A-double combination. The left panel illustrates the spatial parameters of the vehicle model and the right panel illustrates the included motion variables and forces. The spatial parameters are defined as positive if they are in front of the unit's CoG and negative if they are behind the CoG.*

For the A-double combination, the following set of generalised coordinates is chosen

$$\mathbf{q} = \left(\bar{X}_1,\ \bar{Y}_1,\ \psi_1,\ \Delta\psi_1,\ \Delta\psi_2,\ \Delta\psi_3\right) \tag{5.13}$$

where $\bar{X}_1$ and $\bar{Y}_1$ are the longitudinal and lateral position of the CoG for the first vehicle unit, expressed in an inertial coordinate frame. ψ_1 is the heading angle of the first vehicle unit and $\Delta\psi_1, \Delta\psi_2$ and $\Delta\psi_3$ are the articulation angles of the trailing vehicle units.

To improve the usability of the model, the velocities of the first vehicle unit are expressed relative to a body-fixed coordinate frame. However, the longitudinal and lateral velocities, v_{Xv1} and v_{Yv1} respectively, are not derivatives of generalised coordinates. However, they may be regarded as derivatives of quasi-coordinates and can be introduced into the Lagrange equations. To express the Lagrange equations using the quasi-coordinates, the approach presented in [98] can be followed.

The kinetic energy of the system is calculated as

$$T = \frac{1}{2} \cdot \left(\sum_{j=1}^{4} m_j \cdot |\mathbf{v}_j|^2 + J_{Zj} \cdot \dot{\psi}_j^2 \right) \tag{5.14}$$

where $\mathbf{v}_j$ and $\dot{\psi}_j$ are the translational and rotational velocities of unit j. The mass is m_j and J_{Zj} is the yaw moment of inertia of unit j. The translational velocity components in the CoG of the vehicle units are calculated using the corresponding position vectors as a starting point. The position vectors $\mathbf{r}_j$, are expressed relative to the CoG of the first vehicle unit as

$$\mathbf{r}_1 = \begin{pmatrix} \bar{X}_1, & \bar{Y}_1 \end{pmatrix} \begin{pmatrix} \mathbf{e}_{\mathrm{X_E}} \\ \mathbf{e}_{\mathrm{Y_E}} \end{pmatrix} \tag{5.15}$$

$$\mathbf{r}_2 = \mathbf{r}_1 + \begin{pmatrix} l_{12} - l_{1\mathrm{r}}, & 0 \end{pmatrix} \mathbf{R}_{\mathrm{v}1} \begin{pmatrix} \mathbf{e}_{\mathrm{X_E}} \\ \mathbf{e}_{\mathrm{Y_E}} \end{pmatrix} + \begin{pmatrix} l_{2\mathrm{f}}, & 0 \end{pmatrix} \mathbf{R}_{\mathrm{v}2} \begin{pmatrix} \mathbf{e}_{\mathrm{X_E}} \\ \mathbf{e}_{\mathrm{Y_E}} \end{pmatrix} \tag{5.16}$$

$$\mathbf{r}_3 = \mathbf{r}_2 + \begin{pmatrix} l_{21} + l_{2\mathrm{r}}, & 0 \end{pmatrix} \mathbf{R}_{\mathrm{v}2} \begin{pmatrix} \mathbf{e}_{\mathrm{X_E}} \\ \mathbf{e}_{\mathrm{Y_E}} \end{pmatrix} + \begin{pmatrix} l_{3\mathrm{f}}, & 0 \end{pmatrix} \mathbf{R}_{\mathrm{v}3} \begin{pmatrix} \mathbf{e}_{\mathrm{X_E}} \\ \mathbf{e}_{\mathrm{Y_E}} \end{pmatrix} \tag{5.17}$$

$$\mathbf{r}_4 = \mathbf{r}_3 + \begin{pmatrix} l_{31} - l_{3\mathrm{r}}, & 0 \end{pmatrix} \mathbf{R}_{\mathrm{v}3} \begin{pmatrix} \mathbf{e}_{\mathrm{X_E}} \\ \mathbf{e}_{\mathrm{Y_E}} \end{pmatrix} + \begin{pmatrix} l_{4\mathrm{f}}, & 0 \end{pmatrix} \mathbf{R}_{\mathrm{v}4} \begin{pmatrix} \mathbf{e}_{\mathrm{X_E}} \\ \mathbf{e}_{\mathrm{Y_E}} \end{pmatrix} \tag{5.18}$$

where $\mathbf{e}_{\mathrm{X_E}}$ and $\mathbf{e}_{\mathrm{Y_E}}$ are unit vectors of the inertial frame. $\mathbf{R}_{\mathrm{v}j}$ are rotation matrices in 2D Euclidean space, defined as

$$\mathbf{R}_{\mathrm{v}j} = \begin{pmatrix} \cos(\psi_{\mathrm{j}}) & \sin(\psi_{\mathrm{j}}) \\ -\sin(\psi_{\mathrm{j}}) & \cos(\psi_{\mathrm{j}}) \end{pmatrix} \qquad j = 1, ..., 4 \tag{5.19}$$

The position vectors are transformed between the body-fixed coordinate frames and the reference frame using

$$\begin{pmatrix} \mathbf{e}_{\mathrm{X}\mathrm{v}j} \\ \mathbf{e}_{\mathrm{Y}\mathrm{v}j} \end{pmatrix} = \mathbf{R}_{\mathrm{v}j} \begin{pmatrix} \mathbf{e}_{\mathrm{X_E}} \\ \mathbf{e}_{\mathrm{Y_E}} \end{pmatrix} \qquad j = 1, ..., 4 \tag{5.20}$$

where $\mathbf{e}_{\mathrm{X}\mathrm{v}j}$ and $\mathbf{e}_{\mathrm{Y}\mathrm{v}j}$ are body-fixed unit vectors. Starting from (5.15)-(5.18), the translational velocity vectors of the CoG of the vehicle units are calculated as

$$\mathbf{v}_j = \frac{\mathrm{d}\mathbf{r}_j}{\mathrm{d}t} \qquad j = 1, ..., 4 \tag{5.21}$$

The velocities of the first vehicle unit relative a body-fixed coordinate frame are introduced using

$$\mathbf{v}_1 = \begin{pmatrix} \dot{\bar{X}}, & \dot{\bar{Y}} \end{pmatrix} \begin{pmatrix} \mathbf{e}_{\mathrm{X_E}} \\ \mathbf{e}_{\mathrm{Y_E}} \end{pmatrix} = \begin{pmatrix} v_{\mathrm{X}\mathrm{v}1}, & v_{\mathrm{Y}\mathrm{v}1} \end{pmatrix} \mathbf{R}_{\mathrm{v}1}^{\mathrm{T}} \begin{pmatrix} \mathbf{e}_{\mathrm{X_E}} \\ \mathbf{e}_{\mathrm{Y_E}} \end{pmatrix} \tag{5.22}$$

The rotational velocity vectors of the different units are given as $\dot{\psi}_1, \dot{\psi}_2, \dot{\psi}_3$ and $\dot{\psi}_4$.

The external forces acting on the system are the body forces $\mathbf{F}_j = F_{\mathrm{Xv}j} \cdot \mathbf{e}_{\mathrm{Xv}j} + F_{\mathrm{Yv}j} \cdot \mathbf{e}_{\mathrm{Yv}j}$ and the tyre forces $\mathbf{F}_{jk} = F_{\mathrm{Xw}jk} \cdot \mathbf{e}_{\mathrm{Xw}jk} + F_{\mathrm{Yw}jk} \cdot \mathbf{e}_{\mathrm{Yw}jk}$. The lateral body forces are assumed to be zero. The generalised forces represent the external forces applied to the system in terms of components along the generalised coordinates. The body forces in longitudinal direction $F_{\mathrm{Xv}j}$, are calculated using the aerodynamic drag $F_{\mathrm{air},1}$ and the gravitational forces $F_{\mathrm{grav},j}$, according to

$$F_{\mathrm{Xv}j} = \begin{cases} F_{\mathrm{air},1} + F_{\mathrm{grav},j} & j = 1 \\ F_{\mathrm{grav},j} & j = 2,3,4 \end{cases} \tag{5.23}$$

The aerodynamic drag is assumed to act on the CoG of the first vehicle unit and the gravitational forces are assumed to act on the CoG of each vehicle unit. The longitudinal body forces are calculated as

$$F_{\mathrm{air},1} = -\frac{1}{2} \cdot \rho \cdot A_{\mathrm{v}} \cdot C_{\mathrm{D}} \cdot v_{\mathrm{Xv1}}^2 \tag{5.24}$$

$$F_{\mathrm{grav},j} = -m_j \cdot g \cdot \sin\left(\theta_{\mathrm{R}}\left(s_{\mathrm{R}11}\right)\right) \qquad j = 1, ..., 4 \tag{5.25}$$

where ρ is the air density, A_{v} is the vehicle front cross-sectional area, C_{D} is the air drag coefficient. g is the gravitational acceleration, and $\theta_{\mathrm{R}}(s_{R11})$ is the road uphill slope at the first vehicle unit's first axle. Note that the road slope in (5.25) is assumed to be equal for all vehicle units; not necessarily the case for general road conditions. However, in the case of the highway and vertical curvatures mentioned in Section 5.1.1, the approximation is considered valid.

In the derived vehicle body motion model, combined slip is ignored and the tyre forces in the longitudinal direction $F_{\mathrm{Xw}jk}$ are calculated as actuation forces for propulsion and braking. The lateral tyre forces $F_{\mathrm{Yw}jk}$, are calculated using constitutive relations described according to

$$F_{\mathrm{Yw}jk} = -C_{\mathrm{Y}jk} \cdot S_{\mathrm{Y}jk} \tag{5.26}$$

where $C_{\mathrm{Y}jk}$ is the cornering stiffness of unit j axle k. The lateral tyre slip $S_{\mathrm{Y}jk}$ is defined as the ratio of the wheel hub sliding speed in the lateral direction and a reference speed [53]. The reference speed is usually the absolute value of the wheel radius times the wheel rotational speed or the absolute value of the longitudinal velocity. These are equal assuming small longitudinal tyre slip.

Using (5.23)-(5.26), the generalised forces can be calculated as

$$Q_i = \sum_{j=1}^{4} \sum_{k=1}^{p_j} \mathbf{F}_{jk} \bullet \frac{\partial \mathbf{r}_{jk}}{\partial q_i} + \sum_{j=1}^{4} \mathbf{F}_j \bullet \frac{\partial \mathbf{r}_j}{\partial q_i} \tag{5.27}$$

where $i = 1, ..., 6$ are the generalised coordinates, $j = 1, ..., 4$ are the number of vehicle units, and $k = 1, ..., p_j$ with p_j as the number of vehicle axles of unit j. The positions of the tyres are $\mathbf{r}_{jk}$ and $\mathbf{r}_j$ are the positions where the body forces applies.

The dynamic equations of the one-track model representing inertial and kinematic vehicle

properties can be calculated using (5.12)-(5.27). Models for an A-double and a tractor semi-trailer are given in Appendix I.

The longitudinal and lateral accelerations of the first and last vehicle units, expressed relative to body-fixed coordinate frames, are used in the traffic situation predictions to verify the feasibility of the candidate actuation requests. The accelerations of the first vehicle unit $\mathbf{a}_1$ are calculated according to

$$\mathbf{a}_1 = \frac{\mathrm{d}\mathbf{v}_1}{\mathrm{d}t} \tag{5.28}$$

$$\frac{\mathrm{d}\mathbf{v}_1}{\mathrm{d}t} = \frac{\delta}{\delta t}\mathbf{v}_1 + \boldsymbol{\Omega}_1 \times \mathbf{v}_1 \tag{5.29}$$

$$\frac{\delta}{\delta t}\mathbf{v}_1 = \dot{v}_{\mathrm{Xv1}} \cdot \mathbf{e}_{\mathrm{Xv1}} + \dot{v}_{\mathrm{Yv1}} \cdot \mathbf{e}_{\mathrm{Yv1}} \tag{5.30}$$

where $\boldsymbol{\Omega}_1 = \dot{\psi}_1 \cdot \mathbf{e}_{\mathrm{Zv1}}$. Furthermore, a local time derivative operator $\frac{\delta}{\delta t}$ is introduced, see further [17]. The resulting longitudinal and lateral accelerations for the first vehicle unit are described as

$$\mathbf{a}_1 = (\dot{v}_{\mathrm{Xv1}} - v_{\mathrm{Yv1}} \cdot \dot{\psi}_1) \cdot \mathbf{e}_{\mathrm{Xv1}} + (\dot{v}_{\mathrm{Yv1}} + v_{\mathrm{Xv1}} \cdot \dot{\psi}_1) \cdot \mathbf{e}_{\mathrm{Yv1}} \tag{5.31}$$

Starting from (5.21), the accelerations of the last vehicle unit can be calculated as

$$\mathbf{a}_4 = \frac{\mathrm{d}\mathbf{v}_4}{\mathrm{d}t} \tag{5.32}$$

The resulting longitudinal and lateral accelerations are described as

$$\begin{aligned}
\mathbf{a}_4 = & \Big(\cos(\psi_1 - \psi_4) \cdot \Big(\dot{v}_{\mathrm{Xv1}} - \dot{\psi}_1 \cdot \Big(\dot{\psi}_1 \cdot (l_{12} - l_{1\mathrm{r}}) + v_{\mathrm{Yv1}} \Big) \Big) + \\
& \sin(\psi_1 - \psi_4) \cdot \Big((l_{1\mathrm{r}} - l_{12}) \cdot \ddot{\psi}_1 - \dot{\psi}_1 v_{\mathrm{Xv1}} - \dot{v}_{\mathrm{Yv1}} \Big) + \dot{\psi}_4^2 \cdot l_{4\mathrm{f}} \\
& \dot{\psi}_2^2 \cdot (l_{2\mathrm{f}} - l_{2\mathrm{r}} - l_{21}) \cdot \cos(\psi_2 - \psi_4) + \ddot{\psi}_2 \cdot (l_{2\mathrm{f}} - l_{2\mathrm{r}} - l_{21}) \cdot \sin(\psi_2 - \psi_4) + \\
& \dot{\psi}_3^2 \cdot (l_{3\mathrm{f}} + l_{3\mathrm{r}} - l_{31}) \cdot \cos(\psi_3 - \psi_4) + \ddot{\psi}_3 \cdot (l_{3\mathrm{f}} + l_{3\mathrm{r}} - l_{31}) \cdot \sin(\psi_3 - \psi_4) \Big) \cdot \mathbf{e}_{\mathrm{Xv4}} + \\
& \Big(\sin(\psi_1 - \psi_4) \cdot \Big(\dot{v}_{\mathrm{Xv1}} - \dot{\psi}_1 \cdot \Big(\dot{\psi}_1 \cdot (l_{12} - l_{1\mathrm{r}}) + v_{\mathrm{Yv1}} \Big) \Big) + \\
& \cos(\psi_1 - \psi_4) \cdot \Big((l_{12} - l_{1\mathrm{r}}) \cdot \ddot{\psi}_1 + \dot{\psi}_1 \cdot v_{\mathrm{Xv1}} + \dot{v}_{\mathrm{Yv1}} \Big) - l_{4\mathrm{f}} \ddot{\psi}_4 + \\
& \dot{\psi}_2^2 \cdot (l_{2\mathrm{f}} - l_{2\mathrm{r}} - l_{21}) \cdot \sin(\psi_2 - \psi_4) + \ddot{\psi}_2 \cdot (-l_{2\mathrm{f}} + l_{2\mathrm{r}} + l_{21}) \cdot \cos(\psi_2 - \psi_4) + \\
& \dot{\psi}_3^2 \cdot (l_{3\mathrm{f}} + l_{3\mathrm{r}} - l_{31}) \cdot \sin(\psi_3 - \psi_4) + \ddot{\psi}_3 \cdot (-l_{3\mathrm{f}} - l_{3\mathrm{r}} + l_{31}) \cdot \cos(\psi_3 - \psi_4) \Big) \cdot \mathbf{e}_{\mathrm{Yv4}}
\end{aligned} \tag{5.33}$$

5.2.2.2 Vehicle prediction actuation

The model described in this section predicts how the control and actuator systems such as powertrain, brakes and wheels generates longitudinal wheel forces on each axle. The actuations of the vehicle body motion model are the front wheel steering angle δ_{11} and the longitudinal tyre forces $F_{\mathrm{Xw}jk}$. The front wheel steering angle actuation is calculated as

$$\delta_{11} = \operatorname{sgn}\left(\delta^{\mathrm{req,pred}}\right) \cdot \min\left(\frac{|\delta^{\mathrm{req,pred}}|}{\eta_s}, \overline{\delta}\right) \tag{5.34}$$

where $\delta^{\mathrm{req,pred}}$ is the requested steering wheel angle for the prediction, calculated using the driver steering model, see Section 5.3.2. The ratio between the steering wheel angle and the front wheel steering angle is η_s and $\overline{\delta}$ is the steering angle limit.

The requested total longitudinal force is calculated as

$$F_{\mathrm{X}}^{\mathrm{req}} = a_{\mathrm{Xv1}}^{\mathrm{req,pred}} \cdot \sum_{j=1}^{4} m_j - \sum_{j=1}^{4} F_{\mathrm{Xv}j} + c_{\mathrm{r}} \cdot \sum_{j=1}^{4} \sum_{k=1}^{p_j} F_{\mathrm{Zv}jk} \tag{5.35}$$

where $a_{\mathrm{Xv1}}^{\mathrm{req,pred}}$ is the requested longitudinal acceleration for the prediction calculated using the driver acceleration model, see Section 5.3.2. The rolling resistance coefficient is c_{r}, p_j is the number of vehicle axles of unit j, and $F_{\mathrm{Zv}jk}$ is the vertical force of unit j axle k.

The requested total longitudinal force is coordinated between propulsion and braking and the vehicle axles using

$$F_{\mathrm{prop},12} = \max\left(\min\left(F_{\mathrm{X}}^{\mathrm{req}}, \frac{P_{\mathrm{prop}}(v_{\mathrm{Xv1}})}{v_{\mathrm{Xv1}}}, F_{\mathrm{prop}}^{\mathrm{max}}\right), 0\right) \tag{5.36}$$

$$F_{\mathrm{brake},jk} = \min\left(\frac{F_{\mathrm{Zv}jk}}{g \cdot \sum_{j=1}^{4} m_j} \cdot F_{\mathrm{X}}^{\mathrm{req}}, F_{\mathrm{brake},jk}^{\mathrm{max}}, 0\right) \tag{5.37}$$

where $P_{\mathrm{prop}}(v_{\mathrm{Xv1}})$ is the engine power and $F_{\mathrm{prop}}^{\mathrm{max}}$ is the maximum engine torque times the ratio of the lowest gear. The maximum design brake force of unit j axle k is $F_{\mathrm{brake},jk}^{\mathrm{max}}$. Equations (5.36)-(5.37) is an idealised model of control coordination between powertrain and brake systems. The usage of engine brake is not included. Additionally, (5.37) models the brake allocation/distribution on axles. The brake forces are assumed to act on each vehicle axle, whereas the propulsion force is assumed to act on the first vehicle unit's second axle.

Finally, the longitudinal tyre forces are calculated as

$$F_{\mathrm{Xw}jk} = \begin{cases} F_{\mathrm{prop},12} + F_{\mathrm{brake},12} - c_{\mathrm{r}} \cdot F_{\mathrm{Zv}jk} & jk = 12 \\ F_{\mathrm{brake},jk} - c_{\mathrm{r}} \cdot F_{\mathrm{Zv}jk} & \text{else} \end{cases} \tag{5.38}$$

where $j = 1, ..., 4$, $k = 1, ..., p_j$ with p_j as the number of vehicle axles of unit j. The longitudinal force limitation due to road friction and combined slip are disregarded. Equation (5.38) is an idealised model of an actuation system (powertrain and brake) and

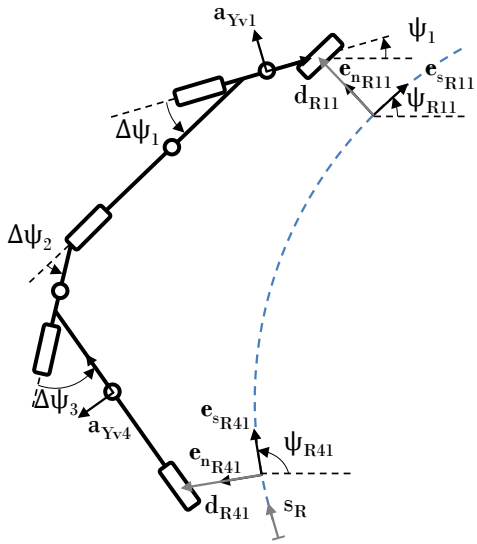

Figure 5.7: *Supplementary motion characteristics that describe the vehicle body motion relative to the road.*

the wheel mechanics. Note that the both the braking and powertrain systems are generally complex modules. The brake system of a heavy vehicle can include both the service brake with pneumatics, brake discs and pads, as well as an auxiliary brake (an engine brake and retarder for example). The powertrain system is composed of an engine, clutch, gearbox, and final gear that transfers fuel energy into a longitudinal propulsion force. To include the dynamics of these systems increases the model complexity beyond the TSP's scope. However, an approximation of the longitudinal dynamics of the powertrain and braking system can be included by using, say, a first-order system including $F_{\mathrm{prop},12}$ and $F_{\mathrm{brake},jk}$.

5.2.2.3 Vehicle in road coordinates

In addition to the vehicle body motion model, supplementary motion characteristics are added to handle the vehicle body's motion relative to the road. Added characteristics are the distance travelled along the road for the first vehicle unit's first axle s_{R11}, and last vehicle unit's last axle, s_{R41}. Furthermore, characteristics are added to capture the lateral distance offset perpendicular to the road geometry for the first vehicle unit's first axle d_{R11}, and last vehicle unit's last axle d_{R41}, see Fig. 5.7.

The absolute velocity of the first vehicle unit's first axle $\mathbf{v}_{11}$, relative to a coordinate frame (moving with the road clothoid spline) can be described as

$$\begin{aligned}\mathbf{v}_{11} =&(v_{\mathrm{Xv11}} \cdot \cos(\psi_1 - \psi_{\mathrm{R11}}) - v_{\mathrm{Yv11}} \cdot \sin(\psi_1 - \psi_{\mathrm{R11}})) \cdot \mathbf{e}_{s_{\mathrm{R11}}} \\ &+(v_{\mathrm{Xv11}} \cdot \sin(\psi_1 - \psi_{\mathrm{R11}}) + v_{\mathrm{Yv11}} \cdot \cos(\psi_1 - \psi_{\mathrm{R11}})) \cdot \mathbf{e}_{n_{\mathrm{R11}}} \qquad (5.39)\\ \mathbf{v}_{11} =&(\dot{s}_{\mathrm{R11}} - d_{\mathrm{R11}} \cdot \dot{\psi}_{\mathrm{R11}}) \cdot \mathbf{e}_{s_{\mathrm{R11}}} + \dot{d}_{\mathrm{R11}} \cdot \mathbf{e}_{n_{\mathrm{R11}}} \qquad (5.40)\end{aligned}$$

where $\dot{s}_{\mathrm{R11}}$ is the velocity of first vehicle unit's first axle along the road clothoid spline and $\dot{d}_{\mathrm{R11}}$ is the first vehicle unit's first axle velocity perpendicular to the road clothoid spline. By combining (5.5), (5.39) and (5.40), the velocities $\dot{s}_{\mathrm{R11}}$ and $\dot{d}_{\mathrm{R11}}$ can be described as

$$\dot{s}_{\mathrm{R11}} = \frac{(v_{\mathrm{Xv11}} \cdot \cos(\psi_1 - \psi_{\mathrm{R11}}) - v_{\mathrm{Yv11}} \cdot \sin(\psi_1 - \psi_{\mathrm{R11}}))}{1 - d_{\mathrm{R11}} \cdot c_{\mathrm{h}}(s_{\mathrm{R11}})} \cdot \mathbf{e}_{s_{\mathrm{R11}}} \qquad (5.41)$$

$$\dot{d}_{\mathrm{R11}} = (v_{\mathrm{Xv11}} \cdot \sin(\psi_1 - \psi_{\mathrm{R11}}) + v_{\mathrm{Yv11}} \cdot \cos(\psi_1 - \psi_{\mathrm{R11}})) \cdot \mathbf{e}_{n_{\mathrm{R11}}} \qquad (5.42)$$

Similarly, the velocities $\dot{s}_{\mathrm{R41}}$ and $\dot{d}_{\mathrm{R41}}$ can be described as

$$\dot{s}_{\mathrm{R41}} = \frac{(v_{\mathrm{Xv41}} \cdot \cos(\psi_4 - \psi_{\mathrm{R41}}) - v_{\mathrm{Yv41}} \cdot \sin(\psi_4 - \psi_{\mathrm{R41}}))}{1 - d_{\mathrm{R41}} \cdot c_{\mathrm{h}}(s_{\mathrm{R41}})} \cdot \mathbf{e}_{s_{\mathrm{R41}}} \qquad (5.43)$$

$$\dot{d}_{\mathrm{R41}} = (v_{\mathrm{Xv41}} \cdot \sin(\psi_4 - \psi_{\mathrm{R41}}) + v_{\mathrm{Yv41}} \cdot \cos(\psi_4 - \psi_{\mathrm{R41}})) \cdot \mathbf{e}_{n_{\mathrm{R41}}} \qquad (5.44)$$

5.2.3 Model comparison

The derived, non-linear, one-track models for a tractor semi-trailer and an A-double combination (see Appendix I) are compared to high-fidelity two-track models developed at Volvo GTT. The high-fidelity models include detailed sub-models of the vehicle axle suspensions, frame, cab suspension, steering system, powertrain and brakes. The tractor semi-trailer that is studied, consists of a 6x4 tractor unit followed by a semi-trailer. The total vehicle length equals 16.5 m and the total weight is 40 t. The A-double combination consists of a 6x4 tractor unit followed by a second three-axle semi-trailer, two-axle converter dolly and a three-axle semi-trailer unit. The total vehicle length equals 32 m and the total weight is 80 t.

The model comparison includes the performance-based characteristics [103]: high-speed steady-state off-tracking (HSSO), high-speed transient off-tracking (HSTO), and rearward amplification (RA_{a_y}). The off-tracking characteristics, HSSO and HSTO, both describe the lateral distance offset between the path of the centre of the front axle and the path of the centre of the most severely off-tracking axle of the last unit, see Section 2.3. These measures express the swept width for a specific steering manoeuvre and vehicle speed. A positive value for the off-tracking means that the last unit is tracking inward of the first one. These off-tracking characteristics have been calculated for constant vehicle speeds in the range of 30-80 km/h. HSSO has been calculated using two levels of constant lateral acceleration of the first vehicle unit: $1\,\mathrm{m/s^2}$ and $2\,\mathrm{m/s^2}$. Furthermore, HSTO has been calculated using a single sine wave lateral acceleration input [51] at a frequency of 0.4 Hz and lateral acceleration of $2\,\mathrm{m/s^2}$. Rearward amplification is the relationship between the maximum movement of the first and last vehicle units during a specified steering manoeuvre and vehicle speed [51]. It is usually given in the metrics yaw velocity amplification or, as here, in lateral acceleration amplification. It expresses the increased risk of a last unit rollover or swing-out, which can occur if a sudden steering manoeuvre is

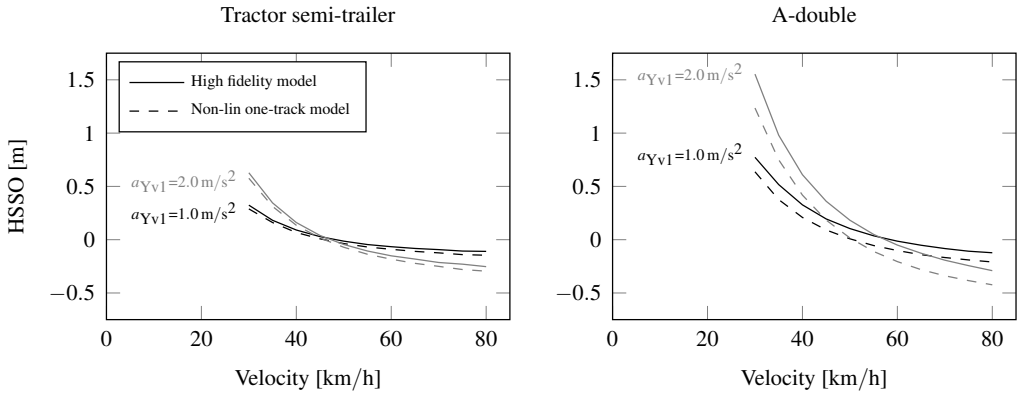

Figure 5.8: *High-speed steady-state off-tracking for tractor semi-trailer (left) and A-double (right).*

executed. The RA_{a_y} has been calculated using a pseudo-random steering input [51], with a_{Yv1} in the range of 0.2-0.5 m/s^2, and constant vehicle speed in the range of 30-80 km/h.

Fig. 5.8 shows the calculated high-speed steady-state off-tracking in the velocity range 30-80 km/h for the high-fidelity and one-track models. For both the tractor semi-trailer and the A-double combination, the HSSO is positive for vehicle speeds lower than 50 km/h. This means that the last axle is tracking inward of the first unit. For vehicle speeds higher than 50 km/h, the HSSO is negative and the last axle is tracking outwards of the first axle. The magnitude of the HSSO is dependent on the lateral acceleration, where high acceleration gives a higher HSSO magnitude. For the A-double, the HSSO is approximately 0.75 m for the velocity of 30 km/h and lateral acceleration 1 m/s^2. This is equivalent to cornering with a constant radius of 70 m.

The calculated high-speed transient off-tracking is shown in Fig. 5.9. Similar to the HSSO, the HSTO is positive for vehicle speeds lower than 50 km/h and negative otherwise. The magnitude of the HSTO increases with increasing vehicle speed. Given the manoeuvre conditions, the magnitude of the HSTO can be as high as 0.75 m for the A-double combination. This should be compared to the available lane width, which is typically 0.5 m for highways in Sweden (assumed lane width is 3.5 m and vehicle width 2.5 m).

Fig. 5.10 shows the calculated rearward amplification. The maximum RA_{a_y} for the studied combinations are 1.2 for the tractor semi-trailer, and 2.5 for the A-double combination.

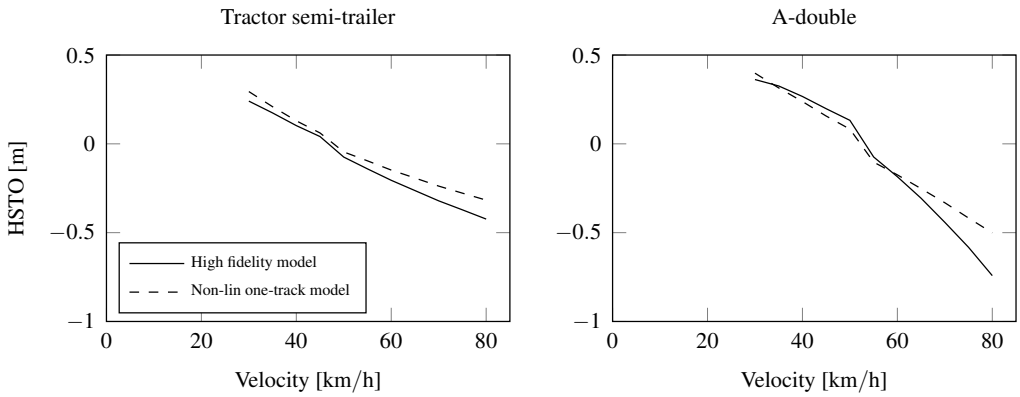

Figure 5.9: *High-speed transient off-tracking for tractor semi-trailer (left) and A-double (right).*

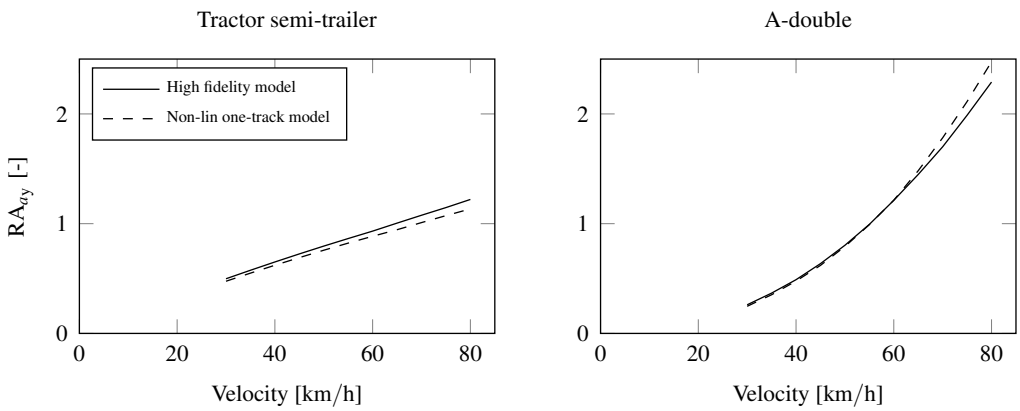

Figure 5.10: *Rearward amplification for tractor semi-trailer (left) and A-double (right).*

5.3 Driver modelling

5.3.1 Background

How to drive a passenger car is considered common knowledge in today's society. The driver controls the planar motion of the vehicle by turning the steering wheel and using the accelerator and brake pedals. Most of us agree that car driving is quite often routine but sometimes requires more focus and attention. The famous psychologist and Nobel laureate Daniel Kahnemann [56] describe driving on an empty road as an activity carried out automatically and quickly, with little or no effort and no sense of voluntary control, see Fig. 5.11a. On the other hand, Kahnemann also states that some driving activities, such as parking in a narrow space, require attention and will most probably fail if the necessary attention is lacking, see Fig. 5.11b. Obviously, from a psychological perspective, driving may be considered an activity of both low and high complexity depending on the circumstances.

Driving a heavy combination-vehicle such as an A-double is a different and often more challenging activity than driving a passenger car. The disparity comprises differences in size and weight dimensions, vehicle dynamics performance (in both longitudinal and lateral directions) and the possible safety impact in case of failure. From a societal perspective, the added complexity is reflected in the fact that heavy combination-vehicle driving requires added training and a special driving licence. On the other hand, heavy combination-vehicles are in generally not allowed in city environments, which can reduce the driving complexity compared to passenger cars.

The term **driver models**, further divided into **driver steering models** and **driver acceleration models**, refers to mathematical models of a driver's steering and longitudinal acceleration control as a function of driver, vehicle and environment states. Driver models are used in the traffic situation predictions to calculate candidate actuation requests. Note that the driver models in question do not necessarily represent complete driver behaviour and assume the existence of long-term driving goals. In the longitudinal

(a) *Transport on empty road using a single-unit vehicle.* (b) *Timber transport in darkness using an articulated vehicle.*

Figure 5.11: *Example of driving activities requiring a different amount of attention from the driver.*

direction, for example, a reference velocity profile is assumed to exists. Typically, this is calculated by the FD-RSiM for, say, optimized fuel consumption. Moreover, in the lateral direction, the driver model associated with traffic situation predictions assumes curvature profiles of current and adjacent lanes. If comparing with the driving assignment carried out by a human driver, the driver models associated with traffic situation predictions can be linked to the tactical level of the driving [79].

Driver models can be categorised based on origin [11] and divided into these main groups: control perspective, behaviour perspective and cognitive perspective. Another option is to categorise the models from the application [100] and divide them into these groups: vehicle perspective, driver perspective, combined system perspective and environment/traffic perspective. Accordingly, the driver models intended for use in the traffic situation predictions are categorised as control perspective and combined system perspective driver models.

According to Plöchl and Edelmann [100], fundamental components of driver models are: general human driver skills and characteristics, information reception, perception and processing, neuromuscular dynamics with thresholds, time delays and limitations, preview, prediction/anticipation, adaptation/learning, planning capabilities and so on. Regardless of the type of road vehicle the driving refers to, one starting point in driver modelling is driver perception abilities. Different sensory systems are used by the human driver to interpret surroundings and vehicle states. The main systems [81] are: visual, vestibular and somatosensory. Perhaps the most important of these is the visual system, used to detect road geometry and the motion of the subject vehicle relative to the surrounding environment. The vestibular organs (located in the inner ear) detect rotations and translations of the driver's head. The somatosensors include a wide range of sensory organs that detect different states of the driver's body. Typically, somatosensors can detect states such as contact pressure, temperature, limb position, joint angles, muscle lengths and tensions. Typical primary visual sensory cues used in driver steering models for single-unit vehicles are: lateral position error and heading angle error of the vehicle, relative to a preferred path. However, in the case of articulated vehicles additional cues, such as lateral acceleration and articulation angle errors are suggested. These are to further assist the driver in carrying out the steering control actions more efficiently. From the perspective of driver models associated with traffic situation predictions, we further limit the focus to exclude neuromuscular dynamics and time delays. Although these can be essential components in driver support systems (such as driver warning systems [6] and shared control systems [128]) they are omitted here.

It is hypothesised that one component (in the overall pursuit of achieving driving automation features with high operator/driver acceptability) is to use driver-models in the TSP calculations, incorporating the following characteristics:

i) in case of a mixed traffic environment with both manually driven and automated vehicles, the generated behaviour is transparent and understandable to the driver/operator as well as to surrounding traffic;

ii) the behaviour of the model can handle the targeted traffic scenarios. Typically maintain-lane manoeuvring includes driving that is affected and unaffected by other vehicles. Affected driving include approaching, braking and following another.

Besides maintain-lane manoeuvring, common traffic scenarios for highway driving are lane changes and possibly non-severe avoidance manoeuvres;

iii) the behaviour of the model is tuneable in that it has a small number of understandable parameters.

The question of whether or not the models need to be fully realistic, in other words able to fully reflect the behaviour exhibited by drivers, likely depends on the driving automation application and is left open.

Considering single-unit vehicles there is a wide range of detailed simulation-ready models, for both steering and acceleration, which meet the characteristics above. However, for articulated vehicles, the range of models is more limited. There now follows a brief review of existing acceleration and steering models. Models based on artificial intelligence (such as fuzzy logic and neural networks) are excluded because they generally do not offer a small number of understandable parameters. In case of steering models, there is particular focus on articulated vehicles.

5.3.1.1 Acceleration models

From a cognitive science perspective, Lee [65] was one of the first to show how braking can be solved using visual sensor cues. Lee proposed that the braking performance can be specified using the parameter τ and its time derivative $\dot{\tau}$, referred to as the $\dot{\tau}$-strategy. τ is defined as the quotient between the angular projection of an object θ_{p} and the angular expansion rate $\dot{\theta}_{\mathrm{p}}$. τ is often cited as an example of an optical invariant, since it uniquely specifies the time-to-collision (TTC) independent of changes in the object size. This is not the case for lower order variables such as the optical angle and expansion rate, referred to as non-specifying variables. In an approaching driving situation where the subject and a lead vehicle are closing, τ and $\dot{\tau}$ specifies whether the vehicles are on a collision course or not. When closing at a constant or acceleration rate $\tau > 0$ and $\dot{\tau} \leq$ -1. When closing at an inadequate deceleration rate $\tau > 0$ and $\dot{\tau} <$ -0.5, and when receding at a decelerating rate $\tau < 0$ and $\dot{\tau} <$ -1. The variable $\dot{\tau}$ directly states whether the deceleration is sufficient or not. Also, if $\dot{\tau} =$ -0.5, the deceleration is the minimum required to avoid a collision.

Considering the important question of when to initiate braking, Lee [65] proposed that the driver should base their decision on his assessment of the urgency of the situation. The variable τ, can as shown above, be used by the driver to determine whether the subject vehicle is on a collision course or not. Lee proposes that it should be used in deciding when to initiate braking. However, depending whether the lead vehicle is stationary or moving, the threshold value for safe braking should differ. Therefore, Lee proposes an additional heuristic value, a margin value of the temporal headway, for use in the braking initiation decision. In principle, the temporal headway could be registered as easily as the time-to-collision. The $\dot{\tau}$-strategy was supported in [134]. However, several studies also indicate deviations from the $\dot{\tau}$-strategy [31]. In general, drivers respond earlier (with greater TTC values) at higher speeds. Likewise, drivers tend to respond earlier (with greater TTC values) for large objects. An alternative to the $\dot{\tau}$ strategy [112], proposed that the optical angle and the expansion rate are independent optical primitives and that the control of braking could be accomplished by weighting these two as sources.

From a control perspective, early work on driver acceleration models for car-following assumed that the driver can perceive the space headway and relative speed between the subject and the lead vehicle. In 1958, Chandler et al. [20] studied car-following and proposed a model based on the relative speed, distance and sensitivity terms. In [40, 41], Gazis et al. assumed that the sensitivity terms were dependent on the vehicle space headway and went on to formulate the GHR-model. Helly [45] added terms to the GHR-model, adapting the driver acceleration to lead vehicle braking and a preferred relative distance. In 1993, Ioannou [50] formulated the autonomous intelligent cruise control for automatic vehicle following. The model includes a safety distance separation rule, based on a constant time headway which reduces oscillation effects and ensures string stability. In [138], a new vehicle-following controller was developed based on a constant time headway. The controller especially targets heavy vehicles which have limited acceleration capabilities.

Driver accelerations models and their implementation into vehicle control functions have received considerable attention in recent decades, with the introduction of cruise control and adaptive cruise control. Differences in acceleration capabilities and between passenger vehicles and heavy vehicles are often handled by tuning gain factors.

5.3.1.2 Steering models

Among the first driver steering models used in the connection with an articulated vehicle was the model proposed by MacAdam [70, 71] in the early 1980s. The driver in this model steers to minimise the path deviation along a preview interval, given specific optimisation criteria. However, in this specific application, the contribution of trailer dynamics was overlooked. Starting in the late 1990s, Yang et al. [133, 132, 131] presented a model that minimised the lateral acceleration, lateral position and orientation errors between the previewed and the actual path of the tractor. Interestingly, Yang identified the lateral acceleration of the vehicle as a main sensor cue based on its importance to lateral and roll stability. As illustrated in Section 5.2, there is a great difference between passenger cars and articulated vehicles in high-speed manoeuvring which needs to be considered by the driver. The model was investigated for a tractor semi-trailer combination using closed-loop simulations in an avoidance manoeuvre.

In 2007, Liu [67] presented a control model for a tracking situation. The steering control was determined by a time-delayed feedback of the vehicle's instantaneous state. The feedback gain factors involved in this model were obtained through optimisation, given a specific optimisation criterion. Moreover, in 2012 Ding and He [24] studied three steering models that minimised lateral position errors based on the perceived motion of a tractor, a trailer and a combined tractor-trailer. The models were compared using closed-loop simulations in low-speed path-following and a high-speed lateral stability manoeuvre.

In 2014, Taheri [118] published a two-stage preview model to characterise human driving behaviour connected to articulated vehicles. The model includes path preview/prediction, error estimation, decision making and hand-arm dynamics. The path-preview part of the model is accomplished using near and far points to manage central lane position and vehicle orientation. The error estimation and decision making contains vehicle orientation

error, lateral position error, and additional vehicle states. The additional vehicle states are lateral accelerations and yaw rate of the tractor and semi-trailer units and the articulation angle rate. The gain factors were identified using minimisation with a performance index, comprising the steering effort, path tracking and directional dynamic measures of the vehicle. In 2016, Zhu [140] presented a preview model generalised for single-unit and multi-unit vehicles. This model is based on a sliding mode control technique [136] and determines the steering based on the lateral position and yaw errors of all vehicle units. The model embraces the MacAdam model [71] as a special case. The model was evaluated for stability and manoeuvrability-orientated modes to characterise high and low-speed manoeuvring.

To conclude, the existing steering models used in connection with articulated vehicles most often have added sensor cues compared to models adapted for single-unit vehicles. This is to meet the added complexity of lateral vehicle dynamics, such as off-tracking and rearward amplification, see Section 2.3. The added sensor cues are: orientation error or lateral error of the trailing units, and lateral acceleration of towing and trailing units. The manoeuvrability and stability aspects of articulated vehicles (low-speed and high-speed manoeuvring) are challenging and often require different gain factors to achieve good overall performance.

5.3.2 Design

In the design of functionalities associated with traffic situation predictions, the main target of the driver modelling is to include the characteristics specified in the hypothesis for high operator/driver acceptability, see Section 5.3.1. One possibility is to use driver models inspired by human cognition and optical flow theory. A model based on relevant perceptual abilities and mechanisms may be applicable to a wide range of driving scenarios and still allow simple formulation as well as effective control.

In Paper A, a simple model based on Lee [65] was used to calculate the requested longitudinal acceleration $a_{\mathrm{Xv1}}^{\mathrm{req,pred}}$ in a combined lane change and lead vehicle braking situation. It was shown that, using simple optical heuristics, the proposed model managed to generate safe and conservative deceleration for lead vehicle deceleration of $0.7g$ and speeds in the range 30-80 km/h. However, this type of simple stimulus model does not have any preferred spatial gap, meaning that if the velocity difference between subject and lead vehicle is zero, the requested acceleration is zero. The model is not suitable for lead vehicle following or cut-in situations.

In Papers B, C and D, the acceleration model was changed to include lead vehicle following. In Paper D, a driving simulator experiment with focusing on maintain-lane and lane-change manoeuvring was carried out and manual and automated driving was compared. The driver's manual brake initiation and execution were compared with the acceleration model and a non-linear model predictive controller. The proposed criterion for brake initiation was based on time-headway and expansion rate. The criterion was not supported by manual driving observations. In general, the manual drivers had smaller lead vehicle time gaps and initiated braking later. The maximum decelerations used in braking were most often higher for manual than automated driving. The maximum deceleration for the manual drivers correlated well with increased levels of the inverse of

time-to-collision.

In the automated driving carried out in the simulator experiment described in Paper E, the requested acceleration for the current lane was calculated as

$$a_{\mathrm{Xv1}}^{\mathrm{req,pred}} = \begin{cases} k_{\dot{\theta}_\mathrm{p}} \cdot \Delta v_{1,n}^{(o)} \cdot \left| \frac{\Delta v_{1,n}^{(o)}}{\Delta s_{1,n}^{(o)}} \right| + k_{\theta_\mathrm{p}} \cdot (\Delta s_{1,n}^{(o)} - \Delta s_{\mathrm{safe}}) & \text{lead vehicle following} \\ k_{\Delta v} \cdot \Delta v_{\mathrm{set}} & \text{speed-control} \end{cases} \tag{5.45}$$

where $\Delta s_{1,n}^{(o)}$ and $\Delta v_{1,n}^{(o)}$ are the distance and speed differences between the rear of the lead vehicle and front of the subject vehicle. The quotient between the relative speed and distance is the inverse of τ (inverse of time-to-collision). $k_{\dot{\theta}_\mathrm{p}}$, k_{θ_p} and $k_{\Delta v}$ are gain factors and Δs_{safe} is a safety distance. Δv_{set} is the speed difference between the desired set speed and the subject vehicle. The first term in the driver acceleration model for lead vehicle following (5.45) is connected to the kinematic expression for the longitudinal acceleration required to bring the relative velocity to zero at the time of the collision [54].

In the case of steering models, it was reported in [75] that the two-point model (5.46) by Salvucci and Gray [106] was able to properly explain the variance in the steering behaviour of human drivers, in both repeated and unexpected stabilization manoeuvring. The model regulates the angular error to both a near-point and a stabilising far-point. How these points are chosen depends on the driving scenario, see examples in [106]. In Papers A-D, the longitudinal near-point location was fixed a short distance in front of the subject vehicle, whereas the longitudinal location of the far-point varied with subject vehicle speed and traffic scenario. In cases where there was a lead vehicle present, its longitudinal position was used as a far-point location.

In Paper A, data collected on-road in highway driving was used to determine the gain factors k_f, k_n, k_nI, for the two-point model (5.46) in lane-change manoeuvring. The two-point model is written as

$$\dot{\delta}^{\mathrm{req,pred}} = k_\mathrm{f} \cdot \dot{\theta}_\mathrm{f} + k_\mathrm{n} \cdot \dot{\theta}_\mathrm{n} + k_\mathrm{nI} \cdot \theta_\mathrm{n} \tag{5.46}$$

where $\dot{\delta}^{\mathrm{req,pred}}$ is the requested steering wheel angle rate and θ_n is the near-point angle. $\dot{\theta}_\mathrm{f}$ and $\dot{\theta}_\mathrm{n}$ are the far and near-point angular rates. In Paper A, the gain factors were tuned using four lane-change manoeuvres and a genetic algorithm [48]. All lane changes were executed on a straight road at 80 km/h with no traffic in the target lane. It was found that the model captured the observed behaviour fairly well, see Fig. 5.12. The main frequency of the steering behaviour was found to be approximately 0.1 Hz, well below the critical subject vehicle yaw mode frequencies. Moreover, it was observed that the steering included a second peak when the vehicle was straightened. This was captured by the model, see Fig. 5.12 time interval 10-20 s.

In Papers B, C and D, the steering model (5.46) was used in functionalities associated with traffic situation predictions for calculation of candidate steering requests for highway driving automation. In Paper B, simulations of lane changes at constant vehicle speeds in the range 20-80 km/h were executed. The lane change durations were in the range of 7-20 s and the main steering wheel frequency was 0.1 Hz. The extremum of the lateral

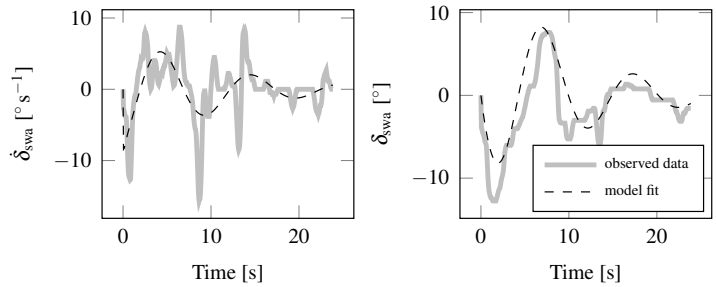

Figure 5.12: *Steering wheel angle rate (left) and steering wheel angle (right) for one of the measured lane-change events. From Paper A.*

accelerations and rearward amplification were approximately 1 m/s^2 and 1.2, respectively. The lane change performances were considered reasonable for the given vehicle combination and driving conditions. The vehicle dynamics performance for lane changes of an A-double combination was compared, between the steering model and a non-linear model predictive controller in Paper C. In general, the non-linear model predictive control showed shorter lane change durations and lower extremum values for the lateral accelerations.

The driver model parameters extracted in Paper A were included in a framework for driving automation used in a driving simulator experiment described in Paper D. In a pre-study for the simulator experiment, it was observed that the gain factors obtained did not perform satisfactorily in maintain-lane cornering manoeuvres. The identified gain factors resulted in poor tracking performance. Furthermore, there was difficulty achieving a common gain factor setting which worked satisfactorily for both maintain-lane and lane-change manoeuvring. A gain factor setting that was capable of producing realistic performance in lane changes resulted in poor tracking performance, whilst a gain factor setting with good tracking performance resulted in unrealistically slow lane-changes. The gain factors used in the final experiment in the paper comprised two different settings; one for maintain-lane and one for lane-change manoeuvring. In Paper D, the driver's manual steering was compared to the steering model (5.46) and a non-linear model predictive controller for lane change execution. The manual driver's lane-change durations were similar to those of the steering model. Both showed considerably longer lane change durations than the automated driving approach based on optimisation. This behaviour also reflected lower mean values on lateral acceleration and jerk, which can describe the level of ride comfort.

5.3.3 Proposed driver steering model for articulated vehicles

As mentioned in Section 2, the main road usage for LCVs are one-way multiple-lane roads. The majority of the driving is envisaged as consisting of maintain-lane manoeuvring, lane changes, road junctions, exit ramps, and overtaking. Typical vehicle speeds are in the range 0-80 km/h. Although in Paper D, satisfactory performance for high-speed maintain-lane manoeuvring was given using the two-point model (5.46), see Section 5.3.2, it was noted that the lateral distance offset of the last vehicle unit last axle was unacceptably

(a) *Front view.*

(b) *View in rear view mirror.*

Figure 5.13: *Front and rear views from the driver position in a right cornering situation when driving an A-double combination.*

large in low-speed cornering.

The proposed driver steering model for articulated vehicles, targeting maintain-lane manoeuvring, includes the concept of a near and far point, as developed by Salvucci and Gray [106], see Section 5.3.2. In addition to the near and far points, the proposed model includes a rear point, representing visual information on the orientation of the last vehicle unit relative to the road. The added sensor cue is motivated using observations from eye movement behaviour of professional truck drivers. In the driving simulator experiment described in Paper D, the drivers' visual focus in cornering situations repeatedly shifted between the front view and nearside rear-view mirror, as the drivers were checking for feasible manoeuvring. For example, the front and rear views shown to the driver in a right-cornering situation, radius approximately 200 m, are illustrated in Fig. 5.13.

Formulation of driver-vehicle model

The positions of a near point n and far point f are assumed to be located on a clothoid spline representing the lane centre at the distances Δs_{Rn} and Δs_{Rf} ahead of the subject vehicle front axle position s_{R11}, see Fig. 5.14. The near and far points are assumed to travel along the lane centre with the velocities $\dot{s}_{\mathrm{Rn}}$ and $\dot{s}_{\mathrm{Rf}}$ respectively. The calculation of the angular velocities $\dot{\theta}_{\mathrm{n}}$ and $\dot{\theta}_{\mathrm{f}}$ are similar and are here only described for $\dot{\theta}_{\mathrm{f}}$. The absolute velocity of point f can be described as

$$\mathbf{v}_{\mathrm{f}} = \dot{s}_{\mathrm{Rf}} \cdot \cos(\theta_{\mathrm{f}} + \Delta\psi_{\mathrm{R1}} - \Delta\psi_{\mathrm{Rf}}) \cdot \mathbf{e}_{s_{\mathrm{R11}}\prime} - \dot{s}_{\mathrm{Rf}} \cdot \sin(\theta_{\mathrm{f}} + \Delta\psi_{\mathrm{R1}} - \Delta\psi_{\mathrm{Rf}}) \cdot \mathbf{e}_{n_{\mathrm{R11}}\prime} \tag{5.47}$$

$$\Delta\psi_{\mathrm{R1}} = \psi_1 - \psi_{\mathrm{R11}} \tag{5.48}$$

$$\Delta\psi_{\mathrm{Rf}} = \psi_{\mathrm{Rf}} - \psi_{\mathrm{R11}} \tag{5.49}$$

where ψ_{R11} and ψ_{Rf} are the road angles at the subject vehicle's front axle position and the far point position, respectively. $\Delta\psi_{\mathrm{R1}}$ is the yaw angle of the subject vehicle's first unit relative to the road.

Furthermore, the absolute velocity of point f can also be described in the moving coordinate frame $(\mathbf{e}_{s_{\mathrm{R11}\prime}}, \mathbf{e}_{n_{\mathrm{R11}\prime}})$ as

$$\begin{aligned}\mathbf{v}_{\mathrm{f}} = &\Big((\dot{s}_{\mathrm{R11}} - \dot{\psi}_{\mathrm{R11}} \cdot d_{\mathrm{R11}}) \cdot \cos(\theta_{\mathrm{f}} + \Delta\psi_{\mathrm{R1}}) + \dot{d}_{\mathrm{R11}} \cdot \sin(\theta_{\mathrm{f}} + \Delta\psi_{\mathrm{R1}}) + \dot{r}_{\mathrm{f/o}\prime}\Big) \cdot \mathbf{e}_{s_{\mathrm{R11}\prime}} \\ &+ \Big(-(\dot{s}_{\mathrm{R11}} - \dot{\psi}_{\mathrm{R11}} \cdot d_{\mathrm{R11}}) \cdot \sin(\theta_{\mathrm{f}} + \Delta\psi_{\mathrm{R1}}) + \dot{d}_{\mathrm{R11}} \cdot \cos(\theta_{\mathrm{f}} + \Delta\psi_{\mathrm{R1}}) \\ &+ (\dot{\theta}_{\mathrm{f}} + \dot{\psi}_1) \cdot r_{\mathrm{f/o}\prime}\Big) \cdot \mathbf{e}_{n_{\mathrm{R11}\prime}} \end{aligned} \tag{5.50}$$

where $\dot{s}_{\mathrm{R11}}$ and $\dot{d}_{\mathrm{R11}}$ are the velocities of the subject vehicle's front axle in the road coordinate frame $(\mathbf{e}_{s_{\mathrm{R11}}}, \mathbf{e}_{n_{\mathrm{R11}}})$. $\dot{\psi}_{\mathrm{R11}}$ and $\dot{\psi}_1$ are the angular velocity of the road at the subject vehicle's front axle position and the angular velocity of the subject vehicle's first unit, respectively. d_{R11} is the subject vehicle's front axle position perpendicular to the road tangent. $\dot{r}_{\mathrm{f/o}\prime}$ and $r_{\mathrm{f/o}\prime}$ are the velocity and position of point f in the moving coordinate frame.

By combining (5.47)-(5.50), the angular velocity $\dot{\theta}_{\mathrm{f}}$ and the velocity, $\dot{r}_{\mathrm{f/o}\prime}$ can be described as

$$\begin{aligned}\dot{\theta}_{\mathrm{f}} = &\frac{-\dot{s}_{\mathrm{Rf}} \cdot \sin(\theta_{\mathrm{f}} + \Delta\psi_{\mathrm{R1}} - \Delta\psi_{\mathrm{Rf}}) + (\dot{s}_{\mathrm{R11}} - \dot{\psi}_{\mathrm{R11}} \cdot d_{\mathrm{R11}}) \cdot \sin(\theta_{\mathrm{f}} + \Delta\psi_{\mathrm{R1}})}{r_{\mathrm{f/o}\prime}} \\ &- \frac{\dot{d}_{\mathrm{R11}} \cdot \cos(\theta_{\mathrm{f}} + \Delta\psi_{\mathrm{R1}})}{r_{\mathrm{f/o}\prime}} - \dot{\psi}_1 \end{aligned} \tag{5.51}$$

$$\begin{aligned}\dot{r}_{\mathrm{f/o}\prime} = &\dot{s}_{\mathrm{Rf}} \cdot \cos(\theta_{\mathrm{f}} + \Delta\psi_{\mathrm{R1}} - \Delta\psi_{\mathrm{Rf}}) - ((\dot{s}_{\mathrm{R11}} - d_{\mathrm{R11}} \cdot \dot{\psi}_{\mathrm{R11}}) \cdot \cos(\theta_{\mathrm{f}} + \Delta\psi_{\mathrm{R1}}) \\ &- \dot{d}_{\mathrm{R11}} \cdot \sin(\theta_{\mathrm{f}} + \Delta\psi_{\mathrm{R1}})) \end{aligned} \tag{5.52}$$

In some cases, it can be useful to simplify (5.51). By assuming a circular road section, equal velocities $\dot{s}_{\mathrm{R11}}$ and $\dot{s}_{\mathrm{Rf}}$, small angles θ_{f}, $\Delta\psi_{\mathrm{R1}}$ and $\Delta\psi_{\mathrm{Rf}}$, (5.51) can be written as

$$\dot{\theta}_{\mathrm{f}} \approx \frac{\dot{s}_{\mathrm{R11}} \cdot c_{\mathrm{h}} \cdot r_{\mathrm{f/o}\prime} - \dot{d}_{\mathrm{R11}}}{r_{\mathrm{f/o}\prime}} - \dot{\psi}_1 \tag{5.53}$$

where c_{h} is the horizontal curvature of the road.

A rear point r is now introduced and is the main extension compared to original model, see (5.46). The rear point is positioned on the inner edge of the lane at the subject vehicles' rearmost axle s_{Rn1}, with n as the number of vehicle units. The rear point is used to estimate the sensory information perceived from the rearmost trailing unit, see illustration in Fig. 5.14a. The associated angle and angular velocity error are described as

$$\Delta\theta_{\mathrm{r}} = \psi_{\mathrm{R}n1\prime} - \psi_n \tag{5.54}$$

$$\Delta\dot{\theta}_{\mathrm{r}} = \dot{\psi}_{\mathrm{R}n1\prime} - \dot{\psi}_n \tag{5.55}$$

where $n = 4$ in case of an A-double combination.

The proposed driver model for steering articulated heavy vehicles is formulated as

$$\dot{\delta}^{\mathrm{req,pred}} = k_{\mathrm{f}} \cdot \dot{\theta}_{\mathrm{f}} + k_{\mathrm{n}} \cdot \dot{\theta}_{\mathrm{n}} + k_{\mathrm{nI}} \cdot \theta_{\mathrm{n}} + k_{\mathrm{r}} \cdot \Delta\dot{\theta}_{\mathrm{r}} + k_{\mathrm{rI}} \cdot \Delta\theta_{\mathrm{r}} \tag{5.56}$$

where k_{f}, k_{n}, k_{nI}, k_{r} and k_{rI} are gain factors.

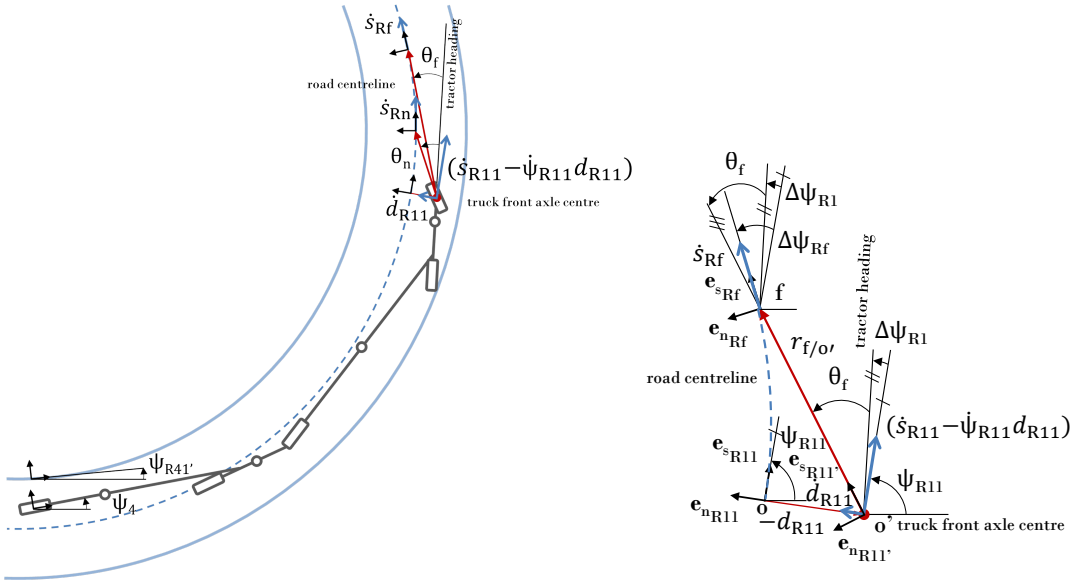

(a) *Overview of geometry.* (b) *Geometry for far-point θ_f.*

Figure 5.14: *Geometry for aim point angles used in driver model for articulated vehicles. The illustrated vehicle is an A-double combination consisting of four vehicle units.*

Analysis

Two driver steering models are analysed. The first is the two-point model by Salvucci and Gray [106] and the second is the proposed steering model for articulated vehicles that includes the concept of a visual cue from the rearmost trailing unit. Furthermore, two vehicle models are used to analyse the performance of the driver steering models. The first vehicle model is a tractor semi-trailer combination and the second is an A-double combination, see Section 2. The assumed vehicle width is in both cases 2.5 m. Moreover, two driving manoeuvres are simulated using two different road sections. Firstly, low speed maintain-lane manoeuvring is studied using an S-curve road section, see Fig. 5.15, where the lane width is 3.5 m and the minimum radius is 100 m. Secondly, high-speed maintain-lane manoeuvring is studied using an S-curve road section, see Fig. 5.15, where the lane width is 3.5 m and the minimum radius is 200 m. In case of low speed maintain-lane manoeuvring the vehicle speed is in the range of 10-50 km/h. For high-speed maintain-lane manoeuvring the vehicle speed is in the range of 50-80 km/h. The minimum radii and vehicle speed are adapted for typical roads and vehicle roll-over margin.

Performance measures

Performance measures are defined to objectively evaluate the driver models during low and high-speed maintain-lane manoeuvring. The tracking performance is described using the extremum of lateral offset of the centre of the first and last vehicle axles $d_{R11,ext}$ and

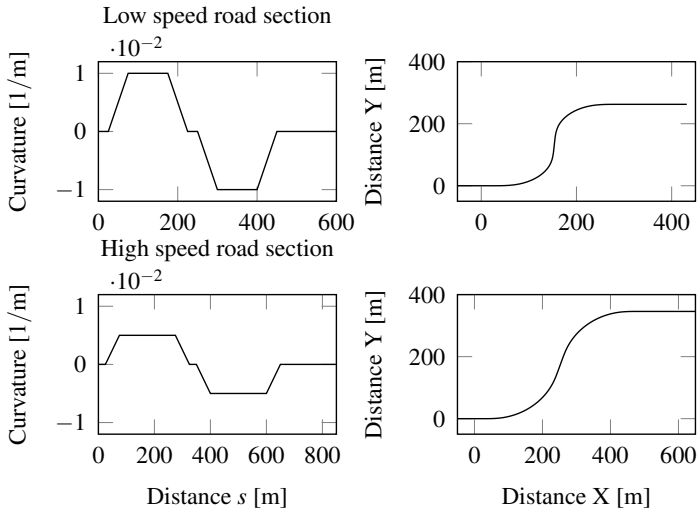

Figure 5.15: *Road section used in simulations. Road sections used in low-speed maintain-lane manoeuvring (top row) and high-speed maintain-lane manoeuvring (bottom row).*

Table 5.1: Performance measures used to evaluate the driver models. In the case of the tractor semi-trailer $n = 2$ and for the A-double $n = 4$.

Variable	Unit	Description
$d_{\mathrm{R11,ext}}$	m	Extremum of lateral distance offset first axle
$d_{\mathrm{R}n1,\mathrm{ext}}$	m	Extremum of lateral distance offset last axle
$a_{\mathrm{Yv1,ext}}$	m/s^2	Extremum of lateral acceleration first unit
$a_{\mathrm{Yv}n,\mathrm{ext}}$	m/s^2	Extremum of lateral acceleration last unit
RA_{a_y}	-	Rearward amplification

$d_{\mathrm{R}n1,\mathrm{ext}}$, respectively. Here, n is the number of vehicle units. Ride comfort is characterised by the extremum of the lateral acceleration of the first and last vehicle unit $a_{\mathrm{Yv1,ext}}$ and $a_{\mathrm{Yv}n,\mathrm{ext}}$, respectively. Safety is characterised using maximum rearward amplification of the lateral acceleration RA_{a_y}.

Driver model gain factors

One possible approach to improving understanding of the model parameters is to assume that the human sensorimotor heuristics are adapted to vehicle dynamics. An initial approach to finding the parameters for the two-point model [106] from vehicle model parameters is carried out by [74]. In the current study, two different parameter settings are used, see Table 5.2. The first setting, A, is without sensory information from the rear point and setting B is with sensory information from the rear point. The parameters are chosen to show the conceptual effect and are not optimised for performance.

Table 5.2: Driver model parameters.

	$k_{\mathrm{f}}[-]$	$k_{\mathrm{n}}[-]$	k_{nI} [1/s]	k_{r} [-]	k_{rI}[1/s]	s_{Rn} [m]	s_{Rf} [m]
Setting A	1.0	10.0	1.0	0.0	0.0	5.0	$v_{Xv1} \cdot 1.5$
Setting B	1.0	10.0	1.0	2.5	1.5	5.0	$v_{Xv1} \cdot 1.5$

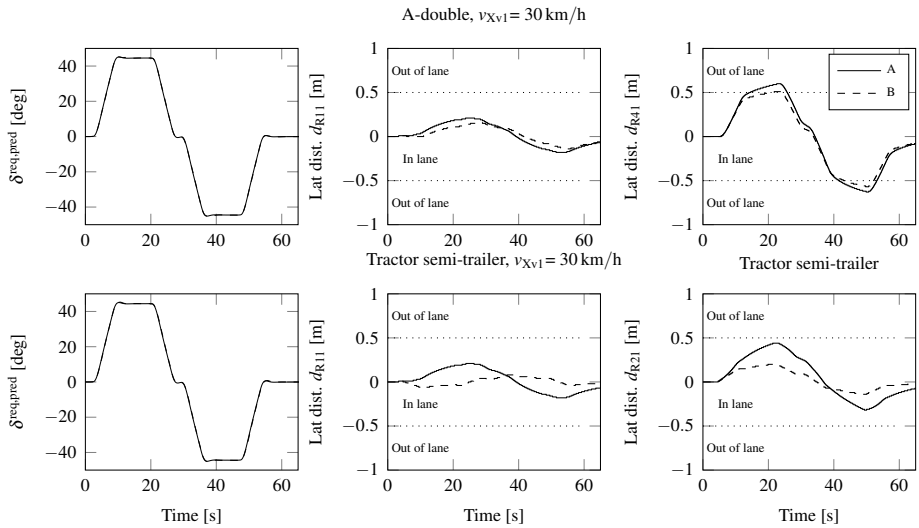

Figure 5.16: *Illustration of low speed, v_{Xv1}=30 km/h, maintain-lane manoeuvring. Steering wheel angle (left), lateral distance offset of first axle (middle) and lateral distance offset of last axle (right) for A-double (top row) and tractor semi-trailer (bottom row).*

Result of low-speed manoeuvring

To illustrate the effects of including a rear point in the driver model formulation for low-speed maintain-lane manoeuvring, Fig. 5.16 shows simulation results for the vehicle speed 30 km/h for an A-double (top row) and a tractor semi-trailer combination (bottom row). Firstly, consider parameter setting A (without rear point) and the situation when the vehicles are approaching the first corner at 10 s. Here, the lateral distance offset of the first vehicle axle d_{R11} (middle panels) shows positive values, meaning that the vehicles try to cut the corner. Due to off-tracking, this means the last vehicle axle will cut the corner even more and possibly end up out of lane; see lateral distance offset of the last vehicle axles $d_{\mathrm{R}n1}$ (right panels). A similar scenario is seen for the second corner at 40 s. Secondly, consider parameter setting B (with rear point) and the first and second corner. The contributions from the rear point cause the front axle of the vehicle to remain out during cornering, resulting in lower magnitudes of d_{R11}. Consequently, the last vehicle axles end up closer to the lane centreline. In this example, this effect is most apparent in the tractor semi-trailer combination.

The extremum of the lateral distance offset for first and last vehicle axles $d_{\mathrm{R11,ext}}$ and $d_{\mathrm{R}n1,\mathrm{ext}}$, and extremum of the lateral acceleration of the last vehicle axle $a_{\mathrm{Y}vn,\mathrm{ext}}$,

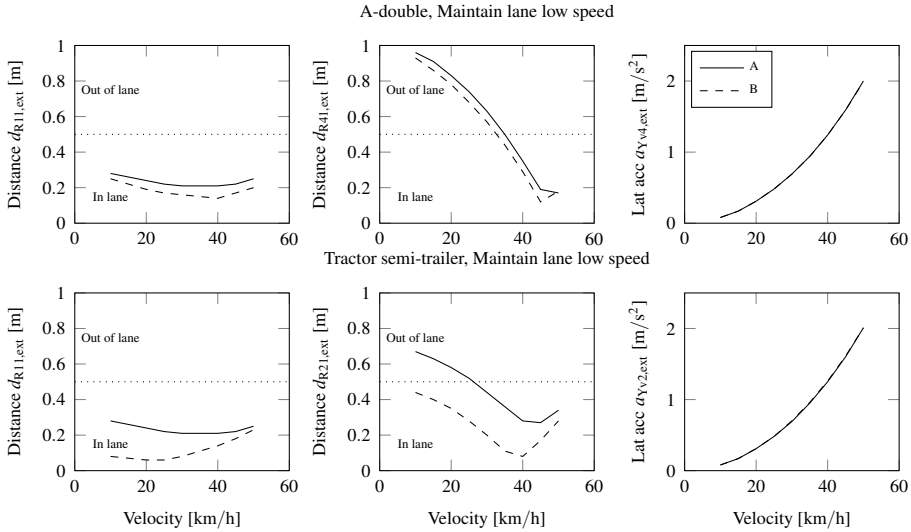

Figure 5.17: *Low-speed maintain-lane manoeuvring.*

are shown in Fig. 5.17 for the vehicle speeds 10-50 km/h. For both vehicles, $d_{\mathrm{R11,ext}}$ is less than 0.3 m for both parameter settings, see Fig. 5.17 (left column). The lateral distance offset $d_{\mathrm{R11,ext}}$ is reduced by approximately 0.1 m for parameter setting B (with rear point) in case of the A-double and 0.2 m for the tractor semi-trailer. For the A-double, both parameter settings show that $d_{\mathrm{R41,ext}}$ is larger than 0.5 m for velocities lower than 35 km/h, see Fig. 5.17 (middle column). None of the parameter settings were able to keep the vehicle within the lane width. In general, the lateral distance offset $d_{\mathrm{R}n1,\mathrm{ext}}$ is reduced by approximately 0.05 m for parameter setting B (with rear point) in case of the A-double and 0.2 m for the tractor semi-trailer. For the tractor semi-trailer, parameter settings A (without rear point) shows that $d_{\mathrm{R21,ext}}$ is larger than 0.5 m for velocities lower than 27 km/h. For parameter setting B (with rear point), the $d_{\mathrm{R21,ext}}$ is maximum 0.45 m. Considering $a_{\mathrm{Yv4,ext}}$, there is no difference between parameter settings A and B, see Fig. 5.17 (right column). In all cases the rearward amplification is close to 1.

Results of high-speed manoeuvring

As in the case of low-speed manoeuvring, we start by exemplify the effects of including the rear point in the driver model formulation for high-speed maintain-lane manoeuvring. In Fig. 5.18, simulation results are shown for the vehicle speed 80 km/h for an A-double (top row) and a tractor semi-trailer combination (bottom row). Initially, when the vehicles are approaching the first corner at 3 s, the lateral distance offset of the first vehicle axle d_{R11} (middle column) shows negative values, meaning that the vehicles keep out of the corner. Due to off-tracking, this means that the last vehicle axle will swing out even more and possibly end up out of lane, see lateral distance offset of the last vehicle axles d_{R41} and d_{R21} (right column). The contributions from the rear point causes the front axle of

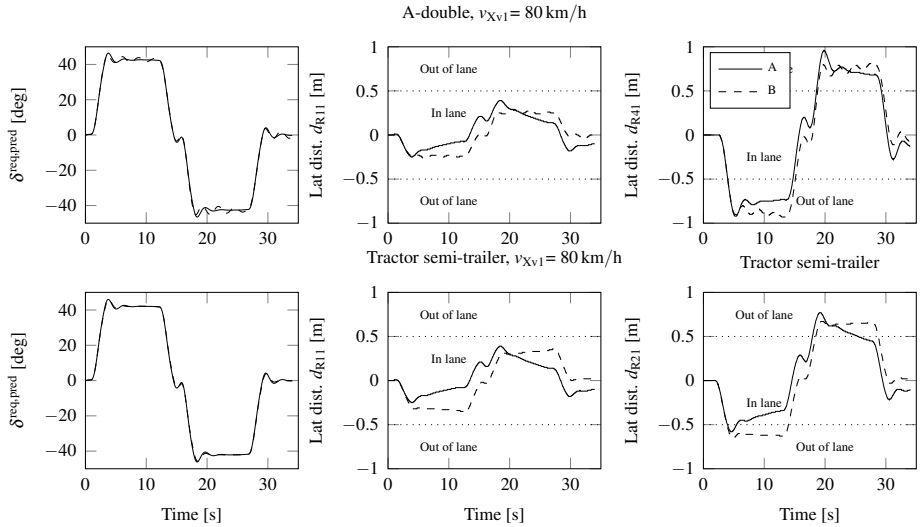

Figure 5.18: *Illustration of high-speed, v_{Xv1}=80 km/h, maintain-lane manoeuvring. Steering wheel angle (left), lateral distance offset of first axle (middle) and lateral distance offset of last axle (right) for A-double (top row) and tractor semi-trailer (bottom row).*

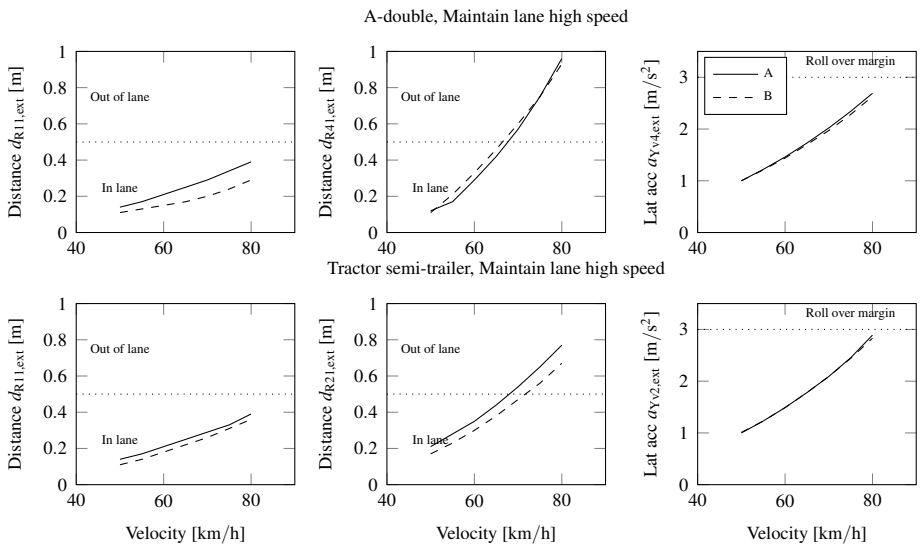

Figure 5.19: *High-speed maintain-lane manoeuvring.*

the vehicles to keep out slightly more during the first corner, giving a higher magnitude of $d_{\mathrm{R}11}$. Consequently, the last vehicle axles end up slightly further away from the lane centreline. However, in the second corner at 15 s, the extremum of $d_{\mathrm{R}11}$ and $d_{\mathrm{R}n1}$ shows

a slightly lower value in setting B (with rear point) than setting A (without rear point). It should be noted that there is no major improvement when using the rear point in the example shown.

The extremum of the lateral distance offset for first and last vehicle axles $d_{\mathrm{R11,ext}}$ and $d_{\mathrm{R}n1,\mathrm{ext}}$, and the extremum of the lateral acceleration of the last vehicle units $a_{\mathrm{Yv}n,\mathrm{ext}}$, are shown in Fig. 5.19 for the vehicle speeds 50-80 km/h. For both vehicles, $d_{\mathrm{R11,ext}}$ is smaller than 0.45 m for both parameter settings, see Fig. 5.19 (left column). The lateral distance offset $d_{\mathrm{R11,ext}}$ is reduced by approximately 0.07 m for parameter setting B for the A-double and 0.03 m for the tractor semi-trailer. For the A-double, both parameter settings show that $d_{\mathrm{R41,ext}}$ is larger than 0.5 m for velocities greater than 70 km/h, see Fig. 5.19 (middle column). None of the parameter settings were able to keep the vehicle within the lane width. In general, the lateral distance offset $d_{\mathrm{R}n1,\mathrm{ext}}$ is similar for both parameter settings in the case of the A-double, and reduced by approximately 0.06 m for setting B (with rear point) for the tractor semi-trailer. Considering $a_{\mathrm{Yv4,ext}}$, there is no difference between parameter settings A and B, see Fig. 5.19 (right column). The rearward amplification is close to 1.0 for the tractor semi-trailer and in the range 1.0-1.2 for the A-double.

5.4 Traffic modelling

5.4.1 Background

In general, highway driving scenarios for articulated vehicles include **surrounding traffic** such as passenger cars, buses, trucks and motorcyclists, see Fig. 5.20. To predict how such driving scenarios will evolve in the future (as in the traffic situation predictions) necessitates models of the surrounding traffic. Moreover, by using models of the subject vehicle and surrounding traffic it is also possible to assess the **risk of a collision** associated with a particular traffic situation. Common motion models for traffic predictions can (according to Lefèvre et al. [66]) be categorised as either physics-based motion models, manoeuvre-based motion models or interaction-aware motion models.

Physics-based motion models represent the surrounding vehicles as dynamic objects controlled by the laws of physics. These are similar to the subject vehicle modelling, see Section 5.2, but are often described with less complexity. The simplest models are kinematic models assuming constant velocity, constant acceleration, constant turn rate and velocity, or constant turn rate and acceleration. In the case of constant acceleration, the motion of a vehicle can be described as

$$\begin{pmatrix} \dot{v}_{m,n}^{(o)} \\ \dot{s}_{m,n}^{(o)} \end{pmatrix} = \begin{pmatrix} 0 & 0 \\ 1 & 0 \end{pmatrix} \begin{pmatrix} v_{m,n}^{(o)} \\ s_{m,n}^{(o)} \end{pmatrix} + \begin{pmatrix} a_{m,n}^{(o)} \\ 0 \end{pmatrix} \tag{5.57}$$

where $s_{m,n}^{(o)}$ and $v_{m,n}^{(o)}$ are the distance and velocity along the road for surrounding vehicle m in lane n, see Fig.5.20. Moreover, $a_{m,n}^{(o)}$ is a given constant acceleration. In the prediction phase, it is possible to include uncertainties on the current surrounding vehicle state and its evolution using normally distributed Gaussian noise. If no assumptions are made on the Gaussianity of the uncertainties, Monte Carlo methods can be used to approximate the uncertainty distributions [27]. Because of the harsh assumptions made in regard to vehicle motion, the models are limited to short prediction intervals, often less than a second [66].

Manoeuvre-based motion models represent the surrounding vehicles as a series of manoeuvres executed independently from the other vehicles. By identifying the manoeuvre intention of a vehicle, pre-calculated trajectories can be used to match the identified manoeuvre. Even though there is a rough assumption that the surrounding vehicles move independent of each other, the inclusion of manoeuvre intention identification generally allows longer prediction intervals than the physics-based models [66].

Interaction-aware motion models represent the surrounding vehicles as a series of manoeuvres that interact with each other. Obviously, the models can be more reliable than the manoeuvre-based motion models as they account for dependencies between the vehicles. However, a major drawback is that computing all potential combinations is very expensive in computational terms, even for just a few surrounding vehicles.

One approach to assessing the risk of a collision during the prediction interval includes these steps *i)* predict potential trajectories for all vehicles in the traffic situation and *ii)* detect any collision between trajectories and derive a risk based on the overall chance of a collision. Perhaps the simplest risk estimation is expressed by using simple physics-based

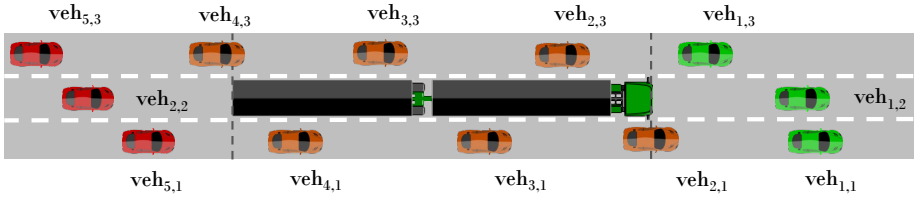

Figure 5.20: *How surrounding vehicles are addressed, based on lane and order.*

motion models that allow analytical solutions for intersections between trajectories. The risk of collision can then be expressed as a binary. However, for more complex motion models, collisions can also can be checked iteratively at each discrete time step. Moreover, the shape of the vehicle can be represented as polygons, ellipses or circles and risk expressed as the overlap between those shapes.

Based on the motion characteristics of articulated vehicles, specific criteria for methods and models for surrounding traffic and risk estimation are:

i) the method is valid in the range of typical subject vehicle manoeuvres. For example, as mention in Paper D, the duration of a smooth lane-change manoeuvre for an A-double is approximately in the range 6-8 s.

ii) the method can handle a large number of surrounding vehicles. Due to the LCV length, the number of surrounding vehicles interacting in a traffic scenario can be relatively large, see Fig. 5.20.

5.4.2 Design

In Papers B-D, the surrounding traffic motion of up to six vehicles was modelled using individual constant acceleration models. The surrounding vehicles were not allowed to change lane. Only single trajectories for each vehicle were simulated and no risk assessment was carried out.

For the driving automation used in the simulator experiment described in Paper E, the motion of the surrounding traffic was modelled using a concept of *dependent* and *independent* vehicles. The term independent is used for a vehicle that is positioned far enough, spatially and temporally, from another vehicle for its behaviour to be deemed significantly unaffected by the actions of the other vehicles. Conversely, a dependent vehicle is one that is close enough for its actions to be influenced by those of other vehicles. This distance is denoted as the dependency distance. An illustration of independent and dependent vehicles appears in Fig. 5.21. The motion for a dependent vehicle is assumed to follow the Intelligent Driver Model (IDM) (5.58)-(5.59)[120], while the motion of an independent vehicle is simulated using a constant acceleration model (5.57). The IDM is a deterministic traffic model for longitudinal motion, originating from research into

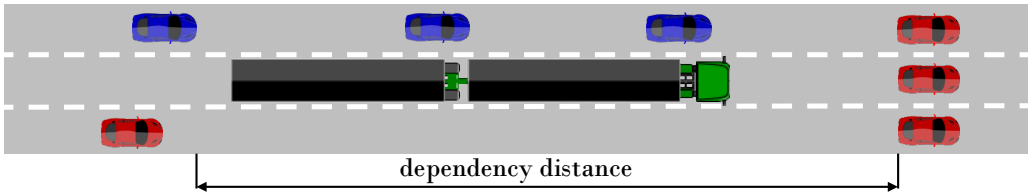

Figure 5.21: *An illustration of dependent and independent vehicles. Blue vehicles are dependant, and red vehicles are independent.*

microscopic traffic simulation. The model is described as

$$\dot{v}_\alpha = a^{(\alpha)} \cdot \left[1 - \left(\frac{v_\alpha}{v_0^{(\alpha)}} \right)^\delta - \left(\frac{s^*(v_\alpha, \Delta v_\alpha)}{s_\alpha} \right)^2 \right] \tag{5.58}$$

$$s^*(v, \Delta v) = s_0^{(\alpha)} + s_1^{(\alpha)} \cdot \sqrt{\frac{v}{v_0^\alpha}} + T^\alpha \cdot v + \frac{v \cdot \Delta v}{2 \cdot \sqrt{a^{(\alpha)} \cdot b^{(\alpha)}}} \tag{5.59}$$

where $\dot{v}_\alpha$ and v_α are the acceleration and velocity of vehicle α. $a^{(\alpha)}$ is the maximum acceleration, $v_0^{(\alpha)}$ is the desired velocity and δ is the acceleration exponent. $s^*(v_\alpha, \Delta v_\alpha)$ is the desired minimum gap and s_α is the gap. $s_0^{(\alpha)}$ and $s_1^{(\alpha)}$ are jam distances, T^α is the safe time headway and $b^{(\alpha)}$ is the desired deceleration. The model behaves as if accident-free and shows self-organised characteristics because of the inclusion of relative velocity. It includes five parameters that are reasonable interpretable and empirically measurable. Furthermore, in a traffic prediction an independent vehicle was modelled using two constant acceleration levels. Either it maintained the current acceleration, hereinafter called the *expected scenario*, or it braked with the maximum deceleration, called *emergency scenario*. The results from the emergency scenario were used to set the distance Δs_{safe}, used in the driver acceleration model (5.45), see Section 5.3.2. To consider one expected and one emergency scenario for each surrounding vehicle, N would lead to 2^N possible combinations. For the sake of simplicity, the work on driving automation (carried out in connection with the manual driving described in Paper E) did not consider different combinations. Instead, only one expected and one emergency scenario was used in the traffic situation predictions. The subject vehicle state-trajectories from previous update instant were included in the traffic predictions, so as to incorporate the interaction with the subject vehicle motion. A possible improvement of this approach may be assumed if the IDM parameters for each surrounding vehicle can be estimated online. More accurate collision risk estimation can be made using tools such as Monte Carlo simulation.

6 Traffic situation predictions

As mentioned in Section 4.2, *traffic situation predictions* (TSPs) refers to the complete set of functions included in FA-TSP. As the name suggests, TSPs are generated to predict how an observed traffic situation will evolve in the future. This includes the evolution of both subject vehicle and surrounding traffic. The objective is to generate feasible manoeuvres for the subject vehicle in such way that the vehicle motion fulfils requirements such as safety, efficiency and ride comfort. The time horizon for TSPs, partially determined by manoeuvre durations and the reliability of predicting surrounding traffic, are in the range 0-10 s for long combination vehicles. Section 6.1 gives a brief background and discuss possible approaches for TSPs. Section 6.2 presents the specific TSP design used in Papers B-D. Section 6.3 presents the main results of Papers B-D.

6.1 Background

Fundamental terms are outlined and discussed by way of a review of possible approaches for TSPs. A **manoeuvre** is a high-level characterisation of the vehicle motion [58]. In this work, **vehicle actuation** refers to the front wheel steering angle and the longitudinal acceleration of the first vehicle unit. Actuation capabilities are the upper and lower limits of the actuation. A candidate actuation request is the actuation generated in the traffic situation predictions, satisfying given constraints.

The attributes that uniquely define the position and orientation of the vehicle body according to an inertial coordinate frame are termed the configuration vector [58]. A configuration vector can be selected which is identical to the generalised coordinates, see Section 5.2.2. All sets of configurations constitute the configuration space. A **path** [58] is a geometric trace (including orientation) that a specific position of the vehicle, say, the centre of the first or the last vehicle axle, should follow whilst satisfying given constraints. The constraints are typically connected to the ODD, see Section 3.2, including traffic rules, road and lane boundaries, surrounding traffic assumptions, static obstacles, vehicle motion and actuator capabilities. Consequently, the **path planning** problem is to find a path in the configuration space that starts at the initial configuration and reaches the target region whilst satisfying the given constraints. The quality of the path is often described using the terms feasible and optimal. Feasible means that the path satisfies the given constraints while optimal refers to finding the best path according to a given cost function.

In this context, a **state trajectory** [111] can be interpreted as a generalisation of a path; prescribing the evolution of the states of a dynamic system in time. As an example, typical states for a one-track single-unit vehicle model can be chosen as the yaw rate and lateral and longitudinal velocities of the first vehicle unit's CoG, see Section 5.2.2. The path of first vehicle unit's CoG can be calculated by integrating the state trajectory given initial state values. **Trajectory planning** (also known as trajectory generation or motion planning) is a generalisation of path planning, involved with planning the state evolution in time while satisfying given constraints on the states and possibly the actuation. In this work **actuation trajectory planning** refers to generating a sequence

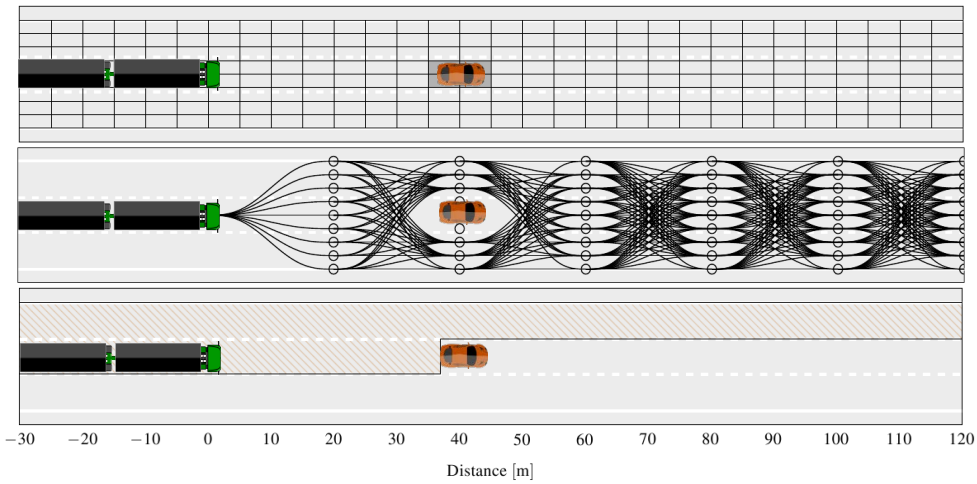

Figure 6.1: *Examples of search spaces. Occupancy grid (top), state lattice (middle) and driving corridor (bottom).*

of feasible control signals for vehicle actuation, whereas **state-trajectory planning** is unambiguous as per trajectory planning outlined above.

The scope and realisation of TSPs are likely to be different depending on the targeted driving automation application. In many cases, methods of path, trajectory and actuation trajectory planning are combined. In [119], local path planning was carried out within estimated road boundaries to generate candidate paths. The candidate paths were run through a vehicle model, meaning that state trajectories were calculated, to ensure kinematic and dynamic vehicle constraints. Finally, vehicle actuations were calculated for velocity control and steering control. In case of steering control, the control law is similar to the driver model proposed by Kondo in 1953 [62]. For further details on the driver model, see [12].

As mentioned in Section 4.1, a passive world model representing an instant observation of a given traffic situation is generated by the perception component. In VeMFRA, this is similar to functionalities associated with FA-TSO. Based on such observation, a search space [63] can be formulated in which path or trajectory planning are carried out. An overview of motion planning approaches is given in [58, 99]. Examples of discrete search space formulations are occupancy grids [130] and state lattices [43], see Fig 6.1. One example of continuous search spaces is driving corridors [72], see Fig 6.1. In an occupancy grid, the environment is discretised into a grid, where each cell in the grid can be associated with a probability of being occupied by an obstacle. State lattices are constructed using segments that connect possible states of the vehicle whereas driving corridors are represented as continuous collision-free spaces bounded by lane-boundaries and obstacles.

The use of different methods of path and trajectory planning is coupled with the chosen representation of search space. Given an occupancy grid or a state lattice, **graph search** algorithms such as Dijkstra [69] or A* [44] can be used to explore the state space

to find a relevant trajectory for the traffic situation. Possible drawbacks are that the planned trajectories may requires smoothing and that the search algorithm may entail a high computational cost, since the number of graph nodes grows exponentially with the number of states [87]. In [43], a two-step trajectory planning is carried out using a state lattice approach accounting for road geometry, obstacles and high-level directives. Based on the result from the first-step state lattice optimisation, a second trajectory planning step is carried out in which trajectories are selected that satisfy kinematic constraints for a single-unit vehicle.

Incremental search methods avoid an explicit representation of the environment. Instead, these methods build a graph based on random sampling. This relies on a collision-checking module that provides information about the feasibility of candidate trajectories [57]. The rapidly-expanding random tree (RRT) method, introduced by LaValle et al. [64], can include both kinematic and dynamic constraints. In [55], an RRT* algorithm [57] was implemented in combination with a single-unit one-track model for autonomous high-speed driving.

In methods based on **numerical optimisation**, used in combination with driving corridors, the trajectory planning problem can be formulated as a constrained optimal control problem. If the constrained optimal control problem is solved online at each time step to determine the actuation over a fixed horizon, the method is referred to as model predictive control (MPC) [16]. In [38], a non-linear MPC was designed for lane-keeping and obstacle avoidance for a passenger car. In [85], MPC was used for longitudinal and lateral trajectory planning for a passenger car by formulating two loosely coupled MPC problems. In this work, a non-linear MPC formulation was used for actuation trajectory planning in connection with Papers C and D.

A **heuristic** approach to the actuation trajectory planning problem, used in combination with driving corridors, would be to use simulations of a vehicle model in combination with steering and longitudinal acceleration control, by using the controllers described in [119] for example. In the case of multiple-lane one-way roads, the lane centrelines constitute possible reference paths for the driving. The planning problem can be approached as how to execute maintain-lane driving and how and when to make transitions between lanes (lane-change manoeuvres for example), such that the target destination can be reached efficiently, safely and comfortably. A heuristic approach was used in this work for actuation trajectory planning in Papers B-E.

To illustrate alternative TSP realisations, examples of two driving automation applications are given. Both assume the presence of traffic observations as well as strategic and control functionalities; FA-TSO, FD-RSiM and FD-VMM. It is assumed that FD-RSiM only provides sparsely separated waypoints. In other words, local path and trajectory planning is carried out by the TSP. Moreover, the request interface to FD-VMM entails actuation trajectories in longitudinal acceleration and the front wheel steering angle.

As a first example, consider automated low-speed manoeuvring of an articulated vehicle in a logistics area, see Fig. 6.2a. In this example, the objective is to manoeuvre the vehicle from its current configuration A to the target configuration B, without interfering with static objects. It is preferable for the manoeuvring to be carried out using the fastest route or the one with the shortest distance and a minimal amount of change in driving direction, such as driving forward and reversing. For this type of application, it is

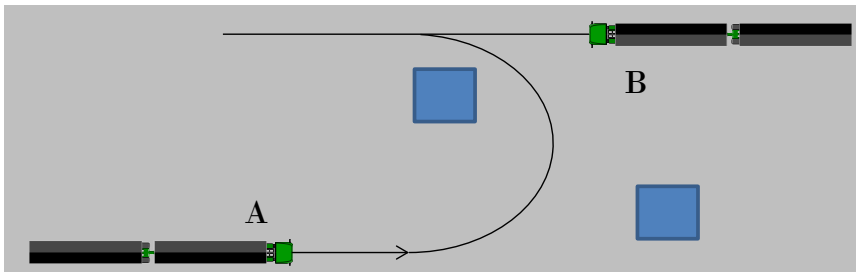

(a) *Illustration of driving automation at low-speed where the reference path, when driving from configuration A-B, has to be planned. The planned path of the centre of the first axle is shown in solid black.*

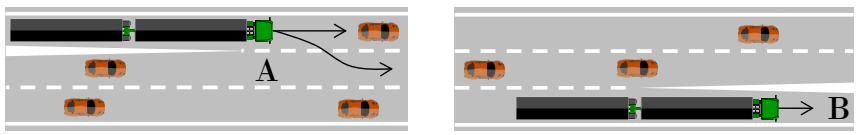

(b) *Illustration of driving automation at high-speed on a multiple-lane one-way road. The lane centrelines constitute candidate reference paths.*

Figure 6.2: *Examples of two driving automation applications.*

important that no pre-defined reference path exists that can be used in the navigation task. Moreover, low vehicle speed means that a kinematic vehicle model can be appropriate as a prediction model. A possible solution approach for this application would be to combine path and trajectory planning (for generation of a local path and trajectory) and convert the trajectory to vehicle actuation, which can be used as a request to FD-VMM. Whether or not path and trajectory need to be updated during the manoeuvre execution depends on the environment as well as on how the vehicle actually moves. Examples of similar approaches used for articulated vehicles are found in [47, 102, 83]. In [47] a Nordic combination vehicle is considered and the presence of surrounding objects is rejected. Pre-defined clothoid path-segments are combined to find the shortest possible path between initial and target configuration. The vehicle states and steering angle are calculated based on the path, using an approximate method. Moreover, an LQ controller with feedforward action is used to track the generated states. In [102], a B-double combination vehicle is given as an example and the presence of surrounding static objects is possible. Pre-defined path segments are used with a state lattice approach to find a candidate path. The path is checked for collisions using vehicle model simulation and the path changed as necessary. In [83], a bug-like path planning algorithm is used in combination with model predictive control. The planning algorithm considers the vehicle kinematics as well as surrounding objects and the model predictive control approach is used to transform the path into an actuation trajectory.

As a second example, consider automated driving of an articulated vehicle on a multiple-lane one-way road between an entry ramp and an exit ramp, see Fig.6.2b. One important distinction compared with the first example is that the general path/trajectory

planning problem is in some sense different. In this case, the road lanes constitute possible reference paths for the driving. The planning problem can instead be considered as how and when to make lane transitions, or lane-change manoeuvres, such that the target destination can be reached efficiently, safely and comfortably. Furthermore, given the uncertainties involved with the predicted motion of the surrounding vehicles (if manually driven) any plan is assumed to be valid only for a short period of time. Furthermore, the vehicle speed vary between zero and the maximum speed limit (in Sweden 80 km/h is the maximum speed for articulated heavy vehicles). In the case of vehicle modelling this means that a kinematic model is not sufficient for capturing the dynamic characteristics of an articulated vehicle at high-speed. Instead, a model like the one described in Section 5.2.2 can be used. Additionally, the preferred manoeuvre in the first example often consists of executing the fastest or shortest route. The preferred manoeuvre in the second example is less obvious, given the vehicle speed and consequences in the event of a system failure.

6.2 Design

In this work, the driving under consideration is limited to one-way multiple lane roads and subject vehicle speeds in the range of 0-80 km/h. The road curvature used in the simulator experiments described in Papers D and E are given in Fig. 5.2. Furthermore, the manoeuvres included are: maintain-lane, lane changes, non-evasive abort lane changes and fall-back braking. Process and measurement noise are ignored and it is assumed that FA-TSO can accurately estimate the signals given in the motion architecture, see Fig. 6.3.

The input to FA-TSP from FA-TSO consists of the road speed limit and observations of surrounding traffic in terms of number of vehicles and their motion states. Also, road data in terms of the subject vehicle position in lane, lane width, lane curvature in front of and behind the subject vehicle, road slope and number of adjacent lanes. Moreover, the input from FA-TSO consists of actual subject vehicle states. It is envisaged that the input could also include actuation and motion capabilities and road friction. The signals from the FA-TSP are one or more candidate actuations and their feasibility.

In Papers B-E, two main approaches for actuation trajectory planning have been used. The first one is based on driver modelling and closed-loop simulations including constraint verification. However, the driver model parameters used are fixed and represents a professional driver during normal maintain-lane or lane-change manoeuvring. A limitation of this approach is that if a specific candidate actuation is infeasible no re-planning is made to generate a new possible solution. Instead, the FA-TSM is restricted using a fall-back solution. In Papers B-D a trivial solution including hard braking was used as a fall-back. This approach was further extended, with a gain factor search method for the driver steering model based on particle swarm optimisation (PSO) [126]. The fundamental idea was to find an acceptable set of gain factors for a given traffic scenario. The second approach uses non-linear model predictive control. Both approaches follow the motion architecture described in Fig. 6.3 and were implemented in C++. The approaches were studied using desktop simulations in Matlab/Simulink in Papers B and C and in a driving simulator environment with real-time performance in Papers D and E. Paper C compared the performance of vehicle dynamics for the two approaches.

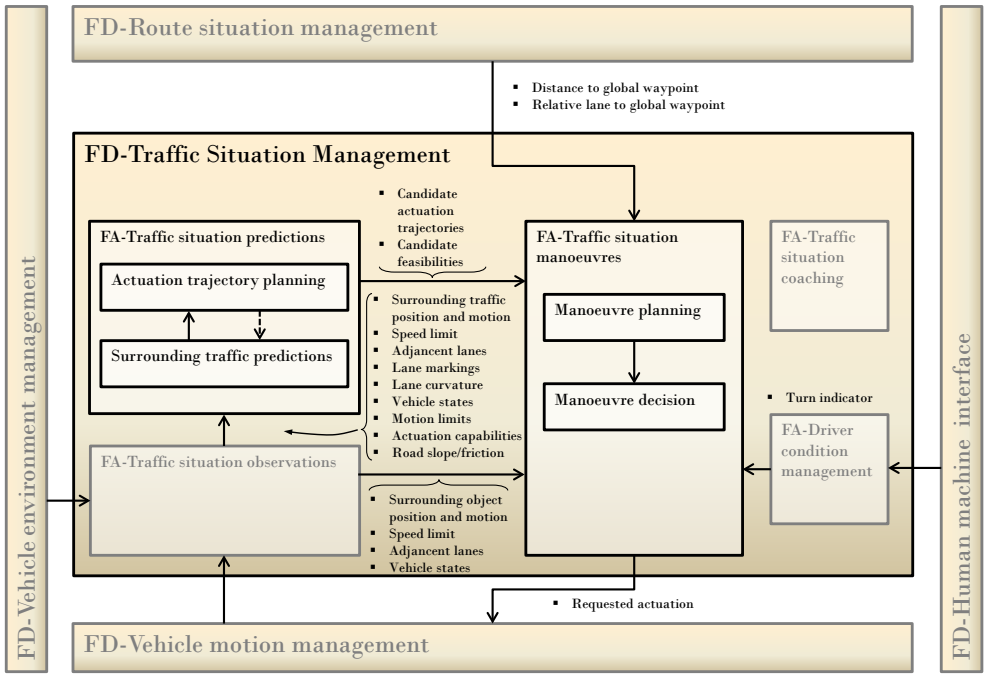

Figure 6.3: *Illustration of the motion architecture including functional domain traffic situation management (FD-TSM).*

As briefly stated in Section 6.1, the main concept of model predictive control (MPC) is to use a model of the system to predict its future evolution. The system model and other relevant constraints are used in conjunction with a cost function to formulate an optimal control problem. The optimal control problem is solved on-line for a finite horizon. The first such calculated optimal actuation is applied to the controlled system, at time t. At the next controller update instant, time $t + \Delta t$, a new optimal control problem is solved for a shifted finite horizon [16]. This process is then repeated. In this context, the benefits of MPC are that it can factor in various control objectives as well as constraints [16]. The drawbacks are the computational burden involved in the numerical optimisation, non-linear dynamics and constraints.

A simplified illustration of the two approaches and their components is given in Fig. 6.4. This illustration does not claim to be complete but focuses on main similarities and differences. In the MPC-based approach, the *model* consists of differential equations representing the road and subject vehicle, see Section 5.2.1. The *constraints* are related to vehicle motion, actuation limits and surrounding traffic. The components of the *cost function* attempt to result in satisficing[1] [113] solutions for the human occupant. This can

[1]Satisficing is defined here as the comfort zone in which the driver is content with good-enough behaviour. Comfort here refers to attributes such as being relaxed, safe and the feeling of being in control.

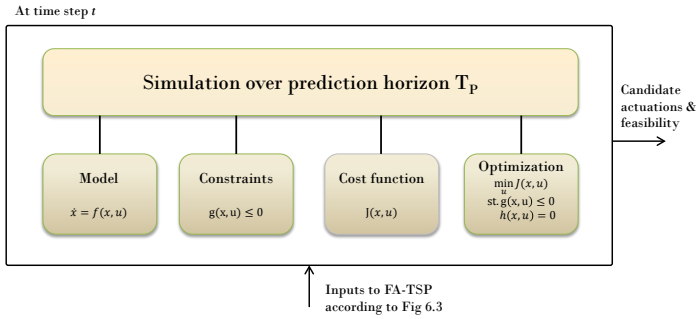

(a) *Model predictive control-based actuation trajectory planning.*

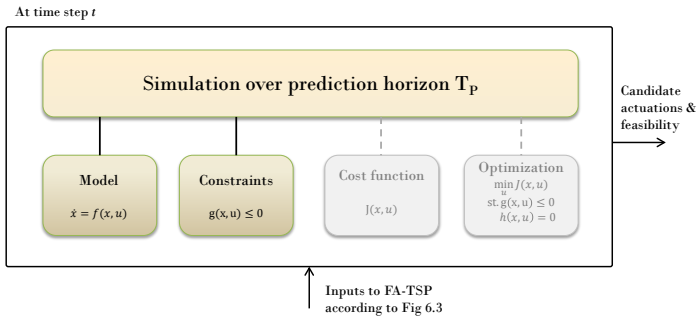

(b) *Driver model-based actuation trajectory planning.*

Figure 6.4: *Simplified illustration of the two actuation trajectory planning approaches and their components. The driver model-based actuation trajectory planning approach can be used both with and without a cost function and optimisation.*

lead to conflicting objectives in the cost function, such as tracking versus comfort. Using an *optimisation* algorithm results in a search of candidate solutions within the solution domain, where the candidate with lowest cost is selected.

In the driver model-based approach, the *model* consists of differential equations representing the road, subject vehicle and the driver, see Sections 5.2.1-5.3.2. The model constitutes a closed-loop system which can be simulated by choosing appropriate reference parameters for the driver model. These parameters are based on heuristics as well as the position of the surrounding vehicles. The *constraints* related to vehicle motion, actuation limits and surrounding traffic are verified during the simulation. Regarding the extended driver-model-based approach, a *cost function* is formulated which aimed to result in solutions in which the driver steering model gain factors are as close as possible to the desired gains. An *optimization* algorithm is used to search candidate solutions within the solution domain and the candidate with lowest cost is selected.

In the driving simulator environment, the driver modelling approach used a prediction

horizon of 3.75 s and was updated at 20 Hz. The non-linear model predictive control approach used a prediction horizon of 100 m and was updated every 2 m. Driving at 20 m/s, this corresponds to a prediction horizon of 5 s and a control rate of 10 Hz. The approaches are described further in Sections 6.2.1-6.2.3.

The constraints for the subject vehicle actuation trajectory planning consist of:

i) keeping the vehicle motion within specified limits (6.1)-(6.5).

ii) keeping the actuation within capability limits (6.6)-(6.7).

iii) avoiding collisions with the surrounding traffic[2] e.g. (6.8).

Using mathematical notation, the constraints for the subject vehicle actuation trajectory planning can be written as:

$$\underline{v}_x \leq v_{\mathrm{Xv1}} \leq \overline{v}_x \tag{6.1}$$
$$-\overline{a}_y \leq a_{\mathrm{Yv}11} \leq \overline{a}_y \tag{6.2}$$
$$-\overline{a}_y \leq a_{\mathrm{Yv}n1} \leq \overline{a}_y \tag{6.3}$$
$$\underline{d} \leq d_{\mathrm{R}11} \leq \overline{d} \tag{6.4}$$
$$\underline{d} \leq d_{\mathrm{R}n1} \leq \overline{d} \tag{6.5}$$
$$\underline{a}_x \leq a_{\mathrm{Xv1}}^{\mathrm{req}} \leq \overline{a}_x \tag{6.6}$$
$$-\overline{\delta} \leq \delta_{11}^{\mathrm{req}} \leq \overline{\delta} \tag{6.7}$$
$$\underline{\Delta s}_{m,n}^{(o)} \leq \Delta s_{m,n}^{(o)} \tag{6.8}$$

where v_{Xv1} is the longitudinal velocity of the first unit's centre of gravity. $a_{\mathrm{Yv}11}$ and $a_{\mathrm{Yv}n1}$ are the lateral accelerations of the first unit's first axle and the nth unit's last axle, respectively. $d_{\mathrm{R}11}$ and $d_{\mathrm{R}n1}$ are the lateral distance offset, perpendicular to the road for the first unit's first axle and nth unit's last axle respectively. $a_{\mathrm{Xv1}}^{\mathrm{req}}$ and $\delta_{11}^{\mathrm{req}}$ are the requested candidate actuation for acceleration and steering. In case of a lead vehicle, $\Delta s_{m,n}^{(o)}$ is the distance between the rear of the surrounding vehicle and front of subject vehicle. In case of a lag vehicle, $\Delta s_{m,n}^{(o)}$ is the distance between front of the surrounding vehicle and rear of the subject vehicle.

6.2.1 Driver model-based TSP

Traffic situation predictions are conducted using simulations, see Fig. 6.6, including models of **road**, **subject vehicle**, **driver** and **surrounding traffic**. The model representations are described in Section 5. In the implementation presented in Papers B-D, and in the automated driving connected to Paper E, the longitudinal vehicle dynamics described under Section 5.2.2 were simplified in respect of resistance, brake and propulsion forces. When driving on roads with considerable horizontal or vertical curvatures, such simplifications are less possible.

[2]The constraints used for collision avoidance are different in driver model-based TSP and MPC-based TSP, see Paper D.

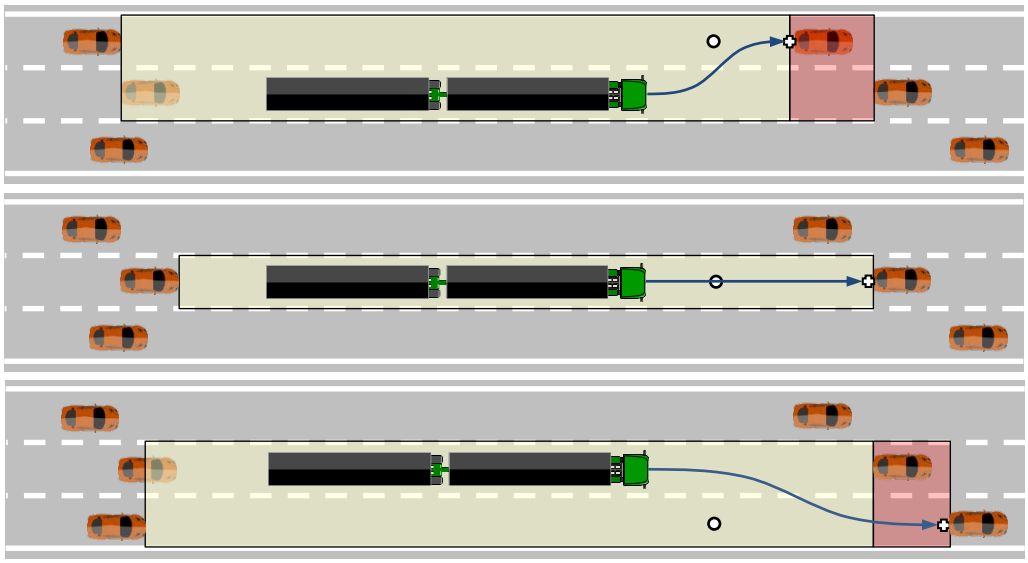

Figure 6.5: *Illustration of driving corridors (yellow areas) for adjacent left-hand lane (top), current lane (middle) and adjacent right-hand lane (bottom), used in each TSP update. White crosses and circles represent the initial far and near-points used in the driver steering model. In case of a lane change prediction, the velocity and distance of the closest lead vehicle is used in the driver acceleration model. The closest lead vehicle is represented with a red area. The blue arrow illustrates the path of the first vehicle's axle centre.*

Consider the highway traffic scenario given in Fig. 6.5. The subject vehicle is driving in the middle lane and has one adjacent lane on either side. When the TSP calculation is started or updated, observed signals are available from FA-TSO.

Firstly, the motion of the surrounding traffic is simulated. In Papers B-D, the motion of surrounding traffic (up to six vehicles) is modelled using constant acceleration models. Only single trajectories for each vehicle are simulated and no risk assessment is carried out. In the driving automation carried out in connection to the manual driving described in Paper E, the surrounding traffic is instead modelled using the concept of dependent and independent vehicles, see Section 5.4.2.

Secondly, three candidate actuation trajectories are calculated by simulating the road, subject vehicle, and driver models. Each candidate actuation trajectory aims for one manoeuvre, such as maintain-lane, lane-change to right and left. Each simulation is made using observed data of initial states and driver model longitudinal and lateral reference parameters corresponding to either the current lane, adjacent right-hand lane or adjacent left-hand lane, see Fig 6.5. The reference parameters for lateral distance used in the driver steering model are the centrelines of the relevant lane. The reference parameters for distance and velocity used in the driver acceleration model are the relative distance

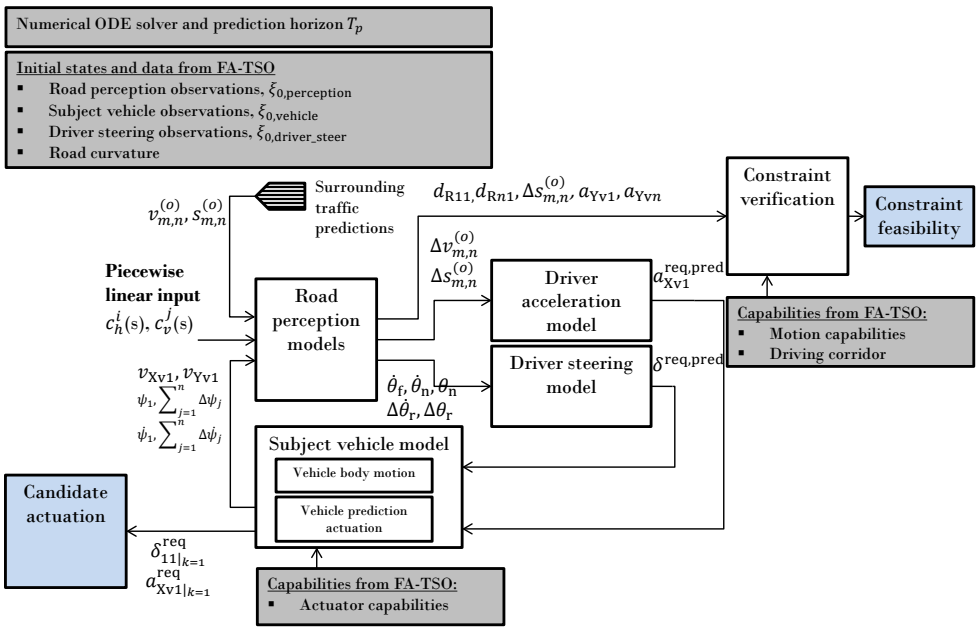

Figure 6.6: *Illustration of a simulation including models of road, driver and subject vehicle, used in the driver model-based TSP calculation.*

and velocity of the closest vehicle ahead in the relevant driving corridor, see Fig. 6.5. In cases where there is no vehicle ahead, the driver acceleration model is shifted to speed control. In Papers B-D, the safety distance used in the driver acceleration model is fixed. In the driving automation carried out in connection with the experiment in Paper E, the safety distance is calculated by assuming emergency braking of the closest vehicle ahead in the relevant driving corridor. The simulations are conducted for a specified prediction horizon T_p using the forward Euler integration method. For each time step in a simulation, the solution is verified against the feasibility constraints (6.1)-(6.8). If any constraint is violated, the specific simulation is stopped and the corresponding candidate actuation request is considered infeasible. The outputs from the TSPs are candidate actuation requests and their feasibility in three individual manoeuvres.

It is likely that using driver models inspired by human cognition in the calculation of TSPs can enable high driver/operator acceptance, considering the manoeuvre execution. If the TSPs are realised in a product aiming for driver-steering assist, such as a lane guidance system, the included driver model can provide good intuitive performance [135]. A possible drawback and limitation of the method is that should a specific proposed actuation be infeasible, no re-planning is made to generate a new prospectively feasible solution. The FA-TSM is restricted to use a fall-back solution instead.

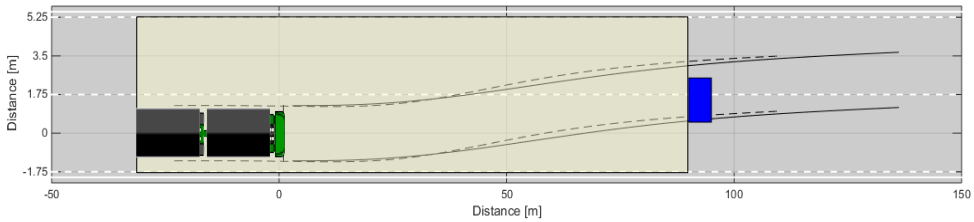

Figure 6.7: *Illustration of a traffic situation in which the candidate actuation-trajectory for a lane change to the left adjacent lane is infeasible. The yellow area is the driving corridor. Black solid and dashed lines are one the left and right sides of the first and last vehicle unit respectively. The blue square represents a static obstacle.*

6.2.2 Driver model-based TSP using driver-steering-model gain factor optimisation

Driver steering and acceleration models, including their use in actuation trajectory calculations for articulated heavy vehicles, were discussed in Section 5.3. Requirements of such driver models include their ability to generate transparent, intelligible vehicle behaviour for a set of targeted highway vehicle manoeuvres. Moreover, the models should preferably include few physically interpretable parameters. This work hypothesises that these requirements can be met by choosing driver models that include, or are correlated to, primitive visual input cues and are based on human cognition. In the driver model-based TSP calculation, discussed in Section 6.2 above, the gain factors of the driver models are fixed and represent a professional driver during normal maintain-lane or lane-change manoeuvring. However, if a candidate actuation is infeasible no re-planning for the targeted manoeuvre is made during the FD-TSM update instant being considered.

One example of a traffic situation that would lead to a vehicle standstill (when using the driver model-based TSP) is illustrated in Fig. 6.7. In the example, the vehicle is driving at a speed of 80 km/h in maintain-lane state and the actuation trajectory calculation seeks a feasible candidate actuation for a lane-change manoeuvre to the adjacent left-hand lane. In this case, the candidate actuation for the lane-change manoeuvre is infeasible due to a collision with a static obstacle positioned 90 m in front of the subject vehicle. The vehicle will therefore continue in maintain-lane state and stop behind the obstacle. However, in the current situation, there is enough space for the vehicle to maintain a constant speed and pass the obstacle on the left-hand side if another, more aggressive, steering actuation is considered.

From a driver behaviour perspective, the gain factors of the driver steering and acceleration models are assumed to be interpretable as driver aggressiveness, given a specific traffic situation [76]. Based on this assumption, a viable option to extend the driver model-based TSP calculation and address actuation infeasibility is to test different sets of driver model gain factors for a targeted manoeuvre.

In the driver steering model (5.46), see Section 5.3.2, the steering wheel angle rate is calculated as a linear combination of three error terms that originate from the visual angles of one near and one far point. The model expresses the steering wheel angle rate

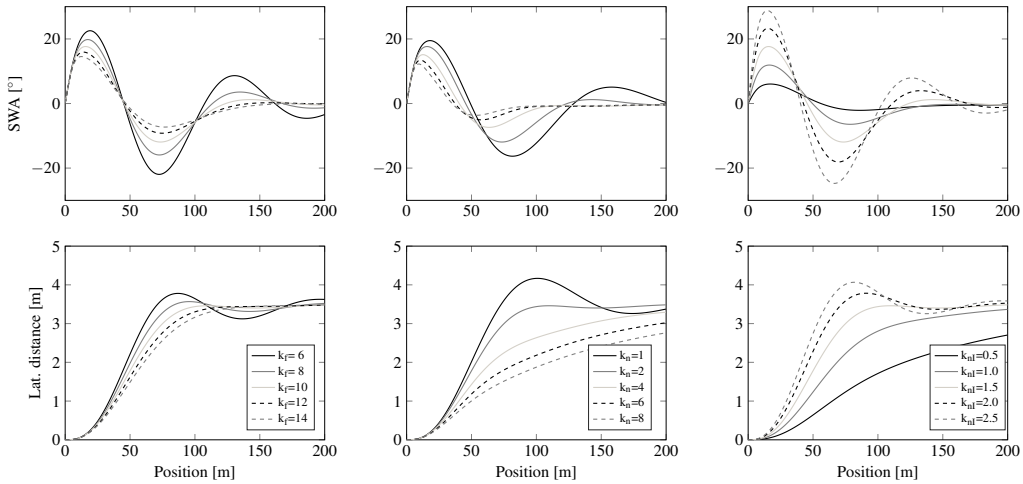

Figure 6.8: *Simulations of a lane change to an adjacent left-hand lane using an A-double at* 80 km/h. *The simulations are executed using different gains in the driver steering model* (5.46). *Top row: steering wheel angle. Bottom row: lateral distance to the centre of the first unit's first axle.*

that aims to reduce the near point angle to zero and keep the angles of both the near and far point constant over time. As an example of the driver steering model behaviour, a lane-change manoeuvre to an adjacent left-hand lane is simulated and illustrated in Fig. 6.8. In the simulation example, the subject vehicle's speed is 80 km/h. The driver model's near point is positioned 5 m ahead and initially 3.5 m to the left of the subject vehicle. The driver model's far point is positioned 44 m ahead and initially 3.5 m to the left of the subject vehicle. In Fig. 6.8, the top row shows the steering wheel angle and the bottom row shows the lateral displacement of the centre of first unit's first axle. The steering gain factors $k_\mathrm{f}, k_\mathrm{n}$ and k_nI, are varied individually. The left-hand column shows variations of k_f, middle column k_n and the right-hand column k_nI. By varying the gains, different driver-vehicle behaviour can be achieved during the lane-change manoeuvre.

Returning to the discussion on the lane-change manoeuvre to the left-hand lane illustrated in Fig 6.7. One possible approach to increasing the search for feasible actuation trajectories in driver model based TSP calculation, would be to test the targeted manoeuvre using tabulated driver model gain factors. The driver model gains could be chosen to represent different driver aggressiveness levels. Another possible approach would be to formulate the search for feasible actuation trajectories as a constrained optimisation problem, defined as

$$\begin{aligned} \min_{\mathbf{x}} \; & J(\mathbf{x}) \\ \text{s.t.} \quad & g_i(\mathbf{x}) \leq 0 \quad i = 1, ..., m \end{aligned}$$

where $\mathbf{x} \in \mathbb{R}^n$ is the optimisation variable, $J(\mathbf{x})$ is the cost function $J : \mathbb{R}^n \to \mathbb{R}$ and $g_i(\mathbf{x})$ are the constraint functions $g_i : \mathbb{R}^n \to \mathbb{R}, i = 1, ..., m$.

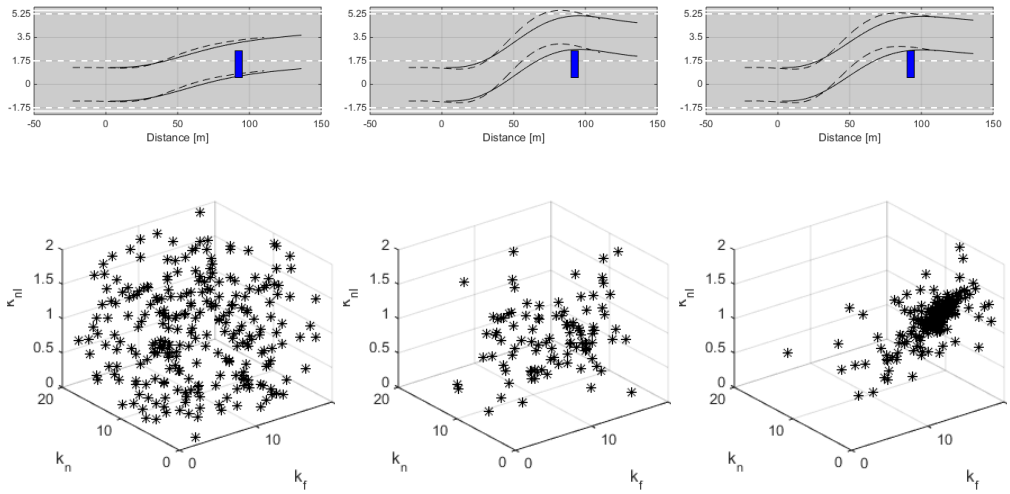

(a) *Iteration 0* (b) *Iteration 10* (c) *Iteration 20*

Figure 6.9: *Illustration of driver steering model gain factor selection using PSO for a lane change to the adjacent left-hand lane. The top row shows X and Y coordinates for the left and right-hand side of first unit's first axle (solid) and last unit's last axle (dashed) at iteration steps 0, 10 and 20. The bottom row shows the gain factors.*

A proposed cost function for the optimisation problem is

$$J(\mathbf{x}) = \sqrt{\frac{(k_{\mathrm{f,des}} - x_1)^2 + (k_{\mathrm{n,des}} - x_2)^2 + (k_{\mathrm{nI,des}} - x_3)^2}{k_{\mathrm{f,des}}^2 + k_{\mathrm{n,des}}^2 + k_{\mathrm{nI,des}}^2}} \tag{6.9}$$

where $\mathbf{x} = [x_1,\ x_2,\ x_3]$, $\mathbf{x} \in [\overline{\mathbf{x}}, \underline{\mathbf{x}}]$. Furthermore, $k_{\mathrm{f,des}}$, $k_{\mathrm{n,des}}$ and $k_{\mathrm{nI,des}}$ are the desired gain factors for normal driving. The constraints $g_i(\mathbf{x})$ are vehicle motion and actuation constraints (6.1)-(6.8).

In the lane change example illustrated in Fig 6.7, the driver model gain factor search was carried out using a PSO algorithm [126] including a penalty method for handling the inequality constraints. In the PSO algorithm (which is a stochastic optimisation method) each candidate solution, often referred to as a particle, is encoded with a position and a velocity in the defined search domain. Each candidate is evaluated against an objective function to obtain a performance. Based on the particle performance, the velocity and position are updated at each iteration step. Due to its highly parallel nature, the PSO algorithm is well-suited to implementation in graphics processing units (GPUs), see example in [124]. Fig. 6.9 shows the results from a PSO search which included 256 particles and 20 iterations. The top row shows the left and right-hand side paths of the first unit's first axle (solid) and last unit's last axle (dashed). The different columns illustrate the results at iterations 0, 10 and 20. The bottom row shows the gain factors for each iteration.

In the driving automation carried out in connection to the manual driving described in Paper E, an actuation trajectory search method (similar to the one described in the

example above) was used [8]. The PSO optimisation was implemented on an external GPU (AMD Radeon R9 380X), using the Open computing language (OpenCL) [80]. At each FD-TSM update instant, the gain factors for two candidate actuation trajectories were calculated using 2000 particles and 3 iterations.

6.2.3 Model predictive control-based TSP

Traffic situation predictions are carried out using simulations of the surrounding traffic followed by actuation trajectory planning using non-linear model predictive control (NMPC). The NMPC formulation includes models of the **subject vehicle** and **road** as well as pre-calculated trajectories of the **surrounding vehicles**. In the implementation presented in Papers C and D, the longitudinal vehicle dynamics described in Section 5.2.2 was simplified in regard to resistance, brake and propulsion forces.

When the TSP calculation is started or updated, observed entities are available from FA-TSO. Firstly, the motions of the surrounding traffic are simulated using individual constant acceleration models. Only single trajectories for each vehicle are simulated and no risk assessment is carried out. Secondly, the candidate actuation trajectory is calculated for one manoeuvre. For example, either maintain-lane manoeuvring or a lane-change manoeuvre. A constrained optimal control problem (OCP) is formulated which describes the desired motion of the vehicle for a finite future horizon. The OCP is transcribed into a non-linear program using a multiple shooting integration technique [15]. The cost function for the infinite dimensional optimal control problem is formulated as [3]

$$\begin{aligned}\min_{\xi,\mathbf{u}} \int_{t=0}^{T_\mathrm{p}} \Big(& K_{d_{\mathrm{R}11}} \cdot (d_{\mathrm{R}11} - d_{\mathrm{R}11,\mathrm{ref}})^2 + K_{d_{\mathrm{R}j1}} \cdot (d_{\mathrm{R}j1} - d_{\mathrm{R}j1,\mathrm{ref}})^2 \\ & + K_{v_{\mathrm{Xv1}}} \cdot (v_{\mathrm{Xv1}} - v_{\mathrm{Xv1,ref}})^2 + K_{j_{\mathrm{Xv1}}} \cdot (j_{\mathrm{Xv1}})^2 + K_{j_{\mathrm{Yv1}}} \cdot (j_{\mathrm{Yv1}})^2 \\ & + K_{a_{\mathrm{Xv1}}} \cdot (a_{\mathrm{Xv1}})^2 + K_{\dot{\delta}} \cdot \dot{\delta}_{11}^2 + \sum_{k=1}^{3} K_{\Delta s} \cdot \Big(f_{\mathrm{dk}} \left(\Delta s_{m,n}^{(o)}, v_{\mathrm{Xv1}} \right) \Big)^2 \Big) \mathrm{d}t \end{aligned} \tag{6.10}$$

where ξ and $\mathbf{u}$ are the vehicle state and actuation vectors. The first two terms in (6.10) can be related to a lane-change efficiency or tracking objective. The reference trajectories $d_{\mathrm{R}11,\mathrm{ref}}$ and $d_{\mathrm{R}j1,\mathrm{ref}}$ are the lane centreline (in case of maintain-lane manoeuvring) and the analytical solution to a point-mass system minimising the lateral jerk (in case of a lane-change manoeuvring). The reference trajectory $v_{\mathrm{Xv1,ref}}$ is based on heuristics that include the speed limit, lateral acceleration caused by road curvature and comfortable lead vehicle following. The variables j_{Xv1} and j_{Yv1} are approximations of the longitudinal and lateral jerk, expressed relative to a local coordinate frame positioned at the CoG of the first vehicle unit. The $\dot{\delta}_{11}$ is the road wheel angle rate. These terms promote smooth and comfortable driving. The term $f_{\mathrm{dk}}(\Delta s_{m,n}^{(o)}, v_{\mathrm{Xv1}})$ is related to distance-keeping and safety, see illustration of distance-keeping in a lane-change-to-right scenario in Fig. 6.10.

[3] In Paper C and [25], the dynamic models are reformulated from the temporal domain to a spatial domain. For the sake of simplicity, the formulation here is in the temporal domain.

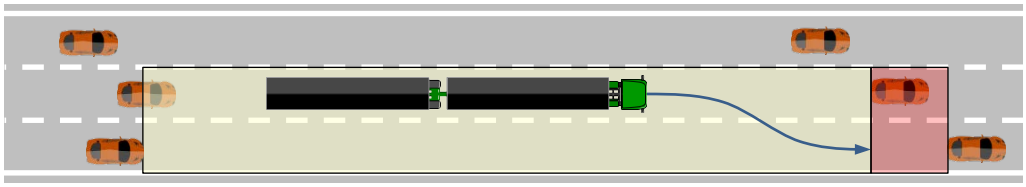

Figure 6.10: *Illustration of the driving corridor (yellow area) in a lane-change-to-the-right situation using NMPC. The corridor is calculated using the lead vehicle in the current lane and lead and lag vehicles in the target lane. For further details see [123]. The blue arrow illustrates the path of the centre of the first vehicle's axles.*

The balance between efficiency, comfort, and safety is weighted with the following factors: $K_{d_{\mathrm{R}11}}$, $K_{d_{\mathrm{R}j1}}$, $K_{v_{\mathrm{Xv}1}}$, $K_{j_{\mathrm{Xv}1}}$, $K_{j_{\mathrm{Yv}1}}$, $K_{a_{\mathrm{Xv}1}}$, $K_{\dot{\delta}}$ and $K_{\Delta s}$.

In direct multiple shooting integration technique, both state trajectory and control input are discretised for the prediction horizon. The system is separately integrated for each interval between the discretisation nodes and continuity constraints between the intervals are introduced. Using the models of the subject vehicle and road, the non-linear system dynamics are discretised using the Euler method to the form

$$\xi(t+1) = f^{\mathrm{dt}}(\xi(t), \mathbf{u}(t)) \tag{6.11}$$

A cost function for the finite time optimal control problem is formulated as

$$J_0(\xi_{t|t}, \mathbf{U}_0) = \sum_{k=1}^{N} \|\xi_{t+k|t} - \xi^{\mathrm{ref}}_{t+k|t}\|^2_{\mathbf{Q}_{\mathrm{MPC}}} + \sum_{k=0}^{N-1} \|\mathbf{u}_{t+k|t} - \mathbf{u}^{\mathrm{ref}}_{t+k|t}\|^2_{\mathbf{R}_{\mathrm{MPC}}} \tag{6.12}$$

where, using standard MPC notation according to [16], $\mathbf{U}_0 = [\mathbf{u}'_0, ..., \mathbf{u}'_{N-1}]$ is the optimisation vector and N is the prediction horizon. $\xi_{t+k|t}$ and $\mathbf{u}_{t+k|t}$ are the state and actuation vector at time $t+k$ measured at time t, respectively. $\xi^{\mathrm{ref}}_{t+k|t}$ and $\mathbf{u}^{\mathrm{ref}}_{t+k|t}$ are the corresponding reference vectors. $\mathbf{Q}_{\mathrm{MPC}}$ and $\mathbf{R}_{\mathrm{MPC}}$ are weighting matrices of appropriate dimensions constituting the gain factors in (6.10).

At each time step t the following constrained finite time optimal control problem is solved

$$J^*_0 = \min_{\mathbf{U}_0} J_0(\xi_{t|t}, \mathbf{U}_0) \tag{6.13}$$

$$\text{s.t} \quad \xi_{t+k+1|t} = f^{\mathrm{dt}}(\xi_{t+k|t}, \mathbf{u}_{t+k|t}), k = 0, ..., N-1 \tag{6.14}$$

$$h(\xi_{t+k|t}, \mathbf{u}_{t+k|t}) \leq 0, k = 0, ..., N-1 \tag{6.15}$$

$$\xi_{t|t} = \xi(t) \tag{6.16}$$

where $h(\xi_{t+k|t}, \mathbf{u}_{t+k|t})$ are state and actuation constraints (6.1)-(6.8). In the NMPC formulation (6.13)-(6.16), neither stability nor feasibility are ensured. The proposed NMPC framework uses the real-time iteration scheme [23]. This is implemented in the open-source ACADO toolkit [2]. Further details on the NMPC are found in [25].

The presented method, referred as model-predictive control-based TSP, was used in Papers C and D. In this method, the candidate actuation is the solution to the optimisation problem (by comparison with the driver model based-TSP in which the actuation is generated by the driver models). If the aim is for human-like behaviour in the MPC approach as well, one solution is to study how the manual drivers prioritise their driving according to the defined cost function and then adjust the weighting parameters accordingly. Another option would be to include the driver models in the MPC formulation, cf [137, 135].

6.3 Results

In Paper B, the combined longitudinal and lateral driver model proposed in Paper A was included in a real-time framework for highway driving automation. Referred to as driver model-based TSP, this framework was used for candidate actuation calculations and the evaluation of constraints related to the subject vehicle dynamics, road boundaries and distance to surrounding traffic. The framework was evaluated using desktop simulations for lane changes at varying constant velocities and during braking. The results showed that the framework could execute lane-keeping and lane-change manoeuvres at constant and varying longitudinal velocities in the range of 20-80 km/h. Moreover, the results showed that the framework can perform abort manoeuvres back to the initial lane or a fall-back manoeuvre, if the feasibility of the initiated lane-change manoeuvre was not fulfilled.

In Paper C, the driver model-based TSP and the model predictive control-based TSP were compared, based on vehicle dynamics performance in lane-change manoeuvring. Desktop simulations showed that both approaches generated feasible lane-change manoeuvres at constant vehicle speed. In addition, lane changes were successfully executed when combined with retardation due to braking by the leading vehicle. In general, the non-linear model predictive control-based TSP showed shorter lane change durations (LCDs) and lower utilisation values for absolute magnitude of longitudinal and lateral acceleration. Paper D evaluated a driving simulator experiment including manual and automated driving. The experiment included three different highway lane-change scenarios, with and without lead vehicle braking. The first scenario was without lead vehicle braking and designed to study driver preferences regarding lane-change initiation and manoeuvring. The second and third scenarios included lead vehicle braking and were constructed to study driver preferences regarding brake initiation and manoeuvring and combined steering and braking respectively. In all scenarios, the subject vehicle was initially prevented from starting a lane-change manoeuvre by two blocking vehicles in the adjacent target lane. The adjacent right-hand lane vehicles were programmed to displace and open a gap once the driver switched on the turn indicator to request a lane change.

The driving automation feature consisted of maintain-lane manoeuvring and lane changes upon the driver's request. In the driving automation, both the driver model-based TSP and the model predictive control-based TSP were used for actuation calculations. One example of actuation and vehicle motion in driving automation for a lane-change manoeuvre in the second scenario is given in Fig. 6.11. The top rows show requested and

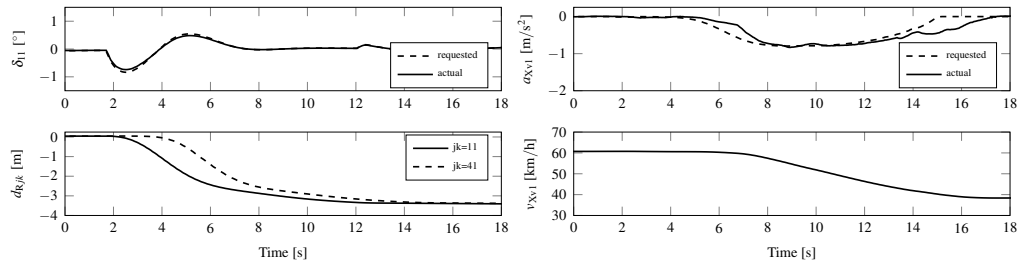

(a) *Driver model-based actuation trajectory planning.*

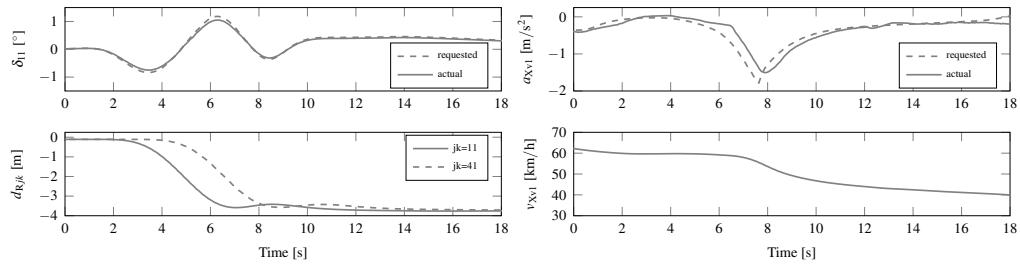

(b) *Model predictive control-based actuation trajectory planning.*

Figure 6.11: *Example of actuation and vehicle motion in driving automation, see Paper D. Top rows: requested and actual front wheel angle and longitudinal acceleration. Bottom rows: lateral distance offset perpendicular to the road for the first unit's first axle and last unit's last axle and longitudinal velocity of the first unit.*

actual front wheel angle and longitudinal acceleration. The bottom rows show lateral distance offset perpendicular to the road for the first unit's first axle and last unit's last axle and longitudinal velocity of the first unit. Note that the actuation and vehicle motion from the driver model based TSP and the model predictive control based TSP should not be directly compared since they occur at different positions along the road.

A similar finite-state machine was used for manoeuvre decision in both approaches. A back-to-back performance comparison of performance characteristics for lane-change manoeuvres and braking were carried out using manual and automated driving observations. The results showed that the mean value of a manual cooperative LCD was approximately 8 s. The driving principle implemented in driver model-based TSP naturally resulted in the same LCD. However, the corresponding value for the model predictive control-based TSP was 4 s. The noticeably lower LCD for the model predictive control-based TSP resulted in a higher extremum for lateral acceleration and lateral jerk. The rearward amplification was similar for both manual and automated driving. Furthermore, evaluation of the second driving scenario showed that the manual drivers braked later and harder than both automated driving approaches. The mean value of the manual drivers' minimum deceleration during braking was $-2.2\,\mathrm{m/s^2}$. The corresponding values for the driver model-based TSP and the model predictive control-based TSP were $-1.4\,\mathrm{m/s^2}$ and $-0.9\,\mathrm{m/s^2}$ respectively. The mean value of the manual drivers' time gap at brake initiation was 1.1 s. The driving principles used in brake initiation for the driver model-based

TSP and the model predictive control-based TSP resulted in 2.4 s and 2.3 s respectively, which leads to lower deceleration values for the driving automation than the manual drivers.

When evaluating the third driving scenario, including combined braking and steering, the results showed that manual drivers often separated braking and steering. This was not the case in automated driving. The interpretation was that the manual drivers were missing the lead vehicle brake onset due to shifted visual focus towards their rear-view mirror, during the first part of the lane change.

7 Traffic situation manoeuvres

As mentioned in Section 4.2, the term *traffic situation manoeuvres* (TSMs) refers to the complete set of functions included in FA-TSM. TSMs are perhaps best described as **decision-making** on the tactical levels of driving principles and control. Section 7.1 gives a brief background and discuss possible approaches for TSMs. Section 7.2 presents the specific TSM design used in Papers B-D and in the automated driving connected to Paper E. Section 7.4 presents the human-machine interface used in the driving simulator experiments to illustrate the decision-making to the driver. Section 7.4 presents the main results of Papers B-E.

7.1 Background

As an example to illustrate TSM, consider the proposed driving automation design in Paper D. In this case, the FA-TSP generates candidate actuations and their feasibilities for a set of defined manoeuvres such as maintain-lane and lane changes to left and right. However, the FA-TSP does not determine why or when to change between maintain-lane and a lane change manoeuvre, in case both are feasible. Rather FA-TSM makes the *manoeuvre planning* and *manoeuvre decision* to achieve both tactical and strategical goals.

Important criteria for TSM are: the methods should be computationally efficient to allow real-time execution; the manoeuvre decisions are consistent in such way that the methods should not frequently change their mind about the choice of manoeuvre; the manoeuvre decisions should be predictable in such way that the function can be evaluated according to functional safety requirements. Major challenges for the manoeuvre decision problem are incomplete and noisy perception and uncertain knowledge about how the traffic situation will evolve over time. Firstly, the intentions of the surrounding traffic is unclear and their behaviour is difficult to predict, see Section 5.4. Secondly, some of the environment may be occluded and sensor measurements may include errors.

Methods of tactical decision-making can vary from being fully deterministic (no uncertainties included) to probabilistic (uncertainties included). The necessary scope and realisation likely depends on the driving automation application. In [42, 141] finite-state-machines (FSMs) were used to handle the decision-making. In [141] predictions of the surrounding traffic were included in the trajectory planner. However, uncertainty in the observation was not considered. In [122, 18], a probabilistic framework was used for lane change decisions and merging manoeuvres.

Another option (proposed by [86]) is to divide methods of tactical decision-making into the groups: rule-based approaches, utility-based approaches and learning approaches. The rule-based approaches are often implemented for specific scenarios using simple heuristics. The drawback is their applicability in more complex traffic scenarios [86]. In utility-based approaches [127], the utility function is used as a common currency for weighting multiple-criteria decisions. Hence, the method might be able to handle more complex traffic situations by selecting appropriate weighting factors. In [4], a utility-based approach was used for highway-driving. The utility was described by means of a

probability distributed stochastic variable. This allows uncertainties of the perception to be regarded in the decision-making process. The learning-based approaches [84, 109] are promising for complex traffic situations, but they require off-line/on-line training and may suffer from non-traceability.

7.2 Design

As stated in Section 6.2, the driving in question is limited to one-way, multiple-lane roads and subject to vehicle speeds in the range of 0-80 km/h. Furthermore, the manoeuvres included are: maintain-lane, lane changes, non-evasive abort lane changes and fall-back braking. Noise from perception is ignored and it is assumed that FA-TSO can accurately estimate the signals given in the motion architecture, see Fig. 6.3. The input to FA-TSM consists of candidate actuation trajectories and their feasibilities for a set of manoeuvres calculated by FA-TSP, see Fig. 6.3. Moreover, FA-TSM also acquires input from FD-RSiM, in terms of distance and relative lane to the next waypoint. Furthermore, inputs to FA-TSM are subject vehicle speed, surrounding traffic observations and turn indicator activation from FA-TSO and FA-DCM respectively. The requests from FA-TSM to FD-VMM are a single vehicle actuation request relating to the front wheel steering angle and longitudinal acceleration of the first vehicle unit. The functionalities of FA-TSM are divided into *manoeuvre planning* and *manoeuvre decision* as discussed in Sections 7.2.1-7.2.2.

7.2.1 Manoeuvre planning

In the simulator experiment described in Paper D, the targeted driving automation included the features maintain-lane and (upon driver's request) lane-changes. In this case, the manoeuvre planning component consisted of the instructions from the manual drivers. The driving automation was started in maintain-lane and the drivers communicated their order to change lane by using the turn indicator switch.

In the driving automation carried out in relation to manual driving (as described in Paper E) the target was to include driving automation which enabled both tactical and strategical goals. The driving automation feature was responsible for maintain-lane driving as well as lane-change manoeuvres, in order to reach the target destination. In this case, it was not possible for the manual operator to influence the manoeuvre planning. Manoeuvre planning was based on a utility-function method in which utility values were calculated for the current and nearest adjacent lanes. The purpose of the utility function was to plan the driving by incorporating properties such as traffic behaviour, efficiency and route-following. Firstly, the subject vehicle preferred driving in the rightmost lane of the road which is the expected driving behaviour for heavy vehicles in Sweden. Secondly, the subject vehicle preferred the lane which had the highest permitted speed, but avoided unnecessary lane changes. Finally, at a specified distance ahead of the next global waypoint, the subject vehicle preferred driving in the target lane. This behaviour was implemented by adapting the lane reference speed in regard to the remaining distance to the upcoming waypoint, see Fig. 7.1. The utility function was customised to work properly in the experiment and was limited to only consider the current and nearest adjacent lanes. The purpose of the

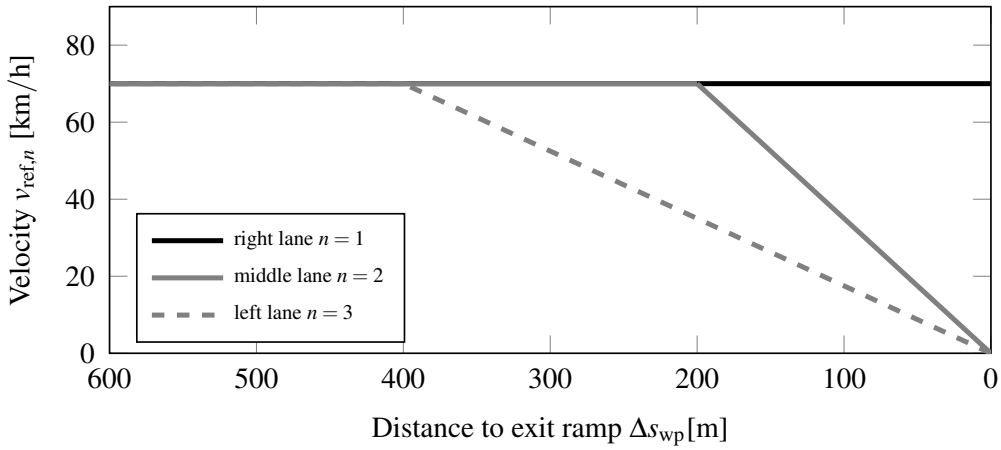

Figure 7.1: *Illustration of lane reference speed, used in the utility calculation, when approaching an upcoming global waypoint. The utility calculation was included in the simulator experiment described in Paper E.*

simulator experiment was to study manual drivers' actions prior to lane changes in dense traffic. The utility U_n is calculated as

$$U_n = \frac{\tilde{v}_n}{v_{\mathrm{Xv1}} \cdot (u_0 + u_1 \cdot \sqrt{n}) + c_{\mathrm{lc}}} \qquad n = 1,\ 2,\ 3 \tag{7.1}$$

$$\tilde{v}_n = \min\left(v^{(o)}_{\mathrm{aver},n},\ v_{\mathrm{ref},n}\right)$$

$$v_{\mathrm{ref},n} = \begin{cases} \overline{v}_{\mathrm{x},n} & : \quad \Delta s_{\mathrm{wp}} \geq \Delta \overline{s}_{\mathrm{wp}} \\ \frac{\Delta s_{\mathrm{wp}}}{T_{\mathrm{lc}} \cdot (N_{\mathrm{rel}}+1)} & : \quad 0 \leq \Delta s_{\mathrm{wp}} < \Delta \overline{s}_{\mathrm{wp}} \end{cases}$$

where $n = 1, 2, 3$ corresponds to the right-hand, middle and left-hand lanes. $\tilde{v}_n$ is the minimum of the average speed of the lead vehicles at a specified distance ahead of the subject vehicle $v^{(o)}_{\mathrm{aver},n}$, and the lane reference speed $v_{\mathrm{ref},n}$. The lane reference speed is calculated using the legal speed limit $\overline{v}_{\mathrm{x},n}$ and the distance and relative lane in regard to the targeted global waypoint, Δs_{wp} and N_{rel}, respectively. T_{lc} is a typical lane change duration. v_{Xv1} is the longitudinal velocity of the subject vehicle's first unit, whilst u_0 and u_1 are tuning parameters. c_{lc} is the cost associated with a lane-change manoeuvre.

7.2.2 Manoeuvring decision

In Papers B-E, the manoeuvring decisions were carried out using a FSM consisting of states and conditional transitions between those states, see Fig. 7.2. The FSM executes the actuation connected to the current state until a transition condition forces it to jump to another state, whose actuation is then executed. Twelve driving states are defined, in order to handle the combination of actuations required to carry out the different manoeuvres. The driving states used for right-side manoeuvres are shown in Fig. 7.2.

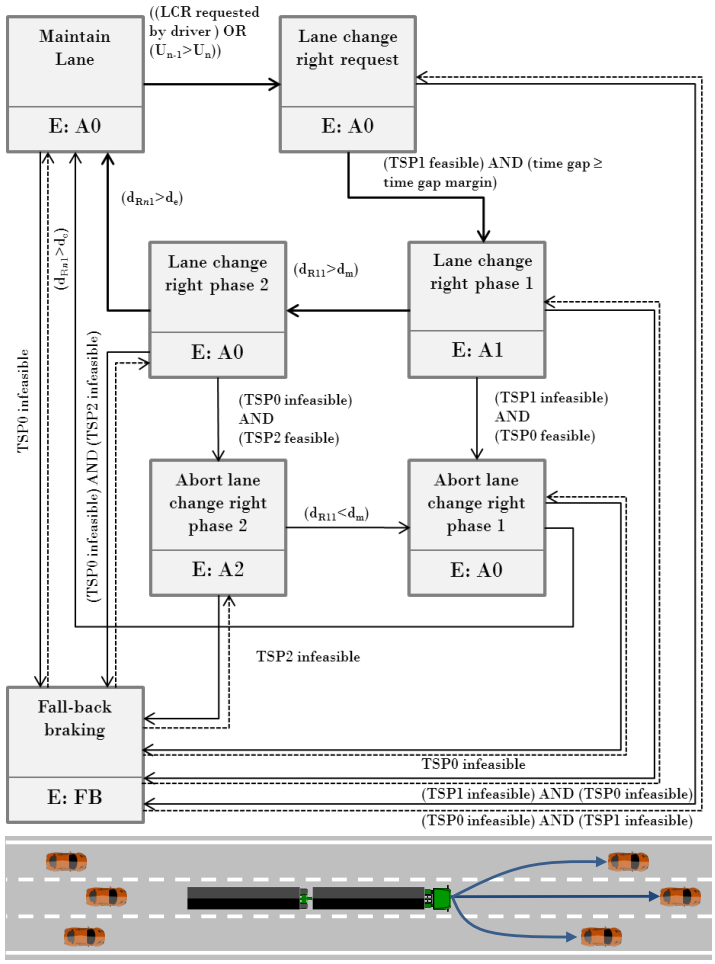

Figure 7.2: *Finite-state machine for manoeuvre-decision making. Conditions for transitions valid for solid lines. Only right-hand side manoeuvres are illustrated. Manoeuvres to the left-hand side are mirrored.*

A simple driving scenario is given to illustrate the FSM. Consider the driving automation described in Paper D, where the driver was responsible for the manoeuvre planning by using the turn indicator switch. The driving automation is started in the *maintain lane* state and the candidate actuation A0 is executed. Once the driver switches the turn indicator, say, to the right, the state is shifted to *lane-change-right-requested*. In this state, the candidate actuation A0 is also executed. If the candidate actuation for lane change to the right is feasible and the fixed margin value for lane change initiation is valid, the state is shifted to *lane-change-right-phase 1* and the candidate actuation A1

(a) *Yellow flashing arrow and display indicating that a lane-change is ordered by human driver or utility function.*

(b) *Green flashing light and display indicating that lane change is started.*

Figure 7.3: *Visual HMI used to inform the driver of manoeuvre planning and decision.*

is executed. When the centre of the first axle of the first vehicle unit passes into the target lane, the state is shifted to *lane-change-right-phase 2* and the candidate actuation A0 is executed. Finally, when the last unit enters the target lane, the state is shifted to *maintain-lane*. There are two states for the complete-lane-change manoeuvre due to the definition of which lane the vehicle is currently in. If the state is shifted to *fall-back braking* a relatively hard braking is executed. However, there is a possibility to return to the previous state within a short time period if the previous state becomes feasible. This is represented with dashed lines in Fig. 7.2.

If considering the driving automation carried out in connection to Paper E, a utility function method (see Section 7.2.1) was used for manoeuvre planning. The utility function replaced the manual lane-change order executed by the operator/driver. Once a lane change was requested, the utility function was no longer used until the state returned to maintain-lane.

7.3 Human-machine interface

In the simulator experiments described in Papers D and E, a visual and audible human-machine interface was developed by Volvo GTT to support the driver in regard to the status of requested and actual manoeuvre, see Fig. 7.3. A yellow flashing arrow (normally green) in combination with a ticking sound (at half the frequency compared to normal), communicated that a lane-change manoeuvre had been ordered but not started.

Furthermore, the information was also given as text on a display, see Fig. 7.3. When a lane change was started, the flashing arrow shifted to green and the frequency of the ticking sound increased to normal and text information appeared on the display.

7.4 Results

In Paper D, a back-to-back performance comparison of manual and automated lane-change manoeuvres was carried out using characteristics variables. The characteristic variables addressed lane change and brake initiation. The comparison included both the driver model-based TSP and the model predictive control-based TSP, see Sections 6.2.1 and 6.2.3. The first scenario studied the time gaps to adjacent lane lead and lag vehicles

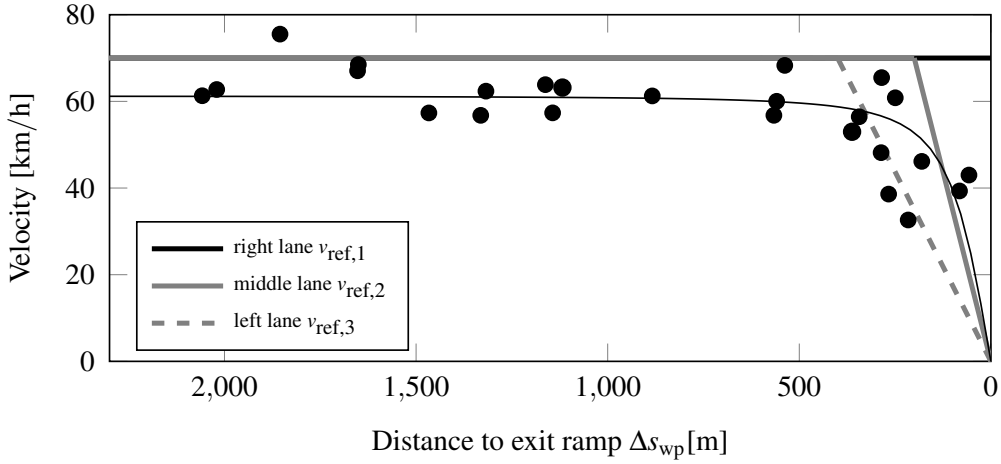

Figure 7.4: *Manual drivers' vehicle speed at lane-change start (black dots). The solid thin black line shows fitted sigmoid function. The solid and dashed thick black and grey lines show the lane reference speed used in the utility calculation.*

at lane-change initiation. For the manual drivers, the mean time gaps at lane-change initiation with respect to adjacent lead and lag vehicles were 0.9 s and −0.8 s respectively. This should be compared with the driver model based-approach in which the margin values for lane change initiation regarding time-gaps were ±2 s. Furthermore, it was found that the time gap at lane-change initiation relating to the lead vehicle in manual driving, varied with the relative speed difference between the subject and target lead vehicle. The time gap at lane change initiation was increased when the relative speed difference was low compared to the time gap when the relative speed difference was high. The results suggest that manual drivers adapt the time gap margin value for lane-change initiation with the relative speed difference. This was not considered in the initial back-to-back automated driving implementation, which used fixed time gap margin values. However, the influence of relative speed difference on time gap margin is a candidate driving principle for automation.

In Papers B-D, it was assumed that the inter-vehicular distances between the traffic in the adjacent target lane were either large enough to allow a lane change, or that the traffic cooperated by displacing to open a gap and allow a lane change. However, it is known that normal highway driving does not always fulfil these assumptions. In many cases, the inter-vehicular distances between the adjacent lane vehicles are shorter than required (see Fig. 1.3) and the traffic does not always cooperate. In Paper E, drivers' actions prior to mandatory lane changes in dense highway traffic were studied using observations from a driving simulator experiment. The studied driver actions were turn indicator activation, speed reduction and lateral intrusion. The experiment consisted of two driving sessions and each session included two lane-change events. The settings of the surrounding traffic were varied for the differing events. The variations consisted of the level of qualifying actions needed by the subject vehicle driver to make the surrounding traffic cooperative.

Cooperative surrounding traffic means that the vehicles displace and open the necessary gap for the subject vehicle's lane-change manoeuvre. Furthermore, the results were categorised in regard to the level of urgency. In this context, urgency was based on the remaining distance to a targeted exit ramp. The results show that, in all started and completed lane-change events, the drivers used their turn indicator prior to starting their lane-change manoeuvre. Moreover, when the subject vehicle was close to the exit ramp the drivers used speed reduction significantly more than when the vehicle was further away. No significant difference was found for the use of lateral intrusion, considering the distance to the exit ramp. Regarding traffic cooperation, significant differences were found for both speed reduction and lateral intrusion. The drivers' speed reduction and lateral intrusion were significantly greater when cooperation by surrounding traffic was low.

In Fig. 7.4, the manual drivers' speeds at lane-change start are compared to the lane reference speed used in the utility function (7.1). The data points of the manual drivers (black dots), are fitted to a sigmoid function using a least-square approximation (thin solid line). The manual drivers' speed at lane change start supports initial back-to-back automated driving implementation, with the driving principle of using speed reduction when approaching a mandatory road exit in an adjacent lane.

8 Concluding remarks

This chapter concludes the thesis with sections on: scientific contributions, appended papers, industrialisation and future research directions.

8.1 Scientific contributions

Driving automation is likely the next revolution to improve the productivity and safety of road transport systems. A primary driving automation application for articulated heavy-vehicle goods transports is in highway driving. Important aspects of highway driving are maintain-lane and lane-change manoeuvres, which have substantial impact on both traffic safety [108] and traffic flow characteristics [139].

Today's professional drivers of articulated heavy-vehicle goods transports are skilled in driving and accounting for the size and dynamic characteristics of these vehicles. Similarly, driving automation features which target articulated heavy vehicles also need to account for these characteristics. In the proposed algorithms for traffic situation predictions, models of the subject vehicle, driver, road and surrounding traffic have been formulated; contribution C1, see Section 1.4. These models capture both subject vehicle dynamics and predicted motion of surrounding traffic. A unique driver steering model for articulated vehicles has been formulated, contribution C1a, see Section 5.3.3. Furthermore, it has been possible to derive traffic situation predictions for multiple-lane one-way road driving by using driver steering and acceleration models in a closed loop with the subject vehicle model; contribution C2. Also, a second approach to calculate actuation trajectories has been developed and evaluated using a MPC framework including on-line optimisation, see Papers C-D. Manoeuvre planning and manoeuvring decisions are made so as to achieve both tactical and strategic goals. The derived traffic situation manoeuvres include maintain-lane, lane changes and non-evasive abort manoeuvres for multiple-lane one-way road driving; contribution C3, see Papers B-E. It is envisaged that studying the important characteristics of manual driving will give insight into how to design driving automation especially in regard to mixed traffic with both manually driven and automated vehicles. Driving principles for driving automation are derived by using back-to-back comparisons of manual and automated driving in simulator experiments; contribution C4. Driving principles for initiation and execution of lane-change manoeuvres with surrounding traffic are studied in Paper D, contribution C4a. Managing mandatory road exits and lane changes in dense traffic are studied in Paper E, contribution C4b.

Paper A - A driver model using optic information for longitudinal and lateral control of a long vehicle combination

In this paper, driver models based on optical information and a one-track vehicle model are used to study a combined lane-change and braking scenario for an A-double combination. The gain factors of the driver steering model were estimated using driving data from a transport mission between Gothenburg and Malmö, measured from an A-double combination during actual lane-changes. Numerical simulations show that the driver models can

generate safe and conservative deceleration and steering for the studied scenario.

Paper B - Driver model based automated driving of long vehicle combinations in emulated highway traffic

This paper presents a framework for highway driving automation, including an A-double combination. Driver models for steering and acceleration are used for the generation of vehicle actuation requests. The behaviour of the driver models is inspired by human cognition and optical flow theory. Traffic situation predictions are calculated using the driver models, in combination with prediction models of the subject vehicle and surrounding traffic. The traffic situation predictions are used for evaluation of constraints relating to vehicle dynamics, road boundaries and distance to surrounding objects. The framework is implemented in a simulation environment, including a high-fidelity vehicle plant model and models of surrounding traffic. Simulations show that the framework can handle both maintain-lane and lane-change manoeuvres at constant speed, as well as and lane changes combined with leading vehicle braking.

Paper C - Automated highway lane changes of long vehicle combinations: A specific comparison between driver model based control and non-linear model predictive control

This paper compares the vehicle dynamics performances of two approaches for automated lane-change manoeuvres. This is achieved by using an A-double combination in simulated highway driving. One of the two approaches is based on non-linear model predictive control and the other on driver modelling. Simulations show that the approach based on non-linear model predictive control includes shorter lane-change durations and lower values for the absolute magnitude of the longitudinal and lateral accelerations. However, when compared to the driver modelling approach, the specific objective function leads to unnecessary variation of longitudinal speed.

Paper D - A Simulator study comparing characteristics of manual and automated driving during lane changes of long combination vehicles

This paper presents a back-to-back performance comparison of lane-change manoeuvres using two driving automation approaches and manual driving. The lane changes were executed in a moving-base truck driving simulator using an A-double combination. One of the approaches for driving automation was based on driver modelling and the other used an MPC framework including on-line optimisation. The comparison addresses lane change and braking (both initiation and execution) from the perspective of driver behaviour and defined characteristic variables.

Paper E - On actions of long combination vehicle drivers prior to lane changes in dense highway trajectory - a driving simulator study

In this paper, we address drivers' actions prior to mandatory lane changes of an A-double combination in dense highway traffic. The studied driver actions were turn indicator

activation, speed reduction and lateral intrusion. We categorised and compared the drivers' actions with respect to the surrounding traffic cooperation and level of urgency. Urgency was based on the remaining distance to a targeted exit ramp. The results show that when the subject vehicle is close to the exit ramp, drivers used speed reduction significantly more than when the vehicle is further away. No significant difference was found for the use of lateral intrusion, considering the distance to the exit ramp.

8.2 Industrialisation

Within goods transport logistics, automated guided vehicles including driving automation features are currently in use on private property, taking over the tasks of human drivers. Such applications often comprise tailored solutions for perception and control that include relatively costly investments. It is envisaged that recent and upcoming developments within driving automation for series-produced road vehicles have great potential to reduce this investment cost.

Moreover (considering the use of driving automation for goods transports on public roads), the first features are expected to target highway applications as highways offer a well-structured environment. High-level or full driving automation features (SAE level 4-5 [104]) have the most promising potential to improve goods transport productivity, since the cost associated with the driver can be removed. However, it is likely that the level of driving automation will instead be gradually increased from driver assistance (SAE level 2 [104]) to ensure road safety.

It is not clear how the instrumentation and potential responsibility split for environment sensors will be handled for articulated vehicles. Today, most truck manufacturers only produce and offer the first vehicle unit whereas the articulated units are produced and offered elsewhere. The proposed algorithms for traffic situation predictions and manoeuvres are expected to undergo initial in-vehicle evaluation and testing using silent mode and then be gradually introduced as product features, when the necessary maturity has been reached.

8.3 Future research direction

The most straightforward way to test driving automation features is through physical vehicle testing. The drawback is that vehicle environment sensors need to be in place and surrounding physical traffic needs to be controlled and included in the test scenarios. To avoid these problems, a high-fidelity moving-base truck driving simulator has been used throughout this work. Driving simulators offer great control and reproducibility, but may have limited physical, perceptual, and behavioural fidelity [10, 101]. Based on the limitations included in driving simulator testing, the proposed functionalities for traffic situation predictions and manoeuvres should be subjected to extensive testing in real-world traffic situations for various highway traffic scenarios.

The algorithms that have been developed for traffic situation predictions and manoeuvres

have only been evaluated for the A-double combination. The performance of these algorithms should be studied using additional vehicle combinations.

The algorithms for traffic situation predictions have assumed certain observed quantities. A realistic sensor instrumentation and sensor fusion might call for changes in these algorithms.

The algorithms for traffic situation predictions and manoeuvres have been evaluated using computing capacity that exceeds that of a current standard vehicle. Even though developments in computer hardware are impressive, the algorithms should be adapted to more limited computational resources.

In case of mixed traffic with both manually driven and automated vehicles, the intention and motion prediction of surrounding traffic is a vital component of the traffic situation predictions. Further development of surrounding traffic predictions using real-world traffic observations is envisaged.

Manoeuvring decision-making in complex traffic situations is a major challenge for human drivers as well as driving automation features. Combining probabilistic methods, including uncertainties from perception and surrounding traffic, with prediction models for articulated vehicles is an area of interest

Using parametrised driver models inspired by human cognition to generate actuation requests is a promising direction for achieving a high level of driver acceptance in regard to manoeuvre execution in lane changes. This should particularly be taken into account for driving automation features which target shared control, or in human driver take-over situations. The used parametrisation was based on one driver in smooth driving conditions and should be extended by using additional drivers and manoeuvres.

The MPC framework that was used showed difficulties in handling both tracking and driving comfort objectives but offers a direct and structured way to include motion and actuation constraints. A promising approach would be to combine the driver model approach with the MPC approach and use the driver models for reference trajectory generation in the MPC framework.

The study of human drivers' actions prior to mandatory lane changes with a final distance to a targeted road exit ramp showed use of speed reduction and lateral intrusion. Imitating the human driver's use of speed reduction can be included relatively easily in a driving automation framework, by using a utility approach for example. However, imitating human drivers' use of lateral intrusion is not obvious and is far more complicated. Additional studies on how to handle mandatory lane changes in driving automation features are envisaged.

Appendix I

Vehicle models

The vehicle body models for a tractor semi-trailer and an A-double are derived using the Lagrange equations, see Section 5.2.2.1. The equations include a linear tyre model and are simplified using an assumption of small steering and articulation angles. The simplifications are in general valid when considering vehicle cornering in high speed and moderate lateral acceleration levels. For each vehicle type, two models are presented. The first model, referred to as the *non-linear model*, includes the equation for longitudinal, lateral and rotational motion. The second model, referred to as the *linear model*, assumes constant longitudinal velocity and neglected body-forces. All terms including the time derivative of v_{Xv1} are consequently zero in the linear models. Further, assuming that the longitudinal forces can be approximated to zero, the equation for longitudinal motion can be neglected. (The character $\times$ is here used for multiplication.)

Tractor semi-trailer

The *non-linear* and the *linear model* are expressed using the vehicle parameters defined in Table 8.1 and Fig. 8.1.

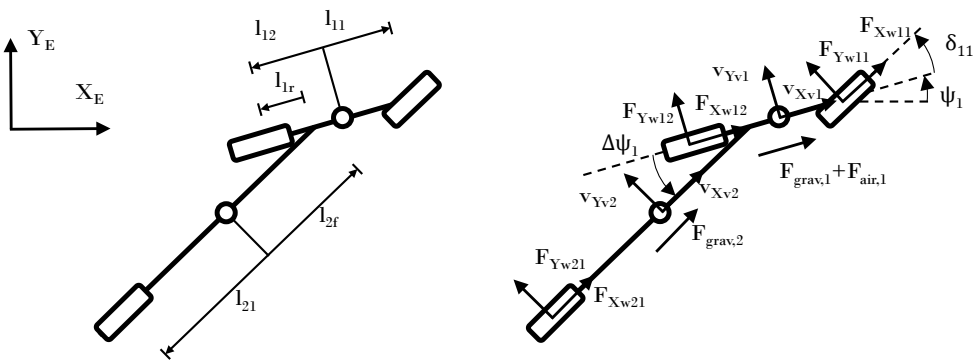

Figure 8.1: *One-track model of tractor semi-trailer combination.*

Non-linear model

The non-linear model (8.1) includes the vehicle states $\xi = [v_{\mathrm{Xv1}},\ v_{\mathrm{Yv1}},\ \dot{\psi}_1,\ \Delta\dot{\psi}_1,\ \Delta\psi_1]$ and the control inputs $\mathbf{u} = [\delta_{11},\ F_{\mathrm{Xw11}},\ F_{\mathrm{Xw12}},\ F_{\mathrm{Xw21}}]$.

Table 8.1: Vehicle model parameters, tractor semi-trailer

Parameter	Symbol	Value	Unit
Mass, unit 1	m_1	8491	[kg]
Mass, unit 2	m_2	31900	[kg]
Inertia z-axis, unit 1	J_{Z1}	37e3	[kgm^2]
Inertia z-axis, unit 2	J_{Z2}	420e3	[kgm^2]
Distance from COG to front axle, unit 1	l_{11}	1.45	[m]
Distance from COG to connection point front, unit 2	$l_{2\mathrm{f}}$	5.27	[m]
Distance from COG to rear axle, unit 1	l_{12}	2.24	[m]
Distance from COG to rear axle, unit 2	l_{21}	3.14	[m]
Distance from connection point rear to rear axle, unit 1	$l_{1\mathrm{r}}$	1.19	[m]
Front axle cornering stiffness, unit 1	C_{Y11}	3.0e5	[N/rad]
Rear axle cornering stiffness, unit 1	C_{Y12}	8.6e5	[N/rad]
Rear axle cornering stiffness, unit 2	C_{Y21}	1.1e6	[N/rad]

$$
\begin{aligned}
\frac{\mathrm{d}}{\mathrm{d}t}v_{\mathrm{Xv1}} =& 2.48\times10^{-5}\cdot(F_{\mathrm{air},1}+\sum_{j=1}^{2}F_{\mathrm{grav,j}}+F_{\mathrm{Xw12}}+\sum_{i=1}^{2}F_{\mathrm{Xw}i1})+\dot{\psi}_1\cdot v_{\mathrm{Yv1}}\\
\frac{\mathrm{d}}{\mathrm{d}t}v_{\mathrm{Yv1}} =& \frac{1}{v_{\mathrm{Xv1}}}\Big(v_{\mathrm{Xv1}}\cdot(\Delta\psi_1\cdot(-1.93\times10^{-5}\cdot(F_{\mathrm{air},1}+F_{\mathrm{grav},1}+F_{\mathrm{Xw11}}+F_{\mathrm{Xw12}})+\\
& 1.68\times10^{-5}\cdot(F_{\mathrm{grav},2}+F_{\mathrm{Xw21}})-3.28)-\dot{\psi}_1\cdot v_{\mathrm{Xv1}}+\delta_{11}\cdot(1.02\times10^{-4}\cdot F_{\mathrm{Xw11}}+30.74))-\\
& 27.58\cdot\Delta\dot{\psi}_1+v_{\mathrm{Yv1}}\cdot(-0.78\cdot\Delta\psi_1\cdot\dot{\psi}_1\cdot v_{\mathrm{Xv1}}-53.63)-19.91\cdot\dot{\psi}_1\Big)\\
\frac{\mathrm{d}}{\mathrm{d}t}\dot{\psi}_1 =& \frac{1}{v_{\mathrm{Xv1}}}\Big(\Delta\psi_1\cdot(8.65\times10^{-6}\cdot(F_{\mathrm{air},1}+F_{\mathrm{grav},1}+F_{\mathrm{Xw11}}+F_{\mathrm{Xw12}})-\\
& 7.50\times10^{-6}\cdot(F_{\mathrm{grav},2}+F_{\mathrm{Xw21}})+1.47)+\delta_{11}\cdot(4.60\times10^{-5}\cdot F_{\mathrm{Xw11}}+13.81)+\\
& 12.34\cdot\Delta\dot{\psi}_1+v_{\mathrm{Yv1}}\cdot(0.35\cdot\Delta\psi_1\cdot\dot{\psi}_1\cdot v_{\mathrm{Xv1}}+3.17)-46.16\cdot\dot{\psi}_1\Big)\\
\frac{\mathrm{d}}{\mathrm{d}t}\Delta\dot{\psi}_1 =& \frac{1}{v_{\mathrm{Xv1}}}\cdot\Big(v_{\mathrm{Xv1}}\cdot(\Delta\psi_1\cdot(-1.65\times10^{-5}\cdot(F_{\mathrm{air},1}+F_{\mathrm{grav},1}+F_{\mathrm{Xw11}}+F_{\mathrm{Xw12}})+\\
& 8.35\times10^{-6}\cdot(F_{\mathrm{grav},2}+F_{\mathrm{Xw21}})-9.34)+\delta_{11}\cdot(-4.44\times10^{-5}\cdot F_{\mathrm{Xw11}}-13.32))-\\
& 78.57\cdot\Delta\dot{\psi}_1+v_{\mathrm{Yv1}}\cdot(-0.67\cdot\Delta\psi_1\cdot\dot{\psi}_1\cdot v_{\mathrm{Xv1}}-3.79)-18.20\cdot\dot{\psi}_1\Big)\\
\frac{\mathrm{d}}{\mathrm{d}t}\Delta\psi_1 =& \Delta\dot{\psi}_1
\end{aligned}
\tag{8.1}
$$

Linear model

The linear model is described in a linear time-invariant state space form $\dot{\mathbf{x}} = \mathbf{A}\mathbf{x} + \mathbf{B}\mathbf{u}$. The model includes the vehicle states $\mathbf{x} = [v_{\mathrm{Yv1}},\ \dot{\psi}_1,\ \Delta\dot{\psi}_1,\ \Delta\psi_1]$ and the control input $\mathbf{u} = \delta_{11}$. The matrices $\mathbf{A}$ and $\mathbf{B}$ are defined in (8.2).

$$\mathbf{A} = \begin{bmatrix} -\dfrac{53.63}{v_{\mathrm{Xv1}}} & -v_{\mathrm{Xv1}} - \dfrac{19.91}{v_{\mathrm{Xv1}}} & -\dfrac{27.58}{v_{\mathrm{Xv1}}} & -3.28 \\ \dfrac{3.17}{v_{\mathrm{Xv1}}} & -\dfrac{46.16}{v_{\mathrm{Xv1}}} & \dfrac{12.34}{v_{\mathrm{Xv1}}} & 1.47 \\ -\dfrac{3.79}{v_{\mathrm{Xv1}}} & -\dfrac{18.20}{v_{\mathrm{Xv1}}} & -\dfrac{78.57}{v_{\mathrm{Xv1}}} & -9.34 \\ 0 & 0 & 1 & 0 \end{bmatrix} \qquad \mathbf{B} = \begin{bmatrix} 30.74 \\ 13.81 \\ -13.32 \\ 0 \end{bmatrix} \tag{8.2}$$

A-double combination

The *non-linear* and the *linear model* are expressed using the vehicle parameters defined in Table 8.2 and Fig. 8.2.

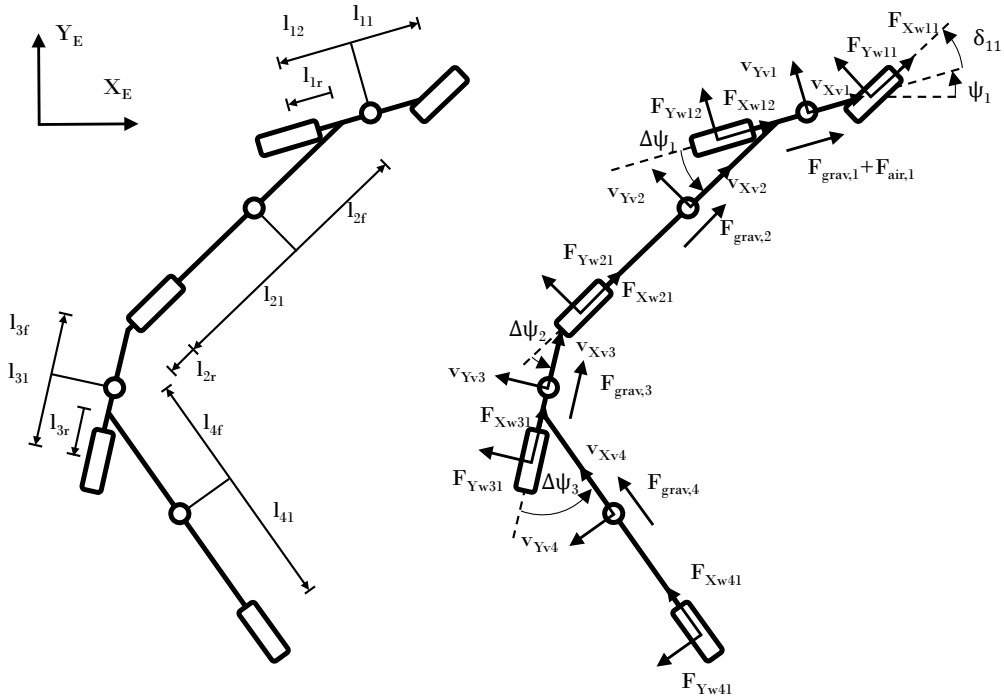

Figure 8.2: *One-track model of A-double combination.*

Non-linear model

Table 8.2: Vehicle model parameters, A-double

Parameter	Symbol	Value	Unit
Mass, unit 1	m_1	9841	[kg]
Mass, unit 2	m_2	33601	[kg]
Mass, unit 3	m_3	2700	[kg]
Mass, unit 4	m_4	33801	[kg]
Inertia z-axis, unit 1	J_{Z1}	20e3	[kgm^2]
Inertia z-axis, unit 2	J_{Z2}	543e3	[kgm^2]

Vehicle model parameters, A-double

Parameter	Symbol	Value	Unit
Inertia z-axis, unit 3	J_{Z3}	2e3	[kgm^2]
Inertia z-axis, unit 4	J_{Z4}	546e3	[kgm^2]
Distance from COG to front axle, unit 1	l_{11}	1.45	[m]
Distance from COG to connection point front, unit 2	$l_{2\mathrm{f}}$	4.43	[m]
Distance from COG to connection point front, unit 3	$l_{3\mathrm{f}}$	4.55	[m]
Distance from COG to connection point front, unit 4	$l_{4\mathrm{f}}$	4.65	[m]
Distance from COG to rear axle, unit 1	l_{12}	2.23	[m]
Distance from COG to rear axle, unit 2	l_{21}	3.27	[m]
Distance from COG to rear axle, unit 3	l_{31}	0.65	[m]
Distance from COG to rear axle, unit 4	l_{41}	3.05	[m]
Distance from connection point rear to rear axle, unit 1	$l_{1\mathrm{r}}$	0.28	[m]
Distance from connection point rear to rear axle, unit 2	$l_{2\mathrm{r}}$	2.70	[m]
Distance from connection point rear to rear axle, unit 3	$l_{3\mathrm{r}}$	0.	[m]
Front axle cornering stiffness, unit 1	C_{Y11}	4.07e5	[N/rad]
Rear axle cornering stiffness, unit 1	C_{Y12}	2.07e6	[N/rad]
Rear axle cornering stiffness, unit 2	C_{Y21}	1.24e6	[N/rad]
Rear axle cornering stiffness, unit 3	C_{Y31}	1.17e6	[N/rad]
Rear axle cornering stiffness, unit 4	C_{Y41}	1.42e6	[N/rad]

The non-linear model (8.3) includes the vehicle states $\xi = [v_{\mathrm{Xv1}},\ v_{\mathrm{Yv1}},\ \dot{\psi}_1,\ \psi_1,\ \Delta\dot{\psi}_1,\ \Delta\psi_1,\ \Delta\dot{\psi}_2,\ \Delta\psi_2\ \Delta\dot{\psi}_3,\ \Delta\psi_3]$ and the control inputs $\mathbf{u} = [\delta_{11},\ F_{\mathrm{Xw11}},\ F_{\mathrm{Xw12}},\ F_{\mathrm{Xw21}},\ F_{\mathrm{Xw31}},\ F_{\mathrm{Xw41}}]$.

$$\frac{\mathrm{d}}{\mathrm{d}t}v_{\mathrm{Xv1}} = 1.25\times10^{-5}\cdot(F_{\mathrm{air},1} + \sum_{j=1}^{4} F_{\mathrm{grav,j}} + \sum_{i=1}^{4} F_{\mathrm{Xw}i1} + F_{\mathrm{Xw12}}) + \dot{\psi}_1\cdot v_{\mathrm{Yv1}}$$

$$\begin{aligned}\frac{\mathrm{d}}{\mathrm{d}t}v_{\mathrm{Yv1}} = &\frac{1}{v_{\mathrm{Xv1}}}(v_{\mathrm{Xv1}}\cdot(\Delta\psi_1\cdot(-1.29\times10^{-5}\cdot(F_{\mathrm{air},1} + F_{\mathrm{Xw12}} + \sum_{j=1}^{4} F_{\mathrm{grav,j}} + \sum_{i=1}^{4} F_{\mathrm{Xw}i1}) + \\ &7.25\times10^{-5}\cdot(\sum_{j=2}^{4} F_{\mathrm{grav,j}} + \sum_{i=2}^{4} F_{\mathrm{Xw}i1}) + 1.93) + \delta_{11}\cdot(1.13\times10^{-4}\cdot F_{\mathrm{Xw11}} + 51.71) + \\ &\Delta\psi_2\cdot(2.43\times10^{-6}\cdot(F_{\mathrm{air},1} + F_{\mathrm{Xw12}} + \sum_{j=1}^{4} F_{\mathrm{grav,j}} + \sum_{i=1}^{4} F_{\mathrm{Xw}i1}) - \\ &5.33\times10^{-6}\cdot(\sum_{j=3}^{4} F_{\mathrm{grav,j}} + \sum_{i=3}^{4} F_{\mathrm{Xw}i1}) + 0.78) + \\ &\Delta\psi_3\cdot(7.23\times10^{-9}\cdot(F_{\mathrm{air},1} + F_{\mathrm{Xw12}} + \sum_{j=1}^{4} F_{\mathrm{grav,j}} + \sum_{i=1}^{4} F_{\mathrm{Xw}i1}) - \\ &2.99\times10^{-8}\cdot(F_{\mathrm{Xw41}} + F_{\mathrm{grav},4}) - 2.24\times10^{-3})) + \\ &21.0\cdot\Delta\dot{\psi}_1 - \dot{\psi}_1\cdot v_{\mathrm{Xv1}}^2 + 71.24\cdot\dot{\psi}_1 + 4.02\cdot\Delta\dot{\psi}_2 - 1.73\times10^{-2}\cdot\Delta\dot{\psi}_3 - 108.1\cdot v_{\mathrm{Yv1}})\end{aligned}$$

$$\frac{\mathrm{d}}{\mathrm{d}t}\dot{\psi}_1 = \frac{1}{v_{\mathrm{Xv1}}}(v_{\mathrm{Xv1}}\cdot(\Delta\psi_1\cdot(1.23\times10^{-5}\cdot(F_{\mathrm{air},1}+F_{\mathrm{Xw12}}+\sum_{j=1}^{4}F_{\mathrm{grav,j}}+\sum_{i=1}^{4}F_{\mathrm{Xw}i1})-$$
$$2.77\times10^{-5}\cdot(\sum_{j=2}^{4}F_{\mathrm{grav,j}}+\sum_{i=2}^{4}F_{\mathrm{Xw}i1})-1.85)+\delta_{11}\cdot(6.17\times10^{-5}\cdot F_{\mathrm{Xw11}}+28.24)+$$
$$\Delta\psi_2\cdot(-2.33\times10^{-6}\cdot(F_{\mathrm{air},1}+F_{\mathrm{Xw12}}+\sum_{j=1}^{4}F_{\mathrm{grav,j}}+\sum_{i=1}^{4}F_{\mathrm{Xw}i1})+$$
$$5.12\times10^{-6}\cdot(\sum_{j=3}^{4}F_{\mathrm{grav,j}}+\sum_{i=3}^{4}F_{\mathrm{Xw}i1})-0.75)+$$
$$\Delta\psi_3\cdot(-6.94\times10^{-9}\cdot(F_{\mathrm{air},1}+F_{\mathrm{Xw12}}+\sum_{j=1}^{4}F_{\mathrm{grav,j}}+\sum_{i=1}^{4}F_{\mathrm{Xw}i1})+$$
$$2.87\times10^{-8}\cdot(F_{\mathrm{grav},4}+F_{\mathrm{Xw41}})+2.15\times10^{-3}))-$$
$$20.15\cdot\Delta\dot{\psi}_1-336.4\cdot\dot{\psi}_1-3.86\cdot\Delta\dot{\psi}_2+1.66\times10^{-2}\cdot\Delta\dot{\psi}_3+95.46\cdot v_{\mathrm{Yv1}})$$
$$\frac{\mathrm{d}}{\mathrm{d}t}\Delta\dot{\psi}_1 = \frac{1}{v_{\mathrm{Xv1}}}\cdot(v_{\mathrm{Xv1}}\cdot(\Delta\psi_1\cdot(-1.84\times10^{-5}\cdot(F_{\mathrm{air},1}+F_{\mathrm{Xw12}}+\sum_{j=1}^{4}F_{\mathrm{grav,j}}+\sum_{i=1}^{4}F_{\mathrm{Xw}i1})+$$
$$2.54\times10^{-5}\cdot(\sum_{j=2}^{4}F_{\mathrm{grav,j}}+\sum_{i=2}^{4}F_{\mathrm{Xw}i1})-4.28)+\delta_{11}\cdot(-6.26\times10^{-5}\cdot F_{\mathrm{Xw11}}-28.65)+$$
$$\Delta\psi_2\cdot(7.10\times10^{-6}\cdot(F_{\mathrm{air},1}+F_{\mathrm{Xw12}}+\sum_{j=1}^{4}F_{\mathrm{grav,j}}+\sum_{i=1}^{4}F_{\mathrm{Xw}i1})-$$
$$1.56\times10^{-5}\cdot(\sum_{j=3}^{4}F_{\mathrm{grav,j}}+\sum_{i=3}^{4}F_{\mathrm{Xw}i1})+2.27)+$$
$$\Delta\psi_3\cdot(2.11\times10^{-8}\cdot(F_{\mathrm{air},1}+F_{\mathrm{Xw12}}+\sum_{j=1}^{4}F_{\mathrm{grav,j}}+\sum_{i=1}^{4}F_{\mathrm{Xw}i1})-$$
$$8.73\times10^{-8}\cdot(F_{\mathrm{grav},4}+F_{\mathrm{Xw41}})-6.56\times10^{-3}))-$$
$$15.04\cdot\Delta\dot{\psi}_1+370.3\cdot\dot{\psi}_1+11.75\cdot\Delta\dot{\psi}_2-0.05\cdot\Delta\dot{\psi}_3-125\cdot v_{\mathrm{Yv1}})$$
$$\frac{\mathrm{d}}{\mathrm{d}t}\Delta\psi_1 = \Delta\dot{\psi}_1$$

$$
\begin{aligned}
\frac{\mathrm{d}}{\mathrm{d}t}\Delta\dot{\psi}_2 =& \frac{1}{v_{\mathrm{Xv1}}}(v_{\mathrm{Xv1}}\cdot(\Delta\psi_1\cdot(9.19\times10^{-6}\cdot(F_{\mathrm{air},1}+F_{\mathrm{Xw12}}+\sum_{j=1}^{4}F_{\mathrm{grav,j}}+\sum_{i=1}^{4}F_{\mathrm{Xw}i1})- \\
& 9.99\times10^{-6}\cdot(\sum_{j=2}^{4}F_{\mathrm{grav,j}}+\sum_{i=2}^{4}F_{\mathrm{Xw}i1})+4.74)+\delta_{11}\cdot(1.36\times10^{-6}F_{\mathrm{Xw11}}+0.62)+ \\
& \Delta\psi_2\cdot(-1.68\times10^{-5}\cdot(F_{\mathrm{air},1}+F_{\mathrm{Xw12}}+\sum_{j=1}^{4}F_{\mathrm{grav,j}}+\sum_{i=1}^{4}F_{\mathrm{Xw}i1})+ \\
& 3.09\times10^{-5}\cdot(\sum_{j=3}^{4}F_{\mathrm{grav,j}}+\sum_{i=3}^{4}F_{\mathrm{Xw}i1})-21.04)+ \\
& \Delta\psi_3\cdot(3.04\times10^{-6}\cdot(F_{\mathrm{air},1}+F_{\mathrm{Xw12}}+\sum_{j=1}^{4}F_{\mathrm{grav,j}}+\sum_{i=1}^{4}F_{\mathrm{Xw}i1})- \\
& 1.26\times10^{-5}\cdot(F_{\mathrm{grav},4}+F_{\mathrm{Xw41}})-0.94))- \\
& 136.4\cdot\Delta\dot{\psi}_1-249.1\cdot\dot{\psi}_1-116.1\cdot\Delta\dot{\psi}_2-7.27\cdot\Delta\dot{\psi}_3+48.92\cdot v_{\mathrm{Yv1}}) \\
\frac{\mathrm{d}}{\mathrm{d}t}\Delta\psi_2 =& \Delta\dot{\psi}_2\ \mathrm{d}t \\
\frac{\mathrm{d}}{\mathrm{d}t}\Delta\dot{\psi}_3 =& \frac{1}{v_{\mathrm{Xv1}}}\cdot(v_{\mathrm{Xv1}}\cdot(\Delta\psi_1\cdot(-3.07\times10^{-6}\cdot(F_{\mathrm{air},1}+F_{\mathrm{Xw12}}+\sum_{j=1}^{4}F_{\mathrm{grav,j}}+\sum_{i=1}^{4}F_{\mathrm{Xw}i1})+ \\
& 3.34\times10^{-6}\cdot(\sum_{j=2}^{4}F_{\mathrm{grav,j}}+\sum_{i=2}^{4}F_{\mathrm{Xw}i1})+2.02)+\delta_{11}\cdot(-4.55\times10^{-6}\cdot F_{\mathrm{Xw11}}-0.21)+ \\
& \Delta\psi_2\cdot(1.20\times10^{-5}\cdot(F_{\mathrm{air},1}+F_{\mathrm{Xw12}}+\sum_{j=1}^{4}F_{\mathrm{grav,j}}+\sum_{i=1}^{4}F_{\mathrm{Xw}i1})- \\
& 7.04\times10^{-5}\cdot(\sum_{j=3}^{4}F_{\mathrm{grav,j}}+\sum_{i=3}^{4}F_{\mathrm{Xw}i1})+20.08)+ \\
& \Delta\psi_3\cdot(-6.32\times10^{-6}\cdot(F_{\mathrm{air},1}+F_{\mathrm{Xw12}}+\sum_{j=1}^{4}F_{\mathrm{grav,j}}+\sum_{i=1}^{4}F_{\mathrm{Xw}i1})+ \\
& 1.98\times10^{-5}\cdot(F_{\mathrm{grav},4}+F_{\mathrm{Xw41}})-7.20))+ \\
& 123.5\cdot\Delta\dot{\psi}_1+168.1\cdot\dot{\psi}_1+53.68\cdot\Delta\dot{\psi}_2-55.43\cdot\Delta\dot{\psi}_3-19.95\cdot v_{\mathrm{Yv1}}) \\
\frac{\mathrm{d}}{\mathrm{d}t}\Delta\psi_3 =& \Delta\dot{\psi}_3
\end{aligned}
\tag{8.3}
$$

Linear model

The linear model is described in a linear time-invariant state space form $\dot{\mathbf{x}} = \mathbf{A}\mathbf{x}+\mathbf{B}\mathbf{u}$. The model includes the vehicle states $\mathbf{x} = [v_{\mathrm{Yv1}},\ \dot{\psi}_1,\ \psi_1,\ \Delta\dot{\psi}_1,\ \Delta\psi_1,\ \Delta\dot{\psi}_2,\ \Delta\psi_2,\ \Delta\dot{\psi}_3,\ \Delta\psi_3]$ and the control input $\mathbf{u} = \delta_{11}$. The matrices $\mathbf{A}$ and $\mathbf{B}$ are defined in (8.4).

$$\mathbf{A} = \begin{bmatrix} -\frac{108.1}{v_{\mathrm{Xv1}}} & \frac{71.24}{v_{\mathrm{Xv1}}} - v_{\mathrm{Xv1}} & 0 & \frac{21.0}{v_{\mathrm{Xv1}}} & 1.93 & \frac{4.02}{v_{\mathrm{Xv1}}} & 0.78 & -\frac{0.017}{v_{\mathrm{Xv1}}} & -0.0022 \\ \frac{95.46}{v_{\mathrm{Xv1}}} & -\frac{336.4}{v_{\mathrm{Xv1}}} & 0 & -\frac{20.15}{v_{\mathrm{Xv1}}} & -1.85 & -\frac{3.86}{v_{\mathrm{Xv1}}} & -0.75 & \frac{0.017}{v_{\mathrm{Xv1}}} & 0.0022 \\ 0 & 1 & 0 & 0 & 0 & 0 & 0 & 0 & 0 \\ -\frac{125}{v_{\mathrm{Xv1}}} & \frac{370.3}{v_{\mathrm{Xv1}}} & 0 & -\frac{15.04}{v_{\mathrm{Xv1}}} & -4.28 & \frac{11.75}{v_{\mathrm{Xv1}}} & 2.27 & -\frac{0.050}{v_{\mathrm{Xv1}}} & -0.0066 \\ 0 & 0 & 0 & 1 & 0 & 0 & 0 & 0 & 0 \\ \frac{48.92}{v_{\mathrm{Xv1}}} & -\frac{249.1}{v_{\mathrm{Xv1}}} & 0 & -\frac{136.4}{v_{\mathrm{Xv1}}} & 4.74 & -\frac{116.1}{v_{\mathrm{Xv1}}} & -21.04 & -\frac{7.27}{v_{\mathrm{Xv1}}} & -0.94 \\ 0 & 0 & 0 & 0 & 0 & 1 & 0 & 0 & 0 \\ -\frac{19.95}{v_{\mathrm{Xv1}}} & \frac{168.1}{v_{\mathrm{Xv1}}} & 0 & \frac{123.5}{v_{\mathrm{Xv1}}} & 2.02 & \frac{53.68}{v_{\mathrm{Xv1}}} & 20.08 & -\frac{55.43}{v_{\mathrm{Xv1}}} & -7.20 \\ 0 & 0 & 0 & 0 & 0 & 0 & 0 & 1 & 0 \end{bmatrix}$$

$$\mathbf{B} = \begin{bmatrix} 51.71 \\ 28.24 \\ 0 \\ -28.65 \\ 0 \\ 0.62 \\ 0 \\ -0.21 \\ 0 \end{bmatrix} \tag{8.4}$$

References

[1] Volvo Trucks Sweden. Accessed August 30, 2017. URL: http://www.volvotrucks.se/sv-se/trucks/volvo-fh-series/features/i-see.html.

[2] ACADO toolkit. Accessed August 30, 2017. URL: http://acado.github.io/.

[3] J. Andersson et al. *Trafiksäkerhetspåverkan vid omkörning av 30-metersfordon*. VTI rapport 732. Swedish National Road and Transport Research Institute (VTI), 2011.

[4] M. Ardelt, C. Coester, and N. Kaempchen. Highly Automated Driving on Freeways in Real Traffic Using a Probabilistic Framework. *IEEE Transactions on Intelligent Transportation Systems* 13.4 (2012), pp. 1576–1585.

[5] J. Aurell and T. Wadman. *Vehicle combinations based on the modular concept*. NVF-reports 1. Nordic Road Association, 2007.

[6] M. L. Aust, J. Engström, and M. Viström. Effects of forward collision warning and repeated event exposure on emergency braking. *Transportation research part F: traffic psychology and behaviour* 18 (2013), pp. 34–46.

[7] A. Bálint et al. "Correlation between truck combination length and injury risk". *Australasian College of Road Safety Conference, 2013, Adelaide, South Australia, Australia*. 2013.

[8] I. Batkovic. "Optimization of driver model parameters for Long Combination Vehicles". Master's thesis. Chalmers University of Technology, 2016.

[9] S. Behere and M. Torngren. "A functional architecture for autonomous driving". *Automotive Software Architecture (WASA), 2015 First International Workshop on*. IEEE. 2015, pp. 3–10.

[10] H. Bellem et al. Can we study autonomous driving comfort in moving-base driving simulators? A validation study. *Human factors* 59.3 (2017), pp. 442–456.

[11] O. Benderius. "Driver modeling: Data collection, model analysis, and optimization". Licentiate thesis. Department of Applied Mechanics, Chalmers University of Technology, 2012.

[12] O. Benderius. "Modelling driver steering and neuromuscular behaviour". PhD thesis. Department of Applied Mechanics, Chalmers University of Technology, 2014.

[13] C. Bergenhem et al. *Challenges of platooning on public motorways*. https://www.researchgate.net/profile/Carl_Bergenhem/publication/228859487_Challenges_Of_Platooning_On_Public_Motorways/links/09e415108e89a8ea18000000/Challenges-Of-Platooning-On-Public-Motorways.pdf. Accessed August 30, 2017.

[14] C. Bergenhem et al. "Overview of platooning systems". *Proceedings of the 19th ITS World Congress, Oct 22-26, Vienna, Austria (2012)*. 2012.

[15] J. T. Betts. *Practical methods for optimal control and estimation using nonlinear programming*. SIAM, 2010.

[16] F. Borrelli, A. Bemporad, and M. Morari. *Predictive control for linear and hybrid systems*. 2014.

[17] A. Boström. *Rigid body dynamics*. Chalmers University of Technology, 2012.

[18] S. Brechtel, T. Gindele, and R. Dillmann. "Probabilistic decision-making under uncertainty for autonomous driving using continuous POMDPs". *17th International IEEE Conference on Intelligent Transportation Systems (ITSC)*. 2014, pp. 392–399.

[19] F. Browand, J. McArthur, and C. Radovich. Fuel saving achieved in the field test of two tandem trucks. *California Partners for Advanced Transit and Highways (PATH)* (2004).

[20] R. E. Chandler, R. Herman, and E. W. Montroll. Traffic dynamics: studies in car following. *Operations research* 6.2 (1958), pp. 165–184.

[21] *COMPANION*. Accessed August 30, 2017. URL: http://www.companion-project.eu/.

[22] Daimler AG. Accessed August 30, 2017. URL: http://media.daimler.com/marsMediaSite/en/instance/ko/Mercedes-Benz-Actros-with-Highway-Pilot---world-premiere-on-public-roads.xhtml?oid=9920353.

[23] M. Diehl, H. G. Bock, and J. P. Schlöder. A real-time iteration scheme for nonlinear optimization in optimal feedback control. *SIAM Journal on control and optimization* 43.5 (2005), pp. 1714–1736.

[24] X. Ding and Y. He. Numerical simulation and analysis of closed-loop driver/articulated vehicle dynamic systems. *SAE International Journal of Commercial Vehicles* 5.2012-01-0244 (2012), pp. 111–118.

[25] N. van Duijkeren et al. Real-Time NMPC for Semi-Automated Highway Driving of Long Heavy Vehicle Combinations. *IFAC-PapersOnLine* 48.23 (2015). 5th IFAC Conference on Nonlinear Model Predictive Control NMPC 2015 Seville, Spain, 17–20 September 2015, pp. 39–46. ISSN: 2405-8963.

[26] S. Edlund and P. O. Fryk. The right truck for the job with global truck application descriptions. *SAE transactions* 113.2 (2004), pp. 344–351.

[27] A. Eidehall and L. Petersson. Statistical Threat Assessment for General Road Scenes Using Monte Carlo Sampling. *IEEE Transactions on Intelligent Transportation Systems* 9.1 (2008), pp. 137–147.

[28] A. Eskandarian. *Handbook of intelligent vehicles*. Springer London, 2012.

[29] *European Truck Platooning Challenge 2016*. Accessed August 30, 2017. URL: https://www.eutruckplatooning.com/PageByID.aspx?sectionID=131542&contentPageID=529927.

[30] Eurostat. *Energy, transport and environment indicators — 2016 edition*. Accessed August 30, 2017. URL: http://ec.europa.eu/eurostat/documents/3217494/7731525/KS-DK-16-001-EN-N.pdf/.

[31] J. M. Flach et al. Collisions: Getting them under control. *Advances in psychology* 135 (2004), pp. 67–91.

[32] H. Flämig. "Autonomous Vehicles and Autonomous Driving in Freight Transport". *Autonomous Driving*. Springer, 2016, pp. 365–385.

[33] Ford Motor Company. *Looking Further - Ford will have a fully autonomous vehicle in operation by 2021*. Accessed August 30, 2017. URL: https://corporate.ford.com/innovation/autonomous-2021.html.

[34] M. Forsberg. *Transmit - Driftstatistik och vägstandardens påverkan på bränsleförbrukningen*. Arbetsrapport 515. Skogforsk, 2002.

[35] Freightliner. Accessed August 30, 2017. URL: http://www.freightlinerinspiration.com/newsroom/press/inspiration-truck-unveiled/.

[36] H. Fritz. "Longitudinal and lateral control of heavy duty trucks for automated vehicle following in mixed traffic: experimental results from the CHAUFFEUR project". *Proceedings of the 1999 IEEE International Conference on Control Applications (Cat. No.99CH36328)*. Vol. 2. 1999, 1348–1352 vol. 2.

[37] H. Fritz et al. "CHAUFFEUR Assistant: a driver assistance system for commercial vehicles based on fusion of advanced ACC and lane keeping". *IEEE Intelligent Vehicles Symposium, 2004*. 2004, pp. 495–500.

[38] Y. Gao et al. A tube-based robust nonlinear predictive control approach to semi-autonomous ground vehicles. *Vehicle System Dynamics* 52.6 (2014), pp. 802–823.

[39] T. M. Gasser et al. Legal consequences of an increase in vehicle automation. *Die Bundesanstalt für Straßenwesen (BASt) Report F* 83 (2009).

[40] D. C. Gazis, R. Herman, and R. B. Potts. Car-following theory of steady-state traffic flow. *Operations research* 7.4 (1959), pp. 499–505.

[41] D. C. Gazis, R. Herman, and R. W. Rothery. Nonlinear follow-the-leader models of traffic flow. *Operations research* 9.4 (1961), pp. 545–567.

[42] T. Gindele et al. "Design of the planner of team AnnieWAY's autonomous vehicle used in the DARPA Urban Challenge 2007". *2008 IEEE Intelligent Vehicles Symposium*. 2008, pp. 1131–1136.

[43] T. Gu et al. "Focused Trajectory Planning for autonomous on-road driving". *2013 IEEE Intelligent Vehicles Symposium (IV)*. 2013, pp. 547–552.

[44] P. E. Hart, N. J. Nilsson, and B. Raphael. A Formal Basis for the Heuristic Determination of Minimum Cost Paths. *IEEE Transactions on Systems Science and Cybernetics* 4.2 (1968), pp. 100–107.

[45] W. Helly. "Simulation of bottlenecks in single lane traffic flow". *Proceedings of the symposium on theory of traffic flow, Research Laboratories, General Motors, New York, pp. 207–238*. 1959.

[46] HHLA. *BESIC Energy Transition Project Successfully Concluded*. Accessed August 30, 2017. URL: http://hhla.de/en/2016/12/besic-energy-transition-project-successfully-concluded.html.

[47] C. J. Hoel and P. Falcone. "Low speed maneuvering assistance for long vehicle combinations". *2013 IEEE Intelligent Vehicles Symposium (IV)*. 2013, pp. 598–604.

[48] J. H. Holland. *Adaptation in natural and artificial systems: An introductory analysis with applications to biology, control, and artificial intelligence*. U Michigan Press, 1975.

[49] Institute for Automotive Engineering (ika). *KONVOI*. Accessed August 30, 2017. URL: https://www.ika.rwth-aachen.de/en/research/projects/driver-assistance-and-vehicle-guidance/1636-konvoi.html.

[50] P. A. Ioannou and C.-C. Chien. Autonomous intelligent cruise control. *IEEE Transactions on Vehicular technology* 42.4 (1993), pp. 657–672.

[51] ISO. *ISO14791:2000(E) Road Vehicles - Heavy Commercial Vehicle Combinations and Articulated Buses - Lateral Stability Test Methods*. Tech. rep. 2002.

[52] ISO/IEC/IEEE. *Systems and software engineering — Architecture description*. Tech. rep. 2011.

[53] B. Jacobson. *Vehicle Dynamics - Compendium for Course MMF062*. Chalmers University of Technology, 2016.

[54] J. Jansson. "Collision Avoidance Theory with Application to Automotive Collision Mitigation". PhD thesis. Department of Electrical Engineering, Linköping University, Sweden, 2005.

[55] J. hwan Jeon et al. "Optimal motion planning with the half-car dynamical model for autonomous high-speed driving". *American Control Conference (ACC), 2013*. IEEE. 2013, pp. 188–193.

[56] D. Kahneman. *Thinking, Fast and Slow*. Farrar, Straus and Giroux, 2011.

[57] S. Karaman and E. Frazzoli. Sampling-based algorithms for optimal motion planning. *The international journal of robotics research* 30.7 (2011), pp. 846–894.

[58] C. Katrakazas et al. Real-time motion planning methods for autonomous on-road driving: State-of-the-art and future research directions. *Transportation Research Part C: Emerging Technologies* 60 (2015), pp. 416 –442.

[59] S. Kharrazi et al. *Performance Based Standards for High Capacity Transports in Sweden FIFFI project 2013-03881 – Report 1, Review of existing regulations and literature*. VTI rapport 859A. Swedish National Road and Transport Research Institute (VTI), 2015.

[60] I. Knight et al. *Longer and/or Longer and Heavier Goods Vehicles (LHVs): A study of the likely effects if permitted in the UK: Final Report*. PPR 285. IHS, 2008.

[61] Komatsu. *Autonomous Haul System (AHS)*. Accessed August 30, 2017. URL: `http://www.komatsu.com.au/AboutKomatsu/Technology/Pages/AHS.aspx`.

[62] M Kondo. Directional stability (when steering is added). *Journal of the Society of Automotive Engineers of Japan (JSAE)* 7.5-6 (1953), p. 9.

[63] S. M. LaValle. *Planning algorithms*. Cambridge university press, 2006.

[64] S. M. LaValle. *Rapidly-exploring random trees: A new tool for path planning*. Technical Report 98-11. Computer Science Dept., Iowa State University, 1998.

[65] D. Lee. A theory of visual control of braking based on information about time to collision. *Perception* 5.4 (1976), pp. 437–459.

[66] S. Lefèvre, D. Vasquez, and C. Laugier. A survey on motion prediction and risk assessment for intelligent vehicles. *ROBOMECH Journal* (2014).

[67] Z. Liu. Characterisation of optimal human driver model and stability of a tractor-semitrailer vehicle system with time delay. *Mechanical Systems and Signal Processing* 21.5 (2007), pp. 2080–2098.

[68] C. Löfroth and G. Svenson. *Två år med ETT: mindre CO2-utsläpp och färre virkesfordon på vägarna*. Resultat från Skogforsk nr 17 2010. Skogforsk.

[69] J. Lundgren, M. Rönnqvist, and P. Värbrand. *Optimization*. Studentlitteratur, Lund, 2010.

[70] C. MacAdam et al. A computerized model for simulating the braking and steering dynamics of trucks, tractor-trailers, doubles, and triples combinations-Users' manual, phase 4, Highway Safety Research Institute. *Ann Arbor, Michigan. Report No. UM-HSRI-80-58. 355p* (1980).

[71] C. C. MacAdam. Application of an optimal preview control for simulation of closed-loop automobile driving. *IEEE Transactions on Systems, Man, and Cybernetics* 11.6 (1981), pp. 393–399.

[72] D. Madås et al. “On path planning methods for automotive collision avoidance”. *2013 IEEE Intelligent Vehicles Symposium (IV)*. 2013, pp. 931–937.

[73] A. Magnusson et al. “A reference architecture for commercial vehicles”. *SAE 2017 Commercial Vehicle Engineering Congress*. To be published. 2017.

[74] G. Markkula. “Driver behavior models for evaluating automotive active safety: From neural dynamics to vehicle dynamics”. PhD thesis. Department of Applied Mechanics, Chalmers University of Technology, 2015.

[75] G. Markkula. “Evaluating vehicle stability support systems by measuring, analyzing, and modeling driver behavior”. Licentiate thesis. Department of Applied Mechanics, Chalmers University of Technology, 2013.

[76] G. Markkula, O. Benderius, and M. Wahde. Comparing and validating models of driver steering behaviour in collision avoidance and vehicle stabilisation. *Vehicle system dynamics* 52.12 (2014), pp. 1658–1680.

[77] D. S. Meek and R. Thomas. A guided clothoid spline. *Computer Aided Geometric Design* 8.2 (1991), pp. 163–174.

[78] A. Mellin and J. Ståhle. *Omvärlds- och framtidsanalys längre och tyngre väg- och järnvägsfordon*. VTI rapport 676. Swedish National Road and Transport Research Institute (VTI), 2010.

[79] J. A. Michon. “A critical view of driver behavior models: what do we know, what should we do?” *Human behavior and traffic safety*. Springer, 1985, pp. 485–524.

[80] A. Munshi. “The opencl specification”. *Hot Chips 21 Symposium (HCS), 2009 IEEE*. IEEE. 2009, pp. 1–314.

[81] C. J. Nash, D. J. Cole, and R. S. Bigler. A review of human sensory dynamics for application to models of driver steering and speed control. *Biological cybernetics* 110.2-3 (2016), pp. 91–116.

[82] National Highway Traffic Safety Administration. *Preliminary statement of policy concerning automated vehicles*. 2013 (Accessed August 30, 2017). URL: `http://www.nhtsa.gov/staticfiles/rulemaking/pdf/Automated_Vehicles_Policy.pdf`.

[83] T. Nayl, G. Nikolakopoulos, and T. Gustafsson. “On-Line path planning for an articulated vehicle based on Model Predictive Control”. *2013 IEEE International Conference on Control Applications (CCA)*. 2013, pp. 772–777.

[84] D. C. K. Ngai and N. H. C. Yung. A multiple-goal reinforcement learning method for complex vehicle overtaking maneuvers. *IEEE Transactions on Intelligent Transportation Systems* 12.2 (2011), pp. 509–522.

[85] J. Nilsson et al. Longitudinal and Lateral Control for Automated Yielding Maneuvers. *IEEE Transactions on Intelligent Transportation Systems* 17.5 (2016), pp. 1404–1414.

[86] J. Nilsson et al. If, When, and How to Perform Lane Change Maneuvers on Highways. *IEEE Intelligent Transportation Systems Magazine* 8.4 (2016), pp. 68–78.

[87] J. Nilsson. “Automated driving maneuvers : trajectory planning via convex optimization in the model predictive control framework”. PhD thesis. Department of Signals and Systems, Chalmers University of Technology, Sweden, 2016.

[90] P. Nilsson, L. Laine, and B. Jacobson. "Performance characteristics for automated driving of long heavy vehicle combinations evaluated in motion simulator". *Intelligent Vehicles Symposium Proceedings, 2014 IEEE*. IEEE. 2014, pp. 362–369.

[94] P. Nilsson and J. Sandin. "Drivers' assessment of driving a 32 meter A-double with and without full automation in a moving simulator base simulator". *13th International Heavy Vehicle Transport Technology Symposium, San Luis, Argentina*. 2014.

[95] Nissan Motor Company. *Nissan Announces Unprecedented Autonomous Drive Benchmarks*. Accessed August 30, 2017. URL: `http://nissannews.com/en-US/nissan/usa/releases/nissan-announces-unprecedented-autonomous-drive-benchmarks#!`.

[96] C Nowakowski, S. E. Shladover, and H.-S. Tan. Heavy Vehicle Automation: Human Factors Lessons Learned. *Procedia Manufacturing* 3 (2015), pp. 2945–2952.

[97] NVIDIA Corporation. *NVIDIA and Bosch Announce AI Self-Driving Car Computer*. Accessed August 30, 2017. URL: `https://blogs.nvidia.com/blog/2017/03/16/bosch/`.

[98] H. B. Pacejka. *Tire and vehicle dynamics*. Butterworth-Heinemann, 2006.

[99] B. Paden et al. A Survey of Motion Planning and Control Techniques for Self-Driving Urban Vehicles. *IEEE Transactions on Intelligent Vehicles* 1.1 (2016), pp. 33–55.

[100] M. Plöchl and J. Edelmann. Driver models in automobile dynamics application. *Vehicle System Dynamics* 45.7-8 (2007), pp. 699–741.

[101] V. Punzo and B. Ciuffo. Integration of driving and traffic simulation: Issues and first solutions. *IEEE transactions on intelligent transportation systems* 12.2 (2011), pp. 354–363.

[102] A. J. Rimmer and D. Cebon. Planning Collision-Free Trajectories for Reversing Multiply-Articulated Vehicles. *IEEE Transactions on Intelligent Transportation Systems* 17.7 (2016), pp. 1998–2007.

[103] M. Sadeghi Kati. *Definitions of Performance Based Characteristics for Long Heavy Vehicle Combinations*. Tech. rep. Department of Signals and Systems, Chalmers University of Technology, 2013.

[104] SAE International. *SAE J3016 Taxonomy and Definitions for Terms Related to Driving Automation Systems for On-Road Motor Vehicles*. Tech. rep. 2016.

[105] SAE International. *SAE J3016 Taxonomy and Definitions for Terms Related to On-Road Motor Vehicles Automated Driving Systems*. Tech. rep. 2014.

[106] D. D. Salvucci and R. Gray. A two-point visual control model of steering. *Perception* 33 (2004), pp. 1233–1248.

[107] K. Sandberg. *Godstransporter i Sverige - en nulägesanalys*. Trafikanalys-report 7. Trafikanalys, 2016.

[108] B Sen, J. Smith, and W. Najm. *Analysis of lane change crashes*. Tech. rep. National Highway Traffic Safety Administration, HS-809 571, DOT-VNTSC-NHTSA-02-03, 2003.

[109] S. Shalev-Shwartz, S. Shammah, and A. Shashua. Safe, multi-agent, reinforcement learning for autonomous driving. *arXiv preprint arXiv:1610.03295* (2016).

[110] S. E. Shladover et al. Demonstration of automated heavy-duty vehicles. *California Partners for Advanced Transit and Highways (PATH)* (2006).

[111] J.-J. E. Slotine and W. Li. *Applied nonlinear control*. Prentice-Hall, Upper Saddle River, NJ, 1991.

[112] M. R. Smith et al. Monocular optical constraints on collision control. *Journal of Experimental Psychology: Human Perception and Performance* 27.2 (2001), p. 395.

[113] H. Summala. "Towards Understanding Motivational and Emotional Factors in Driver Behaviour: Comfort Through Satisficing". *Modelling Driver Behaviour in Automotive Environments*. Ed. by P. Cacciabue. Springer London, 2007, pp. 189–207.

[114] P. Sundström, B. Jacobson, and L. Laine. "Vectorized single-track model in Modelica for articulated vehicles with arbitrary number of units and axles". *Proceedings of the 10 th International Modelica Conference; March 10-12; 2014; Lund; Sweden*. 096. Linköping University Electronic Press. 2014, pp. 265–271.

[115] Swedish Ministry of Enterprise and Innovation. *Government proposal 2016/17:112*. 2016.

[116] Swedish Transport Administration. *Krav för vägars och gators utformning*. Trafikverkets publikation 2015:086. 2015.

[117] Swedish Transport Administration. *Rapport om tyngre och längre fordonståg på det allmänna vägnätet*. TSV 2014-1419. 2014.

[118] S. Taheri. "Steering control characteristics of human driver coupled with an articulated commercial vehicle". PhD thesis. Concordia University, 2014.

[119] S. Thrun et al. Stanley: The robot that won the DARPA Grand Challenge. *Journal of field Robotics* 23.9 (2006), pp. 661–692.

[120] M. Treiber, A. Hennecke, and D. Helbing. Congested traffic states in empirical observations and microscopic simulations. *Physical Review E - Statistical Physics, Plasmas, Fluids, and Related Interdisciplinary Topics* 62.2 B (2000), pp. 1805–1824.

[121] S. Tsugawa, S. Kato, and K. Aoki. "An automated truck platoon for energy saving". *2011 IEEE/RSJ International Conference on Intelligent Robots and Systems*. 2011, pp. 4109–4114.

[122] S. Ulbrich and M. Maurer. "Towards Tactical Lane Change Behavior Planning for Automated Vehicles". *2015 IEEE 18th International Conference on Intelligent Transportation Systems*. 2015, pp. 989–995.

[123] N. Van Duijkeren. "Real-time receding horizon trajectory generation for long heavy vehicle combinations on highways". Master's thesis. Delft University of Technology, 2014.

[124] K. Van Heerden, Y. Fujimoto, and A. Kawamura. "A combination of particle swarm optimization and model predictive control on graphics hardware for real-time trajectory planning of the under-actuated nonlinear Acrobot". *Advanced Motion Control (AMC), 2014 IEEE 13th International Workshop on*. IEEE. 2014, pp. 464–469.

[125] Vinnova 2016-05413. *Highly Automated Freight Transports*. Accessed August 30, 2017. URL: `http://www.vinnova.se/sv/Resultat/Projekt/Effekta/2009-02186/Highly-Automated-Freight-Transports/`.

[126] M. Wahde. *Biologically inspired optimization methods: an introduction*. WIT press, 2008.

[127] M. Wahde. *Introduction to Autonomous Robots*. Chalmers University of Technology, 2016.

[128] D. W. van der Wiel et al. "Driver Adaptation to Driving Speed and Road Width: Exploring Parameters for Designing Adaptive Haptic Shared Control". *Systems, Man, and Cybernetics (SMC), 2015 IEEE International Conference on*. IEEE. 2015, pp. 3060–3065.

[129] C. B. Winkler. Simplified Analysis of the Steady-State Turning of Complex Vehicles. *Vehicle System Dynamics* 29.March 2015 (1998), pp. 141–180.

[130] W. Xu et al. "Motion planning under uncertainty for on-road autonomous driving". *2014 IEEE International Conference on Robotics and Automation (ICRA)*. 2014, pp. 2507–2512.

[131] X Yang, S. Rakheja, and I Stiharu. Structure of the driver model for articulated vehicles. *International Journal of Heavy Vehicle Systems* 9.1 (2002), pp. 27–51.

[132] X. Yang, S. Rakheja, and I. Stiharu. Adapting an articulated vehicle to its drivers. *ASME Journal of Mechanical Design* 123.1 (2000), pp. 132–140.

[133] X. Yang, S. Rakheja, and I. Stiharu. Study of control characteristics of an articulated vehicle driver. *International Journal of Heavy Vehicle Systems* 4.2-4 (1997), pp. 373–397.

[134] E. H. Yilmaz and W. H. Warren. Visual control of braking: A test of the $\dot{\tau}$ hypothesis. *Journal of Experimental Psychology: Human Perception and Performance* 21.5 (1995), p. 996.

[135] C. You and P. Tsiotras. "Optimal two-point visual driver model and controller development for driver-assist systems for semi-autonomous vehicles". *2016 American Control Conference (ACC)*. 2016, pp. 5976–5981.

[136] K. D. Young, V. I. Utkin, and U. Ozguner. A control engineer's guide to sliding mode control. *IEEE Transactions on Control Systems Technology* 7.3 (1999), pp. 328–342.

[137] S. Zafeiropoulos and P. Tsiotras. "Design of a lane-tracking driver steering assist system and its interaction with a two-point visual driver model". *American Control Conference (ACC), 2014*. IEEE. 2014, pp. 3911–3917.

[138] J. Zhang and P. A. Ioannou. Longitudinal control of heavy trucks in mixed traffic: environmental and fuel economy considerations. *IEEE Transactions on Intelligent Transportation Systems* 7.1 (2006), pp. 92–104.

[139] Z. Zheng, S. Ahn, and C. M. Monsere. Impact of traffic oscillations on freeway crash occurrences. *Accident Analysis & Prevention* 42.2 (2010), pp. 626–636.

[140] S. Zhu. "Coordinated control of active safety systems for multi-trailer articulated heavy vehicles". PhD thesis. University of Ontario Institute of Technology, 2016.

[141] J. Ziegler et al. Making Bertha Drive-An Autonomous Journey on a Historic Route. *IEEE Intelligent Transportation Systems Magazine* 6.2 (2014), pp. 8–20.